



Libraries and Learning Services

# University of Auckland Research Repository, ResearchSpace

## Copyright Statement

The digital copy of this thesis is protected by the Copyright Act 1994 (New Zealand).

This thesis may be consulted by you, provided you comply with the provisions of the Act and the following conditions of use:

- Any use you make of these documents or images must be for research or private study purposes only, and you may not make them available to any other person.
- Authors control the copyright of their thesis. You will recognize the author's right to be identified as the author of this thesis, and due acknowledgement will be made to the author where appropriate.
- You will obtain the author's permission before publishing any material from their thesis.

## General copyright and disclaimer

In addition to the above conditions, authors give their consent for the digital copy of their work to be used subject to the conditions specified on the [Library Thesis Consent Form](#) and [Deposit Licence](#).

---

*Department of Mathematics  
The University of Auckland  
New Zealand*

---

**Quasi-steady-state reduction in the  
analysis of biophysical models and  
excitation-contraction coupling in  
airway smooth muscle cells**

---

*Sebastian Daniel Boie*

*June 2016*

*Supervisors: Vivien Kirk*

*James Sneyd*



A THESIS SUBMITTED IN FULFILMENT OF THE REQUIRE-  
MENTS OF DOCTOR OF PHILOSOPHY IN MATHEMATICS



# Co-Authorship Form

This form is to accompany the submission of any PhD that contains research reported in published or unpublished co-authored work. **Please include one copy of this form for each co-authored work.** Completed forms should be included in all copies of your thesis submitted for examination and library deposit (including digital deposit), following your thesis Abstract.

Please indicate the chapter/section/pages of this thesis that are extracted from a co-authored work and give the title and publication details or details of submission of the co-authored work.

The chapters 2-4 are from co-authored work that is submitted to the Journal of Theoretical Biology.

S. Boie, V. Kirk, J. Sneyd and M. Wechselberger. Effects of quasi-steady state reduction on biophysical models with oscillations. Submitted to Journal of Theoretical Biology. Currently under revision

Nature of contribution by PhD candidate

Wrote the paper, performed numerical computations

Extent of contribution by PhD candidate (%)

80%


## CO-AUTHORS

Name	Nature of Contribution
Vivien Kirk	Regular supervision of the work, revision of the paper draft
James Sneyd	Commented on the paper draft, suggested parts for the introduction
Martin Wechselberger	Feedback on paper draft, suggested ideas for proof, revision of the paper draft

## Certification by Co-Authors

The undersigned hereby certify that:

- ❖ the above statement correctly reflects the nature and extent of the PhD candidate's contribution to this work, and the nature of the contribution of each of the co-authors; and
- ❖ in cases where the PhD candidate was the lead author of the work that the candidate wrote the text.

Name	Signature	Date
Vivien Kirk		19/10/16
James Sneyd		19 Jan 2016
Martin Wechselberger		9/12/2015

## Co-Authorship Form

This form is to accompany the submission of any PhD that contains research reported in published or unpublished co-authored work. **Please include one copy of this form for each co-authored work.** Completed forms should be included in all copies of your thesis submitted for examination and library deposit (including digital deposit), following your thesis Abstract.

Please indicate the chapter/section/pages of this thesis that are extracted from a co-authored work and give the title and publication details or details of submission of the co-authored work.

The chapters are from co-authored work that is submitted for publication.

S. Boie, J. Chen, M.J. Sanderson and J.Sneyd. Excitation contraction coupling in airway smooth muscle cells and the role of store-operated Ca<sup>2+</sup> channels.

Nature of contribution by PhD candidate

Data analysis, model construction and simulations, wrote the paper

Extent of contribution by PhD candidate (%)

80%


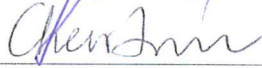

### CO-AUTHORS

Name	Nature of Contribution
James Sneyd	Supervision of the work, revision of the paper
Jun Chen	performed the experiments, commented on the paper
Michael J. Sanderson	performed the experiments, commented on the paper

### Certification by Co-Authors

The undersigned hereby certify that:

- ❖ the above statement correctly reflects the nature and extent of the PhD candidate's contribution to this work, and the nature of the contribution of each of the co-authors; and
- ❖ in cases where the PhD candidate was the lead author of the work that the candidate wrote the text.

Name	Signature	Date
James Sneyd		Click here 19 Jan 2016
Jun Chen		Click here 12/17/15
Michael J. Sanderson		Click here 12/17/15
		Click here
		Click here
		Click here

# Acknowledgements

I would like to express my gratitude to my supervisors Vivien Kirk and James Sneyd. Given continuous guidance and support from them, I was able to explore some aspects of the fields of dynamical systems and mathematical biology. Vivien and James both shared their knowledge on numerous occasions with great patience and clarity. Without their help, I would probably still be stuck in the beginning. Furthermore, I wish to thank Martin Wechselberger for sharing his knowledge about Geometric Singular Perturbation Theory.

I really appreciated the good environment in the Math Department and my office, thanks to my great office mates Jen Creaser, Stefanie Hittmeyer, Pete Langfield, Pingyu Nan, Jeremie Moerenhout, Barak Shani, Tertius Ralph and Anand Rampadarath. Of great help were also discussions with many fellow PhD students, especially Jung Min Han, Andrus Giraldo, Cris Hasan, Jose Mujica, Saeed Farjami, Ben Lawrence, Rebecca Turner, Jurij Volcic, Antoine Nectoux, Ricardo Gutierrez, Demival Vasques and many others. Many have not only inspired me on my work, but also became good friends.

My deepest gratitude goes to my wife Mengnan Ruan, who accompanied me to the far away country of New Zealand, and supported and encouraged me throughout this entire journey. Without whom I would have struggled to find the inspiration and motivation needed to complete this thesis. Furthermore, I want to thank my parents who enabled me to go to University in the first place.

I would also like to thank the Marsden Fund, who funded my PhD research and allowed me to go to multiple international conferences.



# Abstract

This thesis addresses two topics related to the mathematical modelling of biophysical systems.

The first part of the thesis investigates quasi-steady-state reduction (QSSR), which is a technique commonly used for dimension reduction for systems with multiple timescales. Many biophysical models have the property that some variables in the model evolve much faster than others. A common first step in the analysis of such systems is to simplify the model by assuming that some of the fastest variables equilibrate instantaneously; this approach is known as QSSR. QSSR is intuitively satisfying but is not always mathematically justified, with problems known to arise, for instance, in examples in which the full model has oscillatory solutions. In models with oscillations, a simplification by QSSR may lead to a model with significantly different dynamics compared to the original model.

In the first part, we focus on the effect of QSSR on models in which oscillatory solutions arise via one or more Hopf bifurcations. We first illustrate the problems that can arise by applying QSSR to a selection of well-known models. We then prove that Hopf bifurcations that involve fast and slow variables (i.e., singular Hopf bifurcations) are generically preserved under QSSR so long as a fast variable is kept in the simplified system. Furthermore, we argue that Hopf bifurcations that involve only slow variables are not affected by QSSR, and Hopf bifurcations that primarily involve fast variables may be eliminated by QSSR.

The persistence of a Hopf bifurcation does not guarantee that the resulting periodic orbits are unchanged by QSSR. We show that the criticality of a Hopf bifurcation may be changed by QSSR, with a resultant change in the stability of periodic orbits near the Hopf bifurcation. Furthermore, we show that QSSR can affect the amplitude and frequency of periodic orbits and introduce or remove homoclinic bifurcations. Finally, we present some guidelines for the application of QSSR if one wishes to use the method while minimising



the risk of inadvertently destroying essential features of the original model.

In the second part of this thesis we study the feedback between changes in voltage across the plasma membrane and the intracellular  $\text{Ca}^{2+}$  handling in airway smooth muscle cells (ASMC). ASMC are able to contract, and the contraction can result in pathological airway obstruction in asthma or airway hyperresponsiveness. Contraction of ASMC is induced by an increased cytosolic  $\text{Ca}^{2+}$  concentration ( $[\text{Ca}^{2+}]_i$ ). Typically,  $[\text{Ca}^{2+}]_i$  oscillates during prolonged smooth muscle contraction and the oscillation frequency affects the strength of contraction. Oscillations of  $[\text{Ca}^{2+}]_i$  result from either depolarization followed by increased  $[\text{Ca}^{2+}]_i$  and calcium-induced  $\text{Ca}^{2+}$  release from internal stores, or the binding of an agonist which produces inositol (1,4,5)-trisphosphate and leads to  $\text{Ca}^{2+}$  release from internal stores.

Previous models of  $[\text{Ca}^{2+}]_i$  oscillations in ASMC have included the voltage across the plasma membrane as a parameter which modifies the  $\text{Ca}^{2+}$  influx [19, 23, 94]. However, evidence suggests that the voltage changes dynamically during  $[\text{Ca}^{2+}]_i$  oscillations [98]. We combine mathematical models of intracellular  $\text{Ca}^{2+}$  receptors and plasma membrane channels and use experimental data from mouse lung slices to assess the effect of voltage dynamics on the  $[\text{Ca}^{2+}]_i$  oscillations. Furthermore, we look at the contribution of different  $\text{Ca}^{2+}$  channels in the plasma membrane, in particular the voltage-gated and the store-operated  $\text{Ca}^{2+}$  channels.

The main results of this part of the thesis are:

- Agonist-induced  $[\text{Ca}^{2+}]_i$  oscillations are not significantly affected by changes in voltage. Variations in voltage, due to the intrinsic voltage dynamics, only lead to small modulations of the  $\text{Ca}^{2+}$  influxes.
- During depolarization-induced  $[\text{Ca}^{2+}]_i$  oscillations the voltage-gated  $\text{Ca}^{2+}$  channel contributes most to the  $\text{Ca}^{2+}$  influx; during agonist-induced  $[\text{Ca}^{2+}]_i$  oscillations the store-operated  $\text{Ca}^{2+}$  channel contributes most to the  $\text{Ca}^{2+}$  influx.
- During agonist-induced  $[\text{Ca}^{2+}]_i$  oscillations the internal stores do not fully deplete. The  $\text{Ca}^{2+}$  concentration in internal stores plateaus near 80% of the resting concentration during agonist-induced oscillations.

# Contents

<b>Acknowledgements</b>	<b>iii</b>
<b>Abstract</b>	<b>v</b>
<b>1 Introduction</b>	<b>1</b>
<b>2 Quasi-steady-state reduction in mathematical models with oscillations</b>	<b>7</b>
2.1 Introduction . . . . .	7
2.2 Motivating examples . . . . .	9
2.2.1 Hodgkin-Huxley model . . . . .	9
2.2.2 Hindmarsh-Rose model . . . . .	12
2.2.3 Chay-Keizer model . . . . .	14
<b>3 Results on quasi-steady-state reduction</b>	<b>19</b>
3.1 Preliminaries . . . . .	19
3.2 The effect of QSSR on equilibria . . . . .	21
3.3 Note on geometric singular perturbation theory and QSSR . . . . .	22
3.4 Note on $\epsilon$ -dependence of the equations . . . . .	23

---

3.5	The effect of QSSR on oscillatory solutions . . . . .	23
3.6	Singular Hopf bifurcations and QSSR . . . . .	26
3.6.1	Persistence of singular Hopf bifurcations . . . . .	26
3.6.2	Criticality of singular Hopf bifurcations . . . . .	34
3.7	Other effects of QSSR . . . . .	39
3.7.1	Homoclinic bifurcations . . . . .	39
3.7.2	Saddle-node bifurcations of periodic orbits . . . . .	41
<b>4</b>	<b>Applying quasi-steady-state reduction</b>	<b>43</b>
4.1	Appropriate application of quasi-steady-state reduction . . . . .	43
4.2	Conclusions . . . . .	50
<b>5</b>	<b>Excitation-contraction coupling in airway smooth muscle cells</b>	<b>53</b>
5.1	Introduction . . . . .	53
5.2	Model construction . . . . .	56
5.2.1	Calcium transport between the cytosol and the SR . . . . .	58
5.2.2	Calcium transport across the plasma membrane . . . . .	62
5.3	Sodium, potassium and chloride transport across the plasma membrane . . . . .	63
<b>6</b>	<b>Contributions of plasma membrane calcium channels</b>	<b>67</b>
6.1	Importance of voltage-gated $\text{Ca}^{2+}$ entry . . . . .	67
6.2	Importance of store-operated $\text{Ca}^{2+}$ entry . . . . .	70
6.3	Dynamics of store-operated $\text{Ca}^{2+}$ channels . . . . .	72

---

<b>7</b>	<b>Discussion of model predictions</b>	<b>77</b>
<b>8</b>	<b>Concluding remarks and future directions</b>	<b>81</b>
8.1	Quasi-steady-state reduction . . . . .	81
8.2	Airway smooth muscle cells . . . . .	83
<b>A</b>	<b>Model functions and parameters</b>	<b>87</b>
A.1	Hodgkin-Huxley model . . . . .	87
A.2	Chay-Keizer model . . . . .	89
A.3	GnRH neuron model . . . . .	90
	<b>Bibliography</b>	<b>93</b>



# List of Figures

2.1	Partial bifurcation diagrams for various versions of the Hodgkin-Huxley model	11
2.2	Partial bifurcation diagrams for various versions of the Hindmarsh-Rose model . . . . .	13
2.3	Partial bifurcation diagrams for various versions of the Chay-Keizer model	15
2.4	Partial bifurcation diagrams for various versions of the Chay-Keizer model, showing the period of the periodic orbit branches . . . . .	16
2.5	Frequencies of periodic orbits near the left Hopf bifurcation for the Chay-Keizer model . . . . .	17
3.1	Changes in criticality near the left Hopf bifurcation due to QSSR in the HR model . . . . .	40
3.2	Changes in criticality near the left Hopf bifurcation due to QSSR in the CK model . . . . .	40
3.3	Partial bifurcation diagrams for the Gonadotropin Releasing Hormone neuron	42
4.1	Partial bifurcation diagram for the fast subsystem of the HR model . . . .	48
4.2	Partial bifurcation diagram for the fast subsystem of the GnRH model given by Eq. (4.1.3) with $O_{\text{ucl},0}^* = 0.1$ , $c_0 = 0.5$ and $c_{t,0} = 80$ . . . . .	49
4.3	Partial bifurcation diagram for the fast subsystem of the GnRH model given by Eq. (4.1.3) with $O_{\text{ucl},0}^* = 0.0454$ , $c_0 = 50.3688$ and $c_{t,0} = 52.9475$ . .	50

---

5.1	Schematic diagram of $\text{Ca}^{2+}$ fluxes . . . . .	55
5.2	Schematic diagram of airway smooth muscle cell model . . . . .	56
5.3	Sketch of six-state IPR model . . . . .	61
6.1	Comparison of experimental data and simulations of $[\text{Ca}^{2+}]_i$ oscillations upon stimulation by KCl . . . . .	69
6.2	Comparison of experimental data and simulations of $[\text{Ca}^{2+}]_i$ oscillations upon stimulation by MCh . . . . .	70
6.3	Comparison of $\text{Ca}^{2+}$ influxes for different stimuli . . . . .	71
6.4	Comparison of $[\text{Ca}^{2+}]_i$ oscillations for model with fixed voltage and model with oscillating voltage . . . . .	72
6.5	Effect of partially blocking SOCC on oscillations in $[\text{Ca}^{2+}]_i$ . . . . .	73
6.6	Comparison of agonist-induced $[\text{Ca}^{2+}]_i$ oscillations in $\text{Ca}^{2+}$ -free medium to oscillations with blocked SOCC . . . . .	74
6.7	Comparison of $[\text{Ca}^{2+}]_i$ oscillations with different SOCC gating kinetics . . .	75

# List of Tables

5.1	Parameter values for model as presented in 5.2. . . . .	66
A.1	Functions and parameters for the Hodgkin-Huxley model as used in section 2.2. . . . .	88
A.2	Parameter values for the Chay-Keizer model as used in section 2.2. . . . .	90
A.3	Parameter values for the Gonadotropin Releasing Hormone neuron model as used in section 4.1. . . . .	92





# Glossary

**5-HT** - 5-hydroxytryptamine

**ACh** - Acetylcholine

**ASMC** - Airway smooth muscle cells

**Ca<sup>2+</sup>** - Calcium ions

**CICR** - Ca<sup>2+</sup>-induced Ca<sup>2+</sup> release

**CK model** - Chay-Keizer model

**Cl<sup>-</sup>** - Chloride

**CPA** - Cyclopiazonic acid

**FSNII** - Folded saddle-node type II bifurcation

**GSPT** - Geometric singular perturbation theory

**GnRH model** - Gonadotropin Releasing Hormone neuron model

**HR model** - Hindmarsh-Rose model

**HB** - Hopf bifurcation

**HH model** - Hodgkin-Huxley model

**IP<sub>3</sub>** - Inositol (1,4,5)-trisphosphate

**IPR** - IP<sub>3</sub> receptors

**MCh** - Methacholine

**K<sup>+</sup>** - Potassium ions

**PCLSs** - Precision cut lung slices

**PM** - Plasma membrane pump

**QSSR** - Quasi-steady-state reduction

**QSSM** - Quasi-steady-state manifold

**ROCC** - Receptor-operated Ca<sup>2+</sup> channels

**RyR** - Ryanodine receptors

**SP** - Saddle-node bifurcation of periodic orbits

**SR** - Sarcoplasmic reticulum

**Na<sup>+</sup>** - Sodium ions

**SOCC** - Store-operated Ca<sup>2+</sup> channels

**STIM** - Stromal interaction molecules

**tQSSR** - Total quasi-steady-state reduction

**VGCC** - Voltage-gated Ca<sup>2+</sup> channels

# 1

## Introduction

In this thesis we investigate two topics, related to mathematical modelling of biophysical systems.

The first part of this thesis, chapters 2 to 4, investigates the effect of a common dimension reduction technique, which is called *quasi-steady-state reduction* (QSSR). The focus is on establishing conditions for which certain dynamical properties persist after simplifying a given model by QSSR. In the second part of this thesis, chapters 5 to 7, we study the interaction between  $\text{Ca}^{2+}$  handling and changes in membrane voltage of *airway smooth muscle cells* (ASMC). The focus of the second part is on predicting physiological behaviour of ASMC based on a whole-cell, ordinary differential equation model.

Many mathematical models of biological processes are high dimensional and possess multiple timescales. As a consequence, modellers often face stiff systems of differential equations with many variables and parameters. This presents challenges for efficient computation and may obscure the understanding of mathematical mechanisms underlying the observed behaviour. A common approach is to try to exploit the presence of multiple timescales in an attempt to obtain a simplified model (e.g., by assuming that variables equilibrate instantaneously) or to simplify the analysis of a given model by analysing submodels that

evolve on different timescales separately.

A rigorous technique, applicable to systems with two or more distinct timescales, is geometric singular perturbation theory (GSPT). GSPT was pioneered by Fenichel with his seminal work in 1979 [36]. He showed that, under certain conditions, a given system can be divided into slow and fast subsystems, which can be analysed separately and appropriately combined to explain the behaviour of the full system. We discuss some concepts of GSPT in sections 3.3 and 3.6.

The application of GSPT is relatively straightforward if the timescale separation appears explicitly as a parameter in the system. Generally, models are not formulated with explicit timescale separation and various steps may be necessary before GSPT can be applied. If one wishes to use GSPT, one may have to rescale variables and aggregate parameters to identify different timescales. This procedure can become infeasible for large systems with many parameters. Consequently, modellers often revert to techniques that are simpler to use, but are not always mathematically justifiable.

One such technique is quasi-steady-state reduction (QSSR), which was pioneered by [65] and [18], in the analysis of a model of enzyme kinetics. The intuitive idea of QSSR is to identify fast variables based on biophysical intuition and assume they equilibrate instantaneously, thereby effectively removing them from the model. This *ad hoc* removal of fast variables may alter qualitative features of the dynamical behaviour of a model. In particular, it has been demonstrated that oscillations can be removed from a model by QSSR [32, 37]. One aim of this thesis is to study in detail the conditions under which oscillations arising via Hopf bifurcations are robust under QSSR.

In chapters 2 to 4 we study the effect of QSSR in the context of models that show oscillatory solutions. We demonstrate some of the problems that can arise when using QSSR on specific examples in chapter 2. This chapter serves as a motivation for further studies. Chapter 3 explains QSSR in more mathematical detail. We discuss the effect of QSSR on equilibria. While equilibria are preserved, their stability is not necessarily the same in a model simplified by QSSR, compared to the original model. The result is that oscillations arising through Hopf bifurcations can be destroyed. We categorize Hopf bifurcations, depending on whether they involve slow, fast or slow and fast variables, and prove that singular Hopf bifurcations, involving slow and fast variables, persist generically under QSSR. To do this, we use GSPT. Furthermore, we investigate some effects of QSSR on global dynamical structures (e.g., homoclinic bifurcations and saddle-node bifurcations of periodic orbits) in specific examples. In chapter 4 we demonstrate how QSSR can be used while minimizing the risk of inadvertently changing the qualitative behaviour of a

---

given model and give concluding remarks.

The first part of the thesis is co-authored work with Vivien Kirk, James Sneyd and Martin Wechselberger and has been accepted for publication, in modified form, in the Journal of Theoretical Biology [13]. However, the material in subsection 3.6.2 is confined to a comment in that article; the detail appears only in this thesis.

The topic of the second part of this thesis, chapters 5 to 7, is on modelling oscillations of intracellular calcium ions ( $\text{Ca}^{2+}$ ) in airway smooth muscle cells. The focus is on combining a model for voltage dynamics [82] with submodels for intracellular  $\text{Ca}^{2+}$  channels and pumps [19, 23, 94].

Calcium is a ubiquitous messenger important in many cellular processes such as proliferation, fertility, muscle contraction, synaptic transmission and apoptosis [8, 9, 34, 51, 59]. In particular, the cytosolic  $\text{Ca}^{2+}$  concentration,  $[\text{Ca}^{2+}]_i$ , is often the key messenger for diverse cellular processes. Complex spatio-temporal patterns of  $[\text{Ca}^{2+}]_i$  can arise in response to external stimuli or downstream of intracellular processes [9, 29, 34]. For example, in airway smooth muscle cells whole-cell  $\text{Ca}^{2+}$  waves lead to oscillations of  $[\text{Ca}^{2+}]_i$  with periods of 1-60 seconds [74], while in *Xenopus* oocytes changes in the  $\text{Ca}^{2+}$  concentration can take the form of spiral waves and target patterns [2].

The  $[\text{Ca}^{2+}]_i$  is, under normal physiological conditions, significantly lower than the  $\text{Ca}^{2+}$  concentration in the extracellular space and the  $\text{Ca}^{2+}$  concentration in the intracellular stores, such as the endoplasmic reticulum (ER) or sarcoplasmic reticulum (SR) [8, 51, 84]. The  $[\text{Ca}^{2+}]_i$  can be rapidly increased by opening of  $\text{Ca}^{2+}$  selective ion channels in the plasma membrane (influx from extracellular space) or channels in the endo-/sarcoplasmic reticulum (efflux from internal stores) [9, 17, 84].

The most accurate approach to modelling the spatio-temporal patterns of  $[\text{Ca}^{2+}]_i$  would be to take the spatial heterogeneity and diffusion, stochastic release events of  $\text{Ca}^{2+}$  and mobile  $\text{Ca}^{2+}$  buffers into account. Such a formulation would give stochastic partial differential equations with explicit buffer concentrations. A general review of  $\text{Ca}^{2+}$  modelling is given in [34].

Whole-cell models with several simplifying assumptions have been studied extensively and have considerable predictive power in certain cells [19, 23, 60, 84]. First, it is assumed that  $\text{Ca}^{2+}$  is homogeneously distributed within compartments such as the cytosol and the ER/SR, which effectively allows modellers to neglect spatial components [68]. Assuming that  $\text{Ca}^{2+}$  buffers are fast, immobile and linear (e.g., buffers do not saturate) enables

$\text{Ca}^{2+}$  fluxes to be replaced by effective fluxes, thereby neglecting the explicit inclusion of  $\text{Ca}^{2+}$  buffer binding and dissociation [34]. Single channel gating dynamics are governed by stochastic events such as conformational changes and binding of molecules [33]. However, deterministic models have been applied to  $\text{Ca}^{2+}$  signalling components with substantial predictive power [19]. Whether such simplifying assumptions are reasonable depends greatly on the specific question and the cell that is under investigation. Under the assumptions of spatial homogeneity, fast, immobile, non-saturating buffers and deterministic gating mechanisms, the whole-cell  $\text{Ca}^{2+}$  model can be formulated as ordinary differential equations [34].

In the second part of this thesis, we will take the approach of studying the  $\text{Ca}^{2+}$  dynamics in ASMC with ordinary differential equations. Previous work has demonstrated good agreements of whole-cell  $\text{Ca}^{2+}$  fluorescence measurements with predictions by this modelling approach [19, 23, 94].

The motivation for studying  $\text{Ca}^{2+}$  dynamics in ASMC is that the contraction of ASMC during asthma or airway hyperresponsiveness is initiated by increased  $[\text{Ca}^{2+}]_i$ , often in the form of oscillatory changes in  $[\text{Ca}^{2+}]_i$ . The oscillation frequency of  $[\text{Ca}^{2+}]_i$  has been linked directly to the strength of muscle contraction [64, 74], showing that an increased frequency leads to stronger contraction.

In striated skeletal and cardiac muscle the main pathway for contraction is via  $[\text{Ca}^{2+}]_i$  oscillations as a result of electric stimulation by action potentials [78]. An action potential opens voltage-gated  $\text{Ca}^{2+}$  channels and increases  $[\text{Ca}^{2+}]_i$ , which induces  $\text{Ca}^{2+}$ -induced  $\text{Ca}^{2+}$  release from internal stores further increasing  $[\text{Ca}^{2+}]_i$ . Periodic opening of voltage-gated  $\text{Ca}^{2+}$  channels,  $\text{Ca}^{2+}$ -induced  $\text{Ca}^{2+}$  release, reuptake by internal stores, and extrusion of  $\text{Ca}^{2+}$  leads to oscillations. The timescale of these oscillations is set by refilling of internal stores through elevated  $\text{Ca}^{2+}$  influx [84].

In smooth muscle cells stronger contractions, accompanied by faster oscillations of  $[\text{Ca}^{2+}]_i$ , can be elicited by contractile agonists [50]. The pathway is that an agonist binds to G-protein coupled receptors in the plasma membrane. As a downstream effect, inositol (1,4,5)-trisphosphate ( $\text{IP}_3$ ) is produced and diffuses into the cytosol [7]. The  $\text{IP}_3$  can bind to  $\text{IP}_3$ -receptors (IPR), which show an increased open probability in the presence of  $\text{IP}_3$ . The IPR have a biphasic open probability curve, which means that  $\text{Ca}^{2+}$  ions have an activatory effect at low concentrations and an inhibitory effect at high concentrations [87, 93]. Reuptake by pumps and extrusion of  $\text{Ca}^{2+}$  can lead to oscillations in  $[\text{Ca}^{2+}]_i$ , typically much faster than oscillations elicited by external  $\text{Ca}^{2+}$  influx. The timescale of these oscillations is set by the channel gating kinetics of IPR [19, 94].

---

The effect of voltage dynamics during agonist-induced  $[Ca^{2+}]_i$  oscillations is not known. In the second part of this thesis we construct a mathematical model to study the influence of voltage dynamics and the contributions of two types of plasma membrane  $Ca^{2+}$  channels on the intracellular  $Ca^{2+}$  dynamics.

Specifically, in the second part of this thesis, we will study the two following questions:

- Do variations in voltage across the membrane during agonist-induced oscillations have a significant effect on the  $[Ca^{2+}]_i$  oscillation frequency?
- What are the relative contributions to overall  $Ca^{2+}$  influx of different  $Ca^{2+}$  ion channels in the plasma membrane for the two different stimuli?

We introduce the model in detail in chapter 5. In chapter 6 we present a comparison between experimental data and model simulations. In the same chapter, we make predictions about the effect of voltage dynamics during agonist-induced oscillations, and the effect of blocking different plasma membrane  $Ca^{2+}$  channels on  $[Ca^{2+}]_i$  oscillations. In chapter 7, we conclude by identifying predictions that have not been tested experimentally and discuss the general caveats of the model.

The results of the second part of this thesis have been included in a manuscript that will be submitted for publication soon [12]. The model is parametrized to reproduce experimental data, obtained in mouse lung slices, by Jun Chen and Michael J. Sanderson at the University of Massachusetts Medical School. In contrast to the manuscript, this thesis presents a comparison between experimental data and numerical simulations without the experimental details. Furthermore, we introduce the mathematical model in more detail than it appears in the manuscript.





# 2

## Quasi-steady-state reduction in mathematical models with oscillations

### 2.1 Introduction

For well over 50 years, oscillations in cell biology have been of major interest to both theoreticians and experimentalists. In neurons, for example, oscillation of the membrane potential is one of the fundamental behaviours that underlie neuronal function, while in almost every cell type oscillations in the concentration of cytoplasmic calcium control a wide variety of cellular behaviours, including secretion, water transport, movement, gene expression and differentiation. These are but two examples from many of current interest to scientists.

In addition to their physiological interest, models of oscillations in cell physiology often have interesting mathematical properties. In particular, they commonly contain variables that operate on different time scales; thus, mathematical analyses of these models require the use of mathematical techniques that can cope with multiple, widely varying, time scales.

One method that has commonly been used to study such multiple timescale systems is quasi-steady state reduction (QSSR), also sometimes referred to as pseudo-steady state reduction or adiabatic elimination. In this approach, one or more fast variables are assumed to be at quasi-steady state, so transient response in these variables is ignored and the differential equations for their evolution are replaced by algebraic equations, thereby reducing the dimension of the model. QSSR was introduced by Michaelis and Menten over 100 years ago to simplify a mathematical description of enzyme kinetics [65]. The simplification was also discussed by Briggs and Haldane [18] and, more recently, in great detail in [85]. An extension to QSSR, named *total quasi-steady-state reduction* (tQSSR), was introduced in [15], and further developed in [22] and [71]. In tQSSR, a coordinate transformation is first applied, followed by regular QSSR; the coordinate transformation effectively attempts to align model variables more closely with time scales, and thereby to overcome difficulties arising when the evolution equation for a physical variable contains terms corresponding to a mix of timescales.

The approach of equilibrating some variables instantaneously is intuitively satisfying, but it is only justified if the model under consideration possesses a globally attracting slow manifold to which the dynamics are confined after the initial transient phase [85]. Most studies of QSSR (or tQSSR) are devoted to studying the accuracy of the simplified system in comparison to the full system when the system has a globally attracting, slow invariant manifold. Some recent papers note that application of QSSR can lead to qualitatively different predictions compared with the original model, especially with regard to oscillations [32, 37, 71, 97], but a comprehensive understanding of what can go wrong, and why, is still lacking.

Because of the widespread use of QSSR resulting from its ease of use and its ability to present understandable and simplified versions of complex models, it is important to know, as precisely as possible, when a QSSR approach is valid and when it is not.

In section 2.2, we motivate our interest in this issue by showing the effect of QSSR on a selection of well-known biophysical models, all which have oscillatory solutions arising in Hopf bifurcations. In some cases, the dynamics of the original model is minimally disrupted by QSSR but in other cases substantial dynamical changes are induced by QSSR. In chapter 3 we look in more mathematical detail at the effect of QSSR and state our main result about the consequences of QSSR for Hopf bifurcations; this result is proved in section 3.6. Section 4.1 presents some guidelines for the application of QSSR if one wishes to use the method while minimizing the risk of inadvertently destroying essential dynamics of the original model. Concluding remarks are presented in chapter 4.

## 2.2 Motivating examples

In this section we show the effect of QSSR on the dynamics of a selection of well-known ordinary differential equation models, all of which have the feature that oscillatory solutions are introduced via one or more Hopf bifurcations as a bifurcation parameter is varied. It is not *a priori* clear how QSSR affects the onset of oscillations, the interval of parameter values for which the emanating branch of periodic orbit exists, or characteristics of the periodic orbits such as frequency and amplitude. As these examples will demonstrate, it turns out that in some cases the dynamics are minimally disrupted by the application of QSSR but in other cases significant qualitative changes are induced by the reduction.

All the numerical investigations in this section were done with the bifurcation and continuation software AUTO [27].

### 2.2.1 Hodgkin-Huxley model

The first example is the well-known Hodgkin-Huxley (HH) model [45] for the membrane action potential in the squid giant axon. The version of the model we use is formulated as a system of four ordinary differential equations [83]:

$$C_m \frac{dv}{dt} = I - g_{\text{Na}} m^3 h (v - E_{\text{Na}}) - g_{\text{K}} n^4 (v - E_{\text{K}}) - g_{\text{L}} (v - E_{\text{L}}), \quad (2.2.1)$$

$$\frac{dm}{dt} = \frac{1}{\tau_m t_m(v)} (m_{\infty}(v) - m), \quad (2.2.2)$$

$$\frac{dh}{dt} = \frac{1}{\tau_h t_h(v)} (h_{\infty}(v) - h), \quad (2.2.3)$$

$$\frac{dn}{dt} = \frac{1}{\tau_n t_n(v)} (n_{\infty}(v) - n), \quad (2.2.4)$$

where  $v$  represents the membrane potential,  $m$  represents the activation of the sodium channel,  $h$  describes the inactivation of the sodium channel and  $n$  the activation of the potassium channel. The parameter  $I$  represents the applied current, and will be used as the main bifurcation parameter. Expressions for the functions  $m_{\infty}(v)$ ,  $h_{\infty}(v)$ ,  $n_{\infty}(v)$ , etc. and the values of constants used are given in Appendix A.

Since sodium channel activation is observed in experiments to occur more rapidly than sodium channel inactivation or potassium channel activation,  $m$  is usually regarded as a faster variable than either  $n$  or  $h$ . It is common to assume, therefore, that  $m$  relaxes instantaneously to its quasi-steady state value,  $m_{\infty}(v)$ , [31, 51, 66, 79, 83] and to replace  $m$

by  $m_\infty(v)$  in equation (Eq. (2.2.1)). Then the HH equations reduce to a three-dimensional system of ordinary differential equations for  $v$ ,  $h$  and  $n$ :

$$C_m \frac{dv}{dt} = I - g_{\text{Na}}(m_\infty(v))^3 h (v - E_{\text{Na}}) - g_{\text{K}} n^4 (v - E_{\text{K}}) - g_{\text{L}} (v - E_{\text{L}}), \quad (2.2.5)$$

$$\frac{dh}{dt} = \frac{1}{\tau_h t_h(v)} (h_\infty(v) - h), \quad (2.2.6)$$

$$\frac{dn}{dt} = \frac{1}{\tau_n t_n(v)} (n_\infty(v) - n). \quad (2.2.7)$$

A careful nondimensionalization and comparison of the time scales, over the physiologically relevant range of  $v \in (-77 \text{ mV}, 50 \text{ mV})$ , reveals that  $v$ , not  $m$ , is the fastest variable in the HH equations [83]. From a mathematical point of view, therefore,  $v$  might be a more natural candidate for removal via QSSR than  $m$ , although this is not usually done. If we assume that  $v$  equilibrates instantaneously so that  $dv/dt = 0$ , then we can set the right hand side of equation (2.2.1) to zero and use this expression to write  $v$  as a function of the remaining variables:

$$\bar{v}(m, h, n) = \frac{I + g_{\text{Na}} m^3 h E_{\text{Na}} + g_{\text{K}} n^4 E_{\text{K}} + g_{\text{L}} E_{\text{L}}}{g_{\text{Na}} m^3 h + g_{\text{K}} n^4 + g_{\text{L}}}.$$

Substituting this expression into the remaining three equations, we get an alternative simplified form of the HH equations:

$$\frac{dm}{dt} = \frac{1}{\tau_m t_m(\bar{v})} (m_\infty(\bar{v}) - m), \quad (2.2.8)$$

$$\frac{dh}{dt} = \frac{1}{\tau_h t_h(\bar{v})} (h_\infty(\bar{v}) - h), \quad (2.2.9)$$

$$\frac{dn}{dt} = \frac{1}{\tau_n t_n(\bar{v})} (n_\infty(\bar{v}) - n). \quad (2.2.10)$$

It turns out that both variants of quasi-steady state reduction preserve the main features of the dynamics of the HH model. Fig. 2.1 shows the bifurcation diagram for the full HH model, along with the bifurcation diagrams for each simplified version of the model. In the full model, a branch of periodic orbits emanates from a subcritical Hopf bifurcation ( $\text{HB}_1$ ), goes through a sequence of fold bifurcations, and ultimately disappears in a supercritical Hopf bifurcation ( $\text{HB}_2$ ). In the simplified models the positions of the Hopf bifurcations move, and the amplitudes and frequencies of the periodic orbits change, but the basic structure, including criticality of the Hopf bifurcations, is unaffected by QSSR. Note that stability of the equilibrium and periodic solutions is not indicated on the figure. For each version of the model, the equilibrium solutions are unstable between the relevant pair of

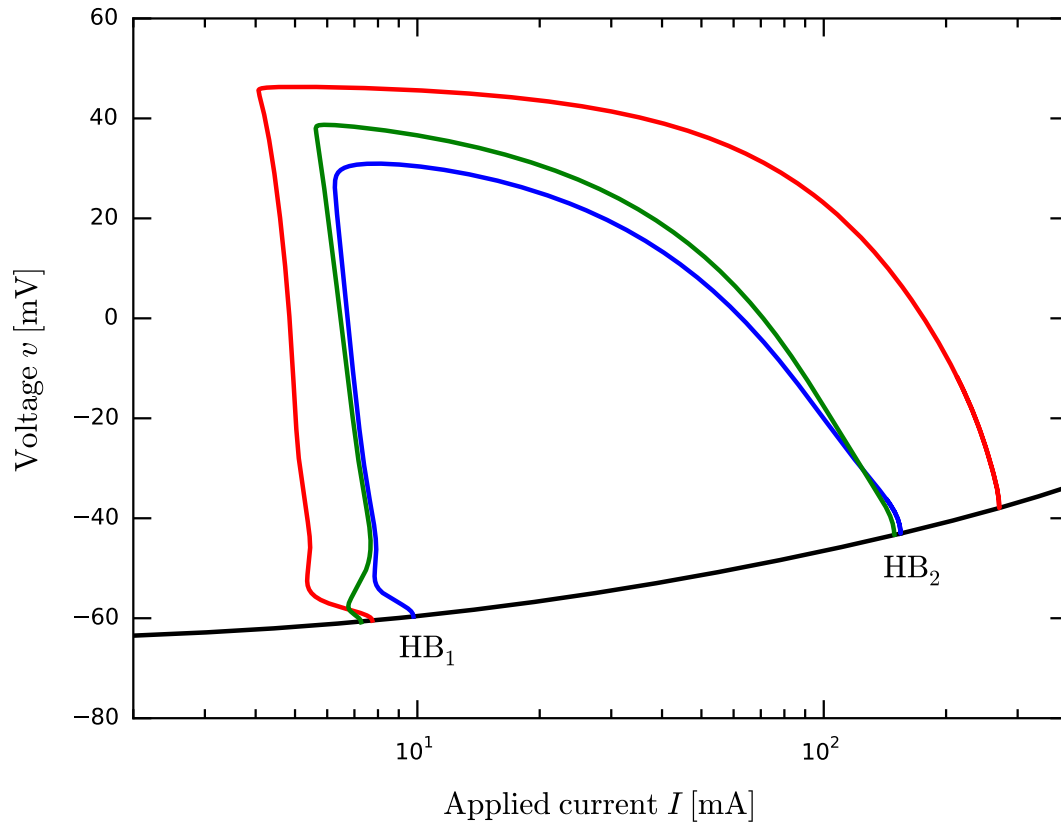


Figure 2.1: Partial bifurcation diagrams for various versions of the Hodgkin-Huxley model. The black curve shows the curve of equilibria, which is common to all versions of the model. Each coloured curve shows the maximum voltage for the periodic orbits in the corresponding model: orbits of the full model, equations (2.2.1)-(2.2.4), are shown in blue; orbits of the model with  $m$  removed, equations (2.2.5)-(2.2.7), are shown in red; and orbits of the model with  $v$  removed, equations (2.2.8)-(2.2.10), are shown in green. Stability of solutions is not indicated.

Hopf bifurcations and stable otherwise, while the branch of periodic solutions is stable from the rightmost Hopf through to the saddle-node of periodic orbits in the top left of each branch. Note that in the case that  $v$  is removed by QSSR, the corresponding curve in Fig. 2.1 was computed by integrating the simplified model and using the resulting  $m$ ,  $h$  and  $n$  values in the formula for  $\bar{v}$  to obtain a ‘time series’ for  $v$ ; the maximum value of this ‘time series’ for each choice of the bifurcation parameter  $I$  was then plotted, producing the curve shown.

Thus, the HH equations provide an example where QSSR does not significantly change the qualitative features of the dynamics of the model; either of the simplified models might be regarded as an acceptable approximation to the full model.

## 2.2.2 Hindmarsh-Rose model

Our second example is the Hindmarsh-Rose (HR) model [44], which was derived as a model of burst generating neurons. The HR equations are

$$\dot{v} = I - v^3 + 3v^2 + m - n, \quad (2.2.11)$$

$$\dot{m} = 1 - 5v^2 - m, \quad (2.2.12)$$

$$\dot{n} = \epsilon(4(v + 1.6) - n), \quad (2.2.13)$$

where  $v$  represents the membrane potential,  $m$  represents the combination of a recovery process and an inward current, and  $n$  is a slow adaptation current which is directed outwards. Once again, we use  $I$  as the main bifurcation parameter.

With the choice  $\epsilon = 0.001$ ,  $n$  evolves much more slowly than  $v$  and  $m$ , and so  $v$  and  $m$  are candidates for removal by QSSR. If we assume that  $m$  equilibrates rapidly, then  $m$  can be replaced by  $m_\infty(v) \equiv 1 - 5v^2$  in equation (2.2.11), yielding the following simplified system:

$$\dot{v} = I - v^3 - 2v^2 + 1 - n, \quad (2.2.14)$$

$$\dot{n} = \epsilon(4(v + 1.6) - n). \quad (2.2.15)$$

This system has significantly different dynamics to the full HR model, as Fig. 2.2 shows. In particular, the full system has four Hopf bifurcations (labelled HB<sub>1</sub> to HB<sub>4</sub> in Fig. 2.2), while the simplified system has just two (at almost the same values of  $I$  as HB<sub>1</sub> and HB<sub>2</sub> in the full system). As a result, the range of values of  $I$  for which there exist oscillatory solutions is significantly smaller in the reduced model compared with the full model. Also, in the full system the branches of periodic orbits created at HB<sub>1</sub> and HB<sub>2</sub> both terminate in homoclinic bifurcations whereas in the simplified system the branch of periodic orbits created at HB<sub>1</sub> terminates at HB<sub>2</sub>. We note that, as is well known, the full HR model has bursting oscillations for some parameter values. For the values of system parameters used in creating Fig. 2.2, bursting occurs for  $I$  in the range 1.26 mA to 3.25 mA, i.e., in the gap between the branches of periodic orbits starting at HB<sub>1</sub> and HB<sub>4</sub>. The bursting involves oscillations in the fast variables and is absent in the simplified system. Since the bursting does not arise via a Hopf bifurcation in this model, we do not investigate it further.

Note that while  $v$  and  $m$  are both fast compared with  $n$ , it is not feasible to remove  $v$  from the full HR model by assuming that  $v$  equilibrates to its quasi-steady state value.

This is because the equation for  $dv/dt$  is cubic in  $v$  and so it is not possible to replace  $v$  in (2.2.12) and (2.2.13) globally as a function of  $m$  and  $n$ .

In summary, the HR equations provide an example in which QSSR substantially alters the dynamics of the model; the simplified version of the HR equations has fewer Hopf bifurcations and a significantly smaller range of parameter values for which periodic solutions exist. The simplified model would not, therefore, normally be regarded as an adequate approximation to the full model.

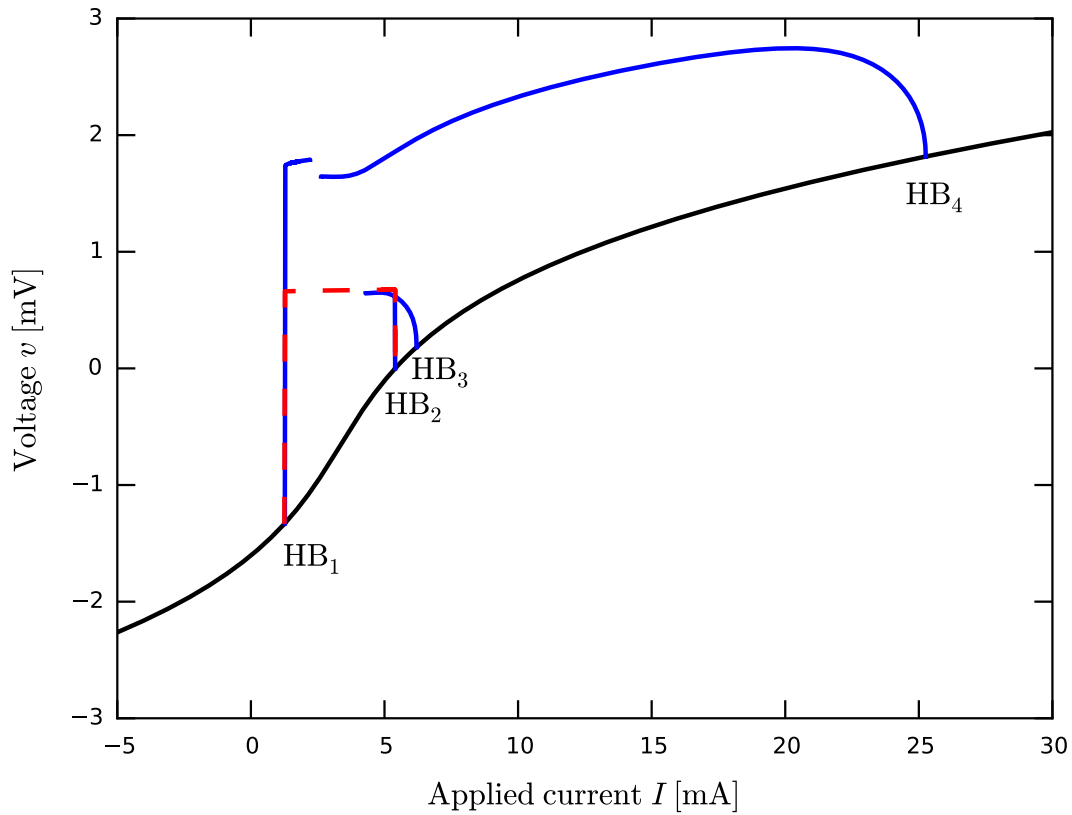


Figure 2.2: Partial bifurcation diagrams for two versions of the Hindmarsh-Rose equations. The black curve shows the curve of equilibria, which is common to both versions of the model. The coloured curves show the maximum voltages for the families of periodic orbits created in the Hopf bifurcations: orbits of the full model, equations (2.2.11)-(2.2.13), are shown in blue; orbits of the model with  $m$  removed, equations (2.2.14)-(2.2.15), are shown in red. Bursting oscillations can be found in the gap of the blue curves ( $I$  in the range of 1.26 mA to 3.25 mA). Stability of solutions is not indicated. Hopf bifurcations of the full model are labelled  $HB_1$ - $HB_4$ . The Hopf bifurcations of the simplified model occur very close to  $HB_1$  and  $HB_2$ . Bursting oscillations are absent in the simplified model.



### 2.2.3 Chay-Keizer model

The Chay-Keizer (CK) model is a minimal model for membrane potential oscillations in pancreatic  $\beta$ -cells [21]. We follow [51] and use the model in the form

$$C_m \frac{dv}{dt} = I - \left( g_{K, Ca} \frac{c}{K_d + c} + g_K n^4 \right) (v - E_K) - 2g_{Ca} m^3 h (v - E_{Ca}) - g_L (v - E_L), \quad (2.2.16)$$

$$\frac{dm}{dt} = \frac{1}{\tau_m t_m(v)} (m_\infty(v) - m), \quad (2.2.17)$$

$$\frac{dh}{dt} = \frac{1}{\tau_h t_h(v)} (h_\infty(v) - h), \quad (2.2.18)$$

$$\frac{dn}{dt} = \frac{1}{\tau_n t_n(v)} (n_\infty(v) - n), \quad (2.2.19)$$

$$\frac{dc}{dt} = f(-k_1 g_{Ca} m^3 h (v - E_{Ca}) - k_c c), \quad (2.2.20)$$

where  $v$  represents the membrane potential,  $m$  and  $h$  describe activation and inactivation of the calcium channel,  $n$  represents the gating variable of the voltage-gated potassium channel and  $c$  represents the intracellular calcium concentration.

The bifurcation diagram for the CK equations is shown in Fig. 2.3; the black curve shows the equilibrium solutions of the model and the dark blue curves show the maximum value of  $v$  for the periodic solutions. As can be seen, the model has two Hopf bifurcations, labelled  $HB_1$  and  $HB_2$ , which are connected by a family of periodic orbits.

From physiological considerations, the variables  $v$  and  $m$  might be regarded as faster than the variables  $h$ ,  $n$  and  $c$  and are thus candidates for removal by QSSR. We first consider the effect of removing  $m$  from the equations, by setting  $m = m_\infty(v)$ , which removes equation (2.2.17) and modifies equations (2.2.16) and (2.2.20). Doing so does not change the equilibrium solutions of the model, but does move the branch of periodic solutions as shown by the red curve in Fig. 2.3. We find that both Hopf bifurcations are preserved under this reduction, with  $HB_1$  staying in essentially the same place but  $HB_2$  moving somewhat to the right. A consequence is that the region for oscillatory solutions is larger and the amplitude of the resulting periodic orbits has increased for a wide range of the applied current.

It is also possible to remove  $v$  via QSSR, just as we did for the HH model earlier. Doing so produces a bifurcation diagram similar in many ways to the original CK model; there are still two Hopf bifurcations, but each produces a branch of periodic orbits that terminates in a homoclinic bifurcation. The rightmost branch is shown in green in Fig. 2.3. The

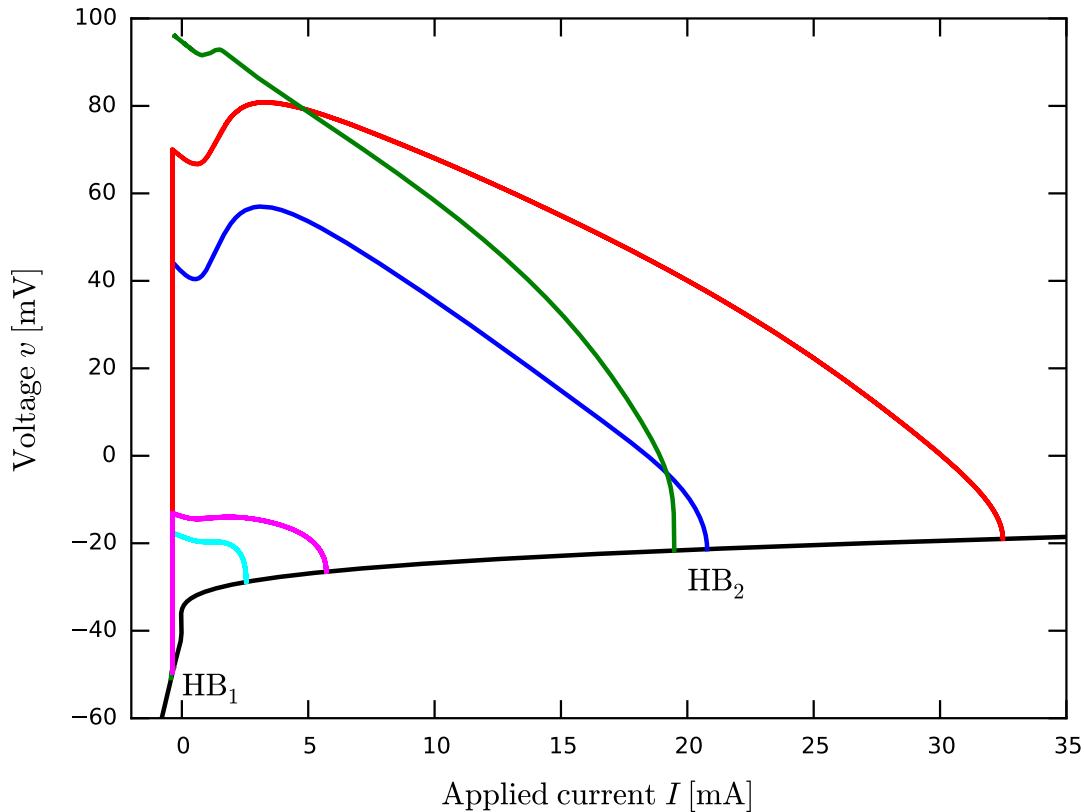


Figure 2.3: Partial bifurcation diagram for various versions of the Chay-Keizer model. The black curve is the curve of equilibria, and is the same for all versions of the model. Each coloured curve shows the maximum voltage for the periodic orbits in the corresponding model: blue corresponds to the original model, red when  $m$  is removed, green when  $v$  is removed, pink when  $h$  is removed and cyan when  $m$  and  $h$  are removed. The Hopf bifurcations of the full model are labelled  $HB_1$  and  $HB_2$ . The blue, red, magenta and cyan curves are all continuous and terminate on the left near the label  $HB_1$ ; near this point they lie on top of one another on the scale of this figure. The green curve has two disjoint pieces: the right one is clearly visible but the left one is a very short, lies near the label  $HB_1$  and is nearly invisible on the scale of this figure.

leftmost branch exists only in a very small interval of  $I$  near  $I = 0$  and is essentially invisible on the scale of Fig. 2.3. A plot of the periods of the orbits corresponding to the blue, red and green curves can be seen in Fig. 2.4, with corresponding frequencies shown in Fig. 2.5. The periods of the orbits on the green branches tend to infinity (or, frequencies tend to zero) at certain parameter values, suggesting that both branches terminate in homoclinic bifurcations. Even though the blue branch and the red branch are unbroken, the corresponding frequencies become very small in a small parameter interval, possibly because the corresponding periodic orbits pass near an equilibrium and are therefore near a homoclinic bifurcation. From Fig. 2.4 it can be seen that the periods of the orbits corresponding to the green, blue and red curves are very similar over a relatively large interval of parameters, suggesting that both of the simplified versions yield reasonable

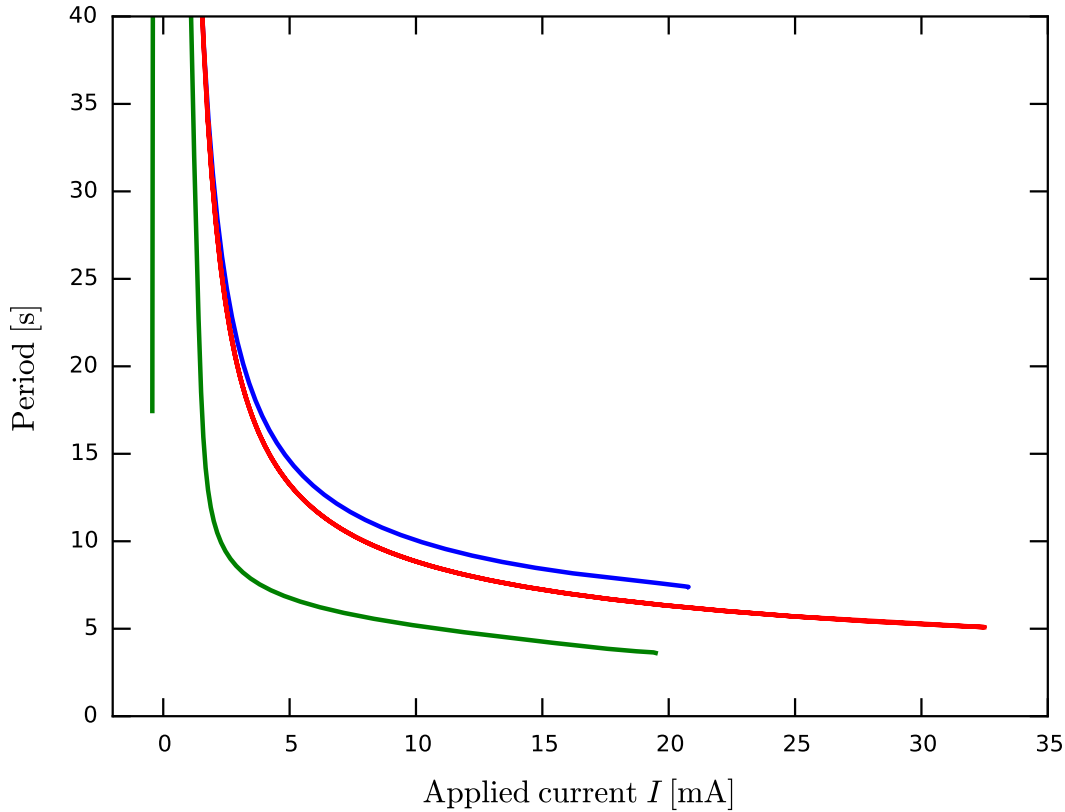


Figure 2.4: Partial bifurcation diagram for various versions of the Chay-Keizer model, showing the period of the periodic orbit branches for the full system (blue), the system with  $m$  removed (red) and the system with  $v$  removed (green). As in Fig. 2.3, the blue and red curves are continuous, but the left ends of both curves lie beyond the upper edge of this figure; see also Fig. 2.5. The green curve has two pieces, with one end of each piece lying beyond the upper edge of this figure.

approximations to the full system dynamics for this range of parameter values.

A different version of the model that has been studied in the literature is obtained by removing both  $m$  and  $h$  via QSSR [28, 35, 80]. Even though  $h$  is not as fast as  $v$  and  $m$ , it evolves faster than  $c$ , and, formally,  $h$  can be removed from the model by setting  $h = h_\infty$  just as if  $h$  were a fast variable. The resulting bifurcation diagram is shown by the black and pink curves in Fig. 2.3. It can be seen that the right Hopf bifurcation is moved significantly to the left, resulting in a smaller interval of parameters for which there exists a periodic solution. By checking the bifurcation diagram for the case where the  $m$  equation is retained but the  $h$  variable is removed by QSSR (pink curve in Fig. 2.3), it can be seen that most of the movement in the second Hopf bifurcation is due to this removal of  $h$ . It is perhaps not surprising that removing  $h$  by assuming that this variable equilibrates rapidly results in a significant change to the bifurcation diagram since  $h$  is known to be a slower variable than  $v$  and  $m$ .

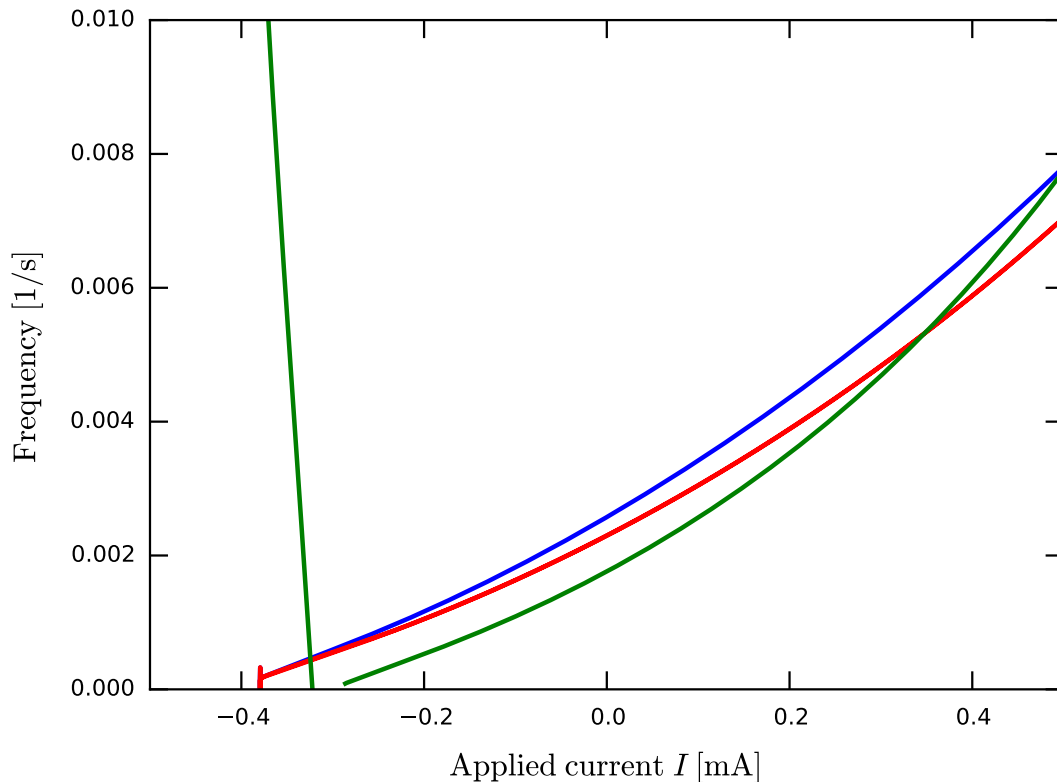


Figure 2.5: Frequencies of the periodic orbits shown in Fig. 2.4 near  $HB_1$ ; colours have the same meaning as in Fig. 2.4. The blue and red curves are continuous but there are two pieces of green curve.

In summary, the CK equations provide an example in which the use of QSSR to remove fast variables of the model preserves the Hopf bifurcations in the model but can move them a significant distance, hence altering the amplitude of the periodic orbits significantly. In one case, QSSR introduced a homoclinic bifurcation to the bifurcation diagram by disconnecting a previously continuous branch of periodic solutions. The CK equations also provide an example from the literature where a slower variable is removed from a model via QSSR, despite the fact that QSSR implicitly assumes that removed variables are fast compared with other variables.



# 3

## Results on quasi-steady-state reduction

The three examples discussed in the previous chapter show that applying QSSR to a model with multiple timescales sometimes leads to minimal disruption of the dynamics of the model and sometimes causes significant changes, such as removing oscillations from the dynamics or changing the amplitude of the oscillations by an order one amount. In this chapter we look in more mathematical detail at the process of QSSR. We show why QSSR works well if we are only concerned with equilibrium solutions of a model and investigate the effect of QSSR on oscillatory solutions by looking at the persistence and criticality of Hopf bifurcations under QSSR.

### 3.1 Preliminaries

We consider models that can be written in standard slow-fast form

$$\begin{aligned}\dot{x} &= \epsilon f(x, y, \alpha), \\ \dot{y} &= g(x, y, \alpha),\end{aligned}\tag{3.1.1}$$

where  $x \in \mathbb{R}^m$ ,  $y \in \mathbb{R}^n$ ,  $f$  and  $g$  are order one vector-valued functions,  $\alpha \in \mathbb{R}$  is a parameter, and  $\epsilon$  is a constant satisfying  $0 < \epsilon \ll 1$ . In such a system, the  $x$  variables evolve much slower than the  $y$  variables and the time scale separation is encoded by  $\epsilon$ . We note that in many models of biological systems, even if different processes are known to evolve on different timescales, it may not be possible to write down a model of the form of (3.1.1) in which there is explicit timescale separation of variables. Nevertheless, it is helpful to start by considering this relatively simple situation.

In QSSR, one or more of the fast variables is assumed to equilibrate instantaneously and is replaced in the model by functions of the remaining variables. Dividing the  $y$  variables into two groups,  $u \in \mathbb{R}^p$  and  $w \in \mathbb{R}^q$  with  $p + q = n$ , we can rewrite (3.1.1) as

$$\begin{aligned}\dot{x} &= \epsilon f(x, u, w, \alpha), \\ \dot{u} &= h(x, u, w, \alpha), \\ \dot{w} &= k(x, u, w, \alpha).\end{aligned}\tag{3.1.2}$$

QSSR can then be applied to remove the  $u$  variables using the following procedure. First it is assumed that  $u$  equilibrates instantaneously, which amounts to assuming

$$h(x, u, w, \alpha) = 0.\tag{3.1.3}$$

So long as the matrix given by

$$D_u h = \left( \frac{\partial h_i}{\partial u_j} \right)_{1 \leq i, j \leq p}\tag{3.1.4}$$

evaluated along  $h = 0$  is invertible, (3.1.3) can be reorganised to give  $u$  as a function of  $x$  and  $w$ , i.e.,  $u = \bar{u}(x, w, \alpha)$ . Here  $\frac{\partial h_i}{\partial u_j}$  is the derivative of the  $i$ -th component of  $h$  with respect to the  $j$ -th component of  $u$ . That this works is a consequence of the Implicit Function Theorem.

Replacing  $u$  in (3.1.2) by this expression for  $\bar{u}$  then yields the following simplified system:

$$\begin{aligned}\dot{x} &= \epsilon f(x, \bar{u}(x, w), w, \alpha), \\ \dot{w} &= k(x, \bar{u}(x, w), w, \alpha).\end{aligned}\tag{3.1.5}$$

It is helpful in what follows to also consider the system in the form

$$\begin{aligned}\dot{x} &= \epsilon f(x, u, w, \alpha), \\ \delta \dot{u} &= h(x, u, w, \alpha), \\ \dot{w} &= k(x, u, w, \alpha),\end{aligned}\tag{3.1.6}$$

where  $\delta$  is a constant with  $0 \leq \delta \leq 1$ . The original system (3.1.1) corresponds to choosing  $\delta = 1$ , and letting  $\delta$  decrease corresponds to speeding up the evolution of  $u$  relative to the other variables. In the limit  $\delta \rightarrow 0$ , Eq. (3.1.6) becomes the differential-algebraic system:

$$\begin{aligned}\dot{x} &= \epsilon f(x, u, w, \alpha), \\ 0 &= h(x, u, w, \alpha), \\ \dot{w} &= k(x, u, w, \alpha),\end{aligned}\tag{3.1.7}$$

which is equivalent to the simplified system (3.1.5). Hence, investigating the behaviour of (3.1.6) as  $\delta$  decreases to zero allows us to understand how the dynamics of (3.1.1) changes in response to QSSR.

## 3.2 The effect of QSSR on equilibria

In this section we show that equilibria cannot be created or destroyed by QSSR.

The set of equilibria of Eq. (3.1.2) is the set of points

$$\{(x, u, w) \in \mathbb{R}^{m+p+q} \mid f = h = k = 0\}.\tag{3.2.1}$$

The simplified system obtained by using QSSR evolves on the quasi-steady-state manifold (QSSM) given by

$$\text{QSSM} = \{(x, u, w) \in \mathbb{R}^{m+p+q} \mid h = 0\}.\tag{3.2.2}$$

Thus, equilibria of Eq. (3.1.2) are contained in the manifold defined by Eq. (3.2.2). This means that if  $(x^*, u^*, w^*)$  is an equilibrium of Eq. (3.1.2), then  $(x^*, w^*)$  is an equilibrium of Eq. (3.1.5).

Eq. (3.1.5) can be equivalently formulated as the differential-algebraic system (3.1.7), meaning that equilibria of Eq. (3.1.5) are equilibria of Eq. (3.1.7) and vice versa. An



equilibrium of Eq. (3.1.7) is a point  $(x^*, u^*, w^*)$  such that

$$\begin{aligned} 0 &= f(x^*, u^*, w^*, \alpha), \\ 0 &= h(x^*, u^*, w^*, \alpha), \\ 0 &= k(x^*, u^*, w^*, \alpha). \end{aligned}$$

These conditions also ensure that  $(x^*, u^*, w^*)$  is an equilibrium of the original system, Eq. (3.1.2).

Thus, we see that equilibria can be neither destroyed nor created by the process of QSSR. However, the stability of an equilibrium can change under QSSR. For instance, the stabilities of some equilibria close to Hopf bifurcations can change and consequently Hopf bifurcations can move or disappear under QSSR, as was seen in the examples in section 2.2.

### 3.3 Note on geometric singular perturbation theory and QSSR

When  $\epsilon = 0$  then equilibria of Eq. (3.1.2) lie on the manifold

$$S_0 = \{(x, u, w) \in \mathbb{R}^{m+p+q} \mid h = k = 0\}. \quad (3.3.1)$$

This manifold is known in geometric singular perturbation theory (GSPT) as the critical manifold for system (3.1.2). GSPT can be used to show that if  $S_0$  is globally attracting when  $\epsilon = 0$ , solutions of Eq. (3.1.2) with  $\epsilon$  small but non-zero will rapidly approach  $S_0$  and thereafter stay close to  $S_0$  [36].

On the other hand, when all fast variables of Eq. (3.1.2) are eliminated by QSSR, the simplified system evolves on  $S_0$ . Thus, if  $S_0$  is globally attracting when  $\epsilon = 0$ , the dynamics of Eq. (3.1.2) after the initial transient has subsided, is well captured by the simplified system (3.1.5) or, indeed, by a simplified system in which both  $u$  and  $w$  are removed by QSSR, i.e., using QSSR to remove fast variables from a multiple timescales model leads to good predictions about the long term behaviour of solutions if the critical manifold  $S_0$  is globally attracting [85]. However, critical manifolds need not be globally attracting, and, in particular, oscillatory solutions are often associated with critical manifolds that are not globally attracting.

### 3.4 Note on $\epsilon$ -dependence of the equations

In the previous section,  $\epsilon$  characterises the time-scale separation between slow and fast variables and does not explicitly appear in the functions  $f, h$  and  $k$ . The more general situation, which occurs frequently in physiological models, is that  $\epsilon$  occurs explicitly in one or more of these functions. In this case system (3.1.2) becomes

$$\begin{aligned}\dot{x} &= \epsilon f(x, u, w, \alpha, \epsilon), \\ \dot{u} &= h(x, u, w, \alpha, \epsilon), \\ \dot{w} &= k(x, u, w, \alpha, \epsilon).\end{aligned}\tag{3.4.1}$$

Most of the arguments of the previous sections are effectively unchanged by this modification. For instance, if we assume that  $u$  equilibrates instantaneously,

$$h(x, u, w, \alpha, \epsilon) = 0,\tag{3.4.2}$$

and the Jacobian matrix of  $h$  with respect to  $u$  (previously defined in Eq. (3.1.4)) is now dependent on  $\epsilon$ . However, provided that the matrix is invertible,  $u$  can be expressed as function of  $(x, w, \alpha, \epsilon)$  and the simplified system can be defined as before. Equilibria of Eq. (3.4.1) are generally dependent on  $\epsilon$ , but the argument of section 3.2 can be carried out as before to show that equilibria cannot be created or destroyed by QSSR. Furthermore, the equilibria of Eq. (3.1.2) are on the critical manifold,  $S_0$ , defined by Eq. (3.3.1) (with  $\epsilon = 0$ ), while the equilibria of Eq. (3.4.1) need not be on  $S_0$  but are within a distance of  $O(\epsilon)$  of  $S_0$ . Under the assumption that  $S_0$  is globally attracting with respect to the dynamics of Eq. (3.1.2) with  $\epsilon = 0$ , removal by QSSR of all fast variables of Eq. (3.4.1) leads to a simplified system that evolves on a manifold that is  $O(\epsilon)$  away from  $S_0$ ; this follows from Fenichel's theorem [36] and is just as was the case for systems of the form of Eq. (3.1.2).

### 3.5 The effect of QSSR on oscillatory solutions

We saw in section 2.2 that Hopf bifurcations may be removed from the dynamics by QSSR. Certain types of Hopf bifurcation might be expected *a priori* to be more robust under QSSR than others. For instance, Hopf bifurcations that involve just slow variables might be expected to persist under QSSR since it removes only fast variables, while Hopf bifurcations that involve only fast variables might disappear if those variables are the ones

removed by QSSR. An aim of this work, therefore, is to derive conditions under which a Hopf bifurcation will persist under QSSR.

We start with a categorization of Hopf bifurcations. We assume that Eq. (3.1.1) has a non-degenerate Hopf bifurcation for  $\alpha = \alpha_H$  and  $\epsilon \neq 0$ . More precisely, we assume that:

**A1:** there is a family of equilibria  $\mu(\alpha) = (x^*(\alpha), y^*(\alpha))$  for  $\alpha$  in a neighbourhood of  $\alpha_H$ , such that the Jacobian matrix has a pair of eigenvalues  $\lambda(\alpha) = \sigma(\alpha) \pm i\omega(\alpha)$  with  $\sigma(\alpha_H) = 0$  and  $\omega(\alpha_H) \in \mathbb{R} \setminus \{0\}$ ;

**A2:**  $\left. \frac{\partial \sigma}{\partial \alpha} \right|_{\alpha=\alpha_H} \neq 0$ ;

**A3:**  $l_1(\alpha_H) \neq 0$ , where  $l_1$  is the first Lyapunov coefficient [57].

The sign of  $l_1(\alpha_H)$  determines the criticality of a Hopf bifurcation and, hence, whether the branch of periodic orbits created in the Hopf bifurcation is stable or unstable.

Depending on the way  $\omega$  scales with variation of  $\epsilon$ , the Hopf bifurcation can be classified in the following way.

(i) If  $\omega = O(1)$ , the Hopf bifurcation involves only fast variables. This means that a corresponding Hopf bifurcation will be seen in the fast subsystem, which is the limit as  $\epsilon \rightarrow 0$  of Eq. (3.1.1).

(ii) If  $\omega = O(\epsilon)$ , the Hopf bifurcation involves only slow variables. More specifically, we can apply the change in variables  $\tau = \epsilon t$  to system (3.1.1) to obtain an equivalent system on the slow timescale,  $\tau$ :

$$\begin{aligned} \frac{\partial x}{\partial \tau} &= f(x, y, \alpha), \\ \epsilon \frac{\partial y}{\partial \tau} &= g(x, y, \alpha). \end{aligned} \tag{3.5.1}$$

If the Hopf bifurcation of the original system involves only slow variables, it will persist in the singular limit as  $\epsilon \rightarrow 0$  of this rescaled system.

(iii) If  $\omega = O(\sqrt{\epsilon})$  the Hopf bifurcation is a singular Hopf bifurcation [42, 55, 97] and involves both fast and slow variables. Singular Hopf bifurcations do not persist in the limit  $\epsilon \rightarrow 0$  of either Eq. (3.1.1) or Eq. (3.5.1). This means that both slow variables and fast variables are crucially involved in the bifurcation.

A Hopf bifurcation of type (i) can be eliminated under QSSR. An example of this was shown in subsection 2.2.2, where a fast Hopf bifurcation was removed from the HR model by QSSR. However, type (i) Hopf bifurcations are not necessarily eliminated by QSSR; whether or not this occurs depends on whether the variable(s) removed by QSSR are involved in the bifurcation. That this is the case is clear if one considers a system in which the fast variables involved in the Hopf bifurcation are decoupled from the fast variable(s) to be removed by QSSR.

Hopf bifurcations involving only slow variables (type (ii)) survive QSSR, at least for  $\epsilon$  sufficiently small. This is independent of how many and which fast variables are kept. The reason for the persistence of slow Hopf bifurcations is that, in the limit of  $\epsilon \rightarrow 0$ , the centre manifold associated with the Hopf bifurcation is contained within the linear subspace tangent to the QSSM at the Hopf bifurcation (the *tangent space* of the QSSM at that point). This ensures that the Hopf bifurcation is preserved in the simplified system, and it will not change from subcritical to supercritical or vice versa. Furthermore, for the same reason, the amplitude and frequency of the periodic orbit are not significantly affected by QSSR, at least sufficiently close to the Hopf bifurcation.

Singular Hopf bifurcations (type (iii)) persist under QSSR as long as the matrix given by Eq. (3.1.4), evaluated along  $h = 0$ , is invertible and  $\epsilon$  is sufficiently small; details of the proof of this statement are contained in section 3.6. The singular Hopf bifurcation may occur at a different parameter value in the simplified system compared to the original system. However, the new parameter value will be within  $O(\epsilon)$  in the simplified system.

We note that for Eq. (3.1.4) to be invertible at least one fast variable must remain after QSSR (see section 3.6), i.e., a singular Hopf bifurcation will be removed if all fast variables are eliminated by QSSR. This is consistent with the observation that a singular Hopf bifurcation involves both fast and slow variables, and so it cannot persist in the dynamics if all fast variables are removed.

**Remark** The persistence of a Hopf bifurcation under QSSR does not, in general, guarantee that the resulting branch of periodic orbits has the same amplitude as the corresponding branch in the original model. In fact, we have seen in the HH model and, more dramatically, in the CK model that the resulting branch of periodic orbits can have a significantly different amplitude. For the HH model, removal of  $m$  by QSSR leads to an increase in the amplitude of the periodic orbit at a given parameter value but removal of  $v$  does not have a significant effect (Fig. 2.1). For the CK model removal of  $m$  or  $v$  via QSSR also leads to an increase in the amplitude of the periodic orbits, but in this

case removal of  $v$  produces a much more significant change in amplitude (Fig. 2.3). We did not observe significant changes in the frequency in response to QSSR applied to HH and CK; see, e.g., Fig. 2.5 and the associated discussion in subsection 2.2.3. QSSR can also induce a change in criticality of a Hopf bifurcation, i.e., the stability of the branch of periodic orbits emanating from the Hopf bifurcation can in principle change after QSSR; this is discussed in subsection 3.6.2 in the context of singular Hopf bifurcations. We note, however, that in many cases, any change in criticality affects only a small portion of the branch of periodic solutions (because the branch is very steep near the Hopf bifurcation) and so may have little overall effect on the system dynamics.

## 3.6 Singular Hopf bifurcations and QSSR

### 3.6.1 Persistence of singular Hopf bifurcations

In this subsection we show that if a system has a singular Hopf bifurcation, the corresponding system obtained by removal of one or more fast variables via QSSR also has a singular Hopf bifurcation so long as the condition given in Assumption 2, below, is satisfied. The proof relies on the observation that a singular Hopf bifurcation is associated with a phenomenon called a *folded saddle-node type II* (FSNII) bifurcation [25, 42, 43]; we prove the persistence of FSNII bifurcations under QSSR and deduce the persistence of singular Hopf bifurcations. The proof relies on some concepts of GSPT, which we introduce in the following few paragraphs.

We begin with the system

$$\begin{aligned}\dot{x} &= \epsilon f(x, y, \alpha, \epsilon), \\ \dot{y} &= g(x, y, \alpha, \epsilon),\end{aligned}\tag{3.6.1}$$

where  $x \in \mathbb{R}^m$  and  $y \in \mathbb{R}^n$ . The dot indicates differentiation with respect to time,  $t$ , and the functions  $f$  and  $g$  are of order one. The parameter  $\alpha$  is the bifurcation parameter for the system, and is assumed to lie in some open interval  $\mathcal{I}$ . The parameter  $\epsilon$  encodes the time-scale separation between  $x$  and  $y$ ; we assume  $0 \leq \epsilon \ll 1$ .

In the case that  $\epsilon \neq 0$ , an equivalent formulation of system (3.6.1) can be obtained by

rescaling time, using  $t = \tau/\epsilon$ , to obtain

$$\begin{aligned}x' &= f(x, y, \alpha, \epsilon), \\ \epsilon y' &= g(x, y, \alpha, \epsilon),\end{aligned}\tag{3.6.2}$$

where the prime now indicates differentiation with respect to  $\tau$ .

In the limit  $\epsilon \rightarrow 0$ , system (3.6.1) gives rise to the *layer problem*

$$\begin{aligned}\dot{x} &= 0, \\ \dot{y} &= g(x, y, \alpha, 0),\end{aligned}\tag{3.6.3}$$

while system (3.6.2) yields the *reduced problem*

$$\begin{aligned}x' &= f(x, y, \alpha, 0), \\ 0 &= g(x, y, \alpha, 0).\end{aligned}\tag{3.6.4}$$

The phase space of the reduced problem is the *critical manifold*,  $S$ , defined by

$$S = \{(x, y) \mid g(x, y, \alpha, 0) = 0\}.\tag{3.6.5}$$

The critical manifold is also the set of equilibria of the layer problem.

The critical manifold may be folded with respect to one or more fast variables. Folds are located at the set of points,  $L \subset S$ , that satisfy

$$\text{rank}(D_y g)(x, y, \alpha, 0) = n - 1,\tag{3.6.6}$$

$$s \cdot [(D_{yy}^2 g)(x, y, \alpha, 0)(r, r)] \neq 0,\tag{3.6.7}$$

$$s \cdot [(D_x g)(x, y, \alpha, 0)] \neq 0,\tag{3.6.8}$$

where  $s$  and  $r$  are the left and right null vectors of  $(D_y g)(x, y, \alpha, 0)$  [95]. The matrices  $(D_y g)(x, y, \alpha, 0)$  and  $(D_x g)(x, y, \alpha, 0)$  are the matrices of first derivatives of  $g$  with respect to  $y$  and  $x$  respectively, and  $(D_{yy}^2 g)(x, y, \alpha, 0)$  is the tensor of second derivatives. Generically, the set of fold points separates sections (usually called *sheets* or *branches*) of the critical manifold that are of different stabilities with respect to the fast dynamics.

It is useful to compute the flow on the critical manifold. This is obtained by differentiating

the expression  $g = 0$  with respect to  $\tau$ , and then rewriting (3.6.4) in the form

$$\begin{aligned} x' &= f(x, y, \alpha, 0), \\ (-D_y g) \cdot y' &= ((D_x g) \cdot f)(x, y, \alpha, 0). \end{aligned} \quad (3.6.9)$$

This can be rearranged as

$$\begin{aligned} x' &= f(x, y, \alpha, 0), \\ -\det(D_y g) \cdot y' &= (\text{adj}(D_y g) \cdot (D_x g) \cdot f)(x, y, \alpha, 0), \end{aligned} \quad (3.6.10)$$

where  $\text{adj}(D_y g)$  is the adjoint matrix of  $(D_y g)$ . This flow is singular when  $\det(D_y g) = 0$  (e.g., on folds of  $S$ ); we remove the singularity by rescaling time by  $\det(D_y g)$ , yielding the *desingularized reduced problem*

$$\begin{aligned} \frac{dx}{dT} &= -(\det(D_y g) \cdot f)(x, y, \alpha, 0), \\ \frac{dy}{dT} &= (\text{adj}(D_y g) \cdot (D_x g) \cdot f)(x, y, \alpha, 0), \end{aligned} \quad (3.6.11)$$

where time has been rescaled so that  $dT = -\det(D_y g)(x, y, \alpha, 0) \cdot d\tau$ .

An equilibrium point of the desingularised reduced system that also lies on the fold curve  $L$  is called a *folded singularity*. Thus,  $(x_F, y_F) \in L$  is a folded singularity when  $\alpha = \alpha_F$  if

$$(\text{adj}(D_y g) \cdot (D_x g) \cdot f)(x_F, y_F, \alpha_F, 0) = 0. \quad (3.6.12)$$

The equation (3.6.12) represents a single condition, since  $\text{adj}(D_y g)$  has rank one along  $L$ .

The eigenvalues of the Jacobian of Eq. (3.6.11) determine the type of folded singularity; a folded singularity is a *folded saddle-node* if there is just one non-zero eigenvalue [95]. A folded singularity is a *type II folded saddle-node* if it has the additional property that  $f(x_F, y_F, \alpha_F, 0) = 0$ .

In order to study the effect of QSSR on the persistence of singular Hopf bifurcations it is convenient to split the fast variables of the model by writing  $y = \begin{pmatrix} u \\ w \end{pmatrix}$ . Here we assume that  $u \in \mathbb{R}^{n-1}$  and  $w \in \mathbb{R}$ . This simplifies the notation in the following proof. A proof for  $u \in \mathbb{R}^p$  and  $w \in \mathbb{R}^q$  works using the same argumentation, albeit with more indices.

Consider the system in the form

$$\begin{aligned}\dot{x} &= \epsilon f(x, u, w, \alpha, \epsilon), \\ \dot{u} &= h(x, u, w, \alpha, \epsilon), \\ \dot{w} &= k(x, u, w, \alpha, \epsilon),\end{aligned}\tag{3.6.13}$$

where  $g = \begin{pmatrix} h \\ k \end{pmatrix}$ . We will assume that  $u$  reaches quasi-steady state rapidly, so that  $\dot{u}$  rapidly approaches 0 and we can approximate the differential equation for  $u$  by the algebraic equation  $h = 0$ . The following generic condition on  $h$  then allows us to remove  $u$  from Eq. (3.6.13).

**Assumption 1**  $D_u h$  evaluated at points such that  $h(x, u, w, \alpha, 0) = 0$  is invertible, for all  $\alpha \in \mathcal{I}$ , where  $\mathcal{I}$  is an open interval.

Under Assumption 1,  $u$  can be written as a function of the remaining variables and the parameters, i.e.,  $u = \bar{u}(x, w, \alpha, \epsilon)$  for some function  $\bar{u}$  and for  $\epsilon$  sufficiently small. Substituting this into Eq. (3.6.13) yields

$$\begin{aligned}\dot{x} &= \epsilon f(x, \bar{u}(x, w, \alpha, \epsilon), w, \alpha, \epsilon) \equiv \epsilon F(x, w, \alpha, \epsilon), \\ \dot{w} &= k(x, \bar{u}(x, w, \alpha, \epsilon), w, \alpha, \epsilon) \equiv K(x, w, \alpha, \epsilon).\end{aligned}\tag{3.6.14}$$

The desingularized reduced system corresponding to Eq. (3.6.14) can be obtained by the process outlined above, and is

$$\begin{aligned}\frac{dx}{d\tilde{T}} &= -(D_w K \cdot F)(x, w, \alpha, 0), \\ \frac{dw}{d\tilde{T}} &= (D_x K \cdot F)(x, w, \alpha, 0),\end{aligned}\tag{3.6.15}$$

where time has been rescaled so that  $d\tilde{T} = -(D_w K)(x, w, \alpha, 0)d\tau$ , and  $\tau$  is related to  $t$  just as earlier. Note that we have used  $\text{adj}(D_w K) = 1$  and  $\det(D_w K) = D_w K$ , since  $D_w K$  is a scalar.

We make a further assumption about system (3.6.13).

**Assumption 2** *The critical manifold of system (3.6.13) is locally folded for all  $\alpha \in \mathcal{I}$ , i.e., conditions (3.6.6)-(3.6.8) are satisfied.*



We now show that certain properties of system (3.6.13) are inherited by (3.6.14).

**Proposition 1** *If Assumptions 1 and 2 hold for system (3.6.13), then the critical manifold of system (3.6.14) is locally folded for all  $\alpha \in \mathcal{I}$ .*

**Proof of Proposition 1** The Jacobian of the fast subsystem of (3.6.13) is

$$D_y g(x, y, \alpha, 0) = \begin{pmatrix} D_u h & D_w h \\ D_u k & D_w k \end{pmatrix} (x, y, \alpha, 0). \quad (3.6.16)$$

From Assumption 2 it follows that the Jacobian has a zero eigenvalue for all  $(x, y) \in L$ . Assumption 1 guarantees the regularity of the submatrix  $D_u h$ . Using the Leibniz formula for determinants then yields

$$\det(D_y g) = \det(D_u h) \det(D_w k - D_u k (D_u h)^{-1} D_w h) = 0 \quad (3.6.17)$$

for  $(x, y) \in L$ , i.e.,

$$\det(D_w k - D_u k (D_u h)^{-1} D_w h) = 0 \quad (3.6.18)$$

or

$$D_w k - D_u k (D_u h)^{-1} D_w h = 0 \quad (3.6.19)$$

since the matrix in (3.6.18) is just a scalar.

To prove Proposition 1, we need to show that equivalent conditions to Eq. (3.6.6)-(3.6.8) are satisfied for system (3.6.14). The Jacobian of the fast subsystem of Eq. (3.6.14) is

$$\begin{aligned} D_w K &= D_u k D_w \bar{u} + D_w k \\ &= -D_u k (D_u h)^{-1} D_w h + D_w k, \end{aligned} \quad (3.6.20)$$

since  $h = 0$  implies that

$$D_w h + D_u h D_w \bar{u} = 0, \quad (3.6.21)$$

and, hence, that

$$D_w \bar{u} = -(D_u h)^{-1} D_w h. \quad (3.6.22)$$

Comparing (3.6.19) and (3.6.20), we see that  $D_w K$  is zero at points on  $L$  and thus the zero eigenvalue from (3.6.13) is preserved under QSSR, i.e., condition (3.6.6) is satisfied for Eq. (3.6.14).

Now we turn to condition (3.6.7). If  $s$  is the left null vector of  $(D_y g)(x, y, \alpha, 0)$  we write

$s = (s_1, s_2)$  where  $s_1$  is a row vector of dimension  $n - 1$  and  $s_2 \in \mathbb{R}$ . Then

$$\begin{pmatrix} s_1 & s_2 \end{pmatrix} \begin{pmatrix} D_u h & D_w h \\ D_u k & D_w k \end{pmatrix} = 0 \quad (3.6.23)$$

from which it follows, using Assumption 1, that

$$s = \left( -s_2 D_u k (D_u h)^{-1} \quad s_2 \right). \quad (3.6.24)$$

Similarly, if  $r$  is the right null vector of  $D_y g(x, y, \alpha, 0)$  we write

$$r = \begin{pmatrix} r_1 \\ r_2 \end{pmatrix}$$

where  $r_1$  is a column vector of dimension  $n - 1$  and  $r_2 \in \mathbb{R}$ , and find that

$$r = \begin{pmatrix} -(D_u h)^{-1} D_w h & r_2 \\ & r_2 \end{pmatrix}. \quad (3.6.25)$$

We see from Eq. (3.6.24) that  $s_2 \neq 0$ ; otherwise  $s$  would be the zero vector and would not be a valid eigenvector of  $(D_y g)$ . By the same argument, we see from Eq. (3.6.25) that  $r_2$  is non-zero. A straightforward calculation then shows that condition (3.6.7) is satisfied for (3.6.13) if and only if

$$\begin{aligned} & D_{ww}^2 k - 2D_{wu}^2 k \xi + D_{uu}^2 k \xi^2 \\ & - \zeta D_{ww}^2 h + 2\zeta D_{wu}^2 h \xi - \zeta D_{uu}^2 h \xi^2 \neq 0, \end{aligned} \quad (3.6.26)$$

where  $\xi = (D_u h)^{-1} D_w h$  and  $\zeta = D_u k (D_u h)^{-1}$ . Note that we use the fact that  $s_2$  and  $r_2$  are nonzero here.

A similar calculation shows an analogous result for Eq. (3.6.14), i.e.,

$$\hat{s} \cdot \left[ (D_{ww}^2 K)(x, w, \alpha, 0)(\hat{r}, \hat{r}) \right] \neq 0$$

if and only if Eq. (3.6.26) is satisfied, where  $\hat{s}$  and  $\hat{r}$  are the left and right null vectors of  $(D_w K)$ . Note that, because of the dimensions involved,  $\hat{s}$  and  $\hat{r}$  are scalar and therefore necessarily non-zero. Thus we conclude that if (3.6.7) holds for (3.6.13) then the equivalent condition holds for (3.6.14).

We now check condition (3.6.8). Condition (3.6.8) written in terms of  $h$  and  $k$  for (3.6.13)

is

$$s \cdot [(D_x g)(x, y, \alpha, 0)] = s_2 (-D_u k (D_u h)^{-1} D_x h + D_x k) \neq 0. \quad (3.6.27)$$

For system (3.6.14), the condition equivalent to (3.6.8) is

$$\hat{s} \cdot (D_x K) \neq 0. \quad (3.6.28)$$

Since  $\hat{s}$  is scalar and since  $h = 0$  implies that  $D_x \bar{u} = -(D_u h)^{-1} D_x h$

$$D_x K = D_x k + D_u k D_x \bar{u} = D_x k - D_u k (D_u h)^{-1} D_x h \neq 0. \quad (3.6.29)$$

Equation (3.6.29) is equivalent to condition (3.6.27). Hence, if (3.6.8) is fulfilled for Eq. (3.6.13) then the equivalent condition is also satisfied for Eq. (3.6.14). This completes the proof of Proposition 1.

We now make another assumption about the dynamics of the original system (3.6.1), or, more specifically, about the dynamics of (3.6.11), the desingularized reduced system corresponding to (3.6.1).

**Assumption 3** *System (3.6.11) has a folded saddle-node type II singularity,  $(x_F, y_F)$ , for some  $\alpha_F \in \mathcal{I}$ .*

**Proposition 2** *If Assumptions 1, 2 and 3 are satisfied for system (3.6.11) then system (3.6.15) has a folded saddle-node singularity of type II for the same parameter value,  $\alpha_F \in \mathcal{I}$ , as in Assumption 3.*

**Proof of Proposition 2** Using the notation  $(x_F, y_F) = (x_F, u_F, w_F)$ , it follows from Assumption 1 that  $u_F = \bar{u}(x_F, w_F, \alpha_F, 0)$ . Since  $(x_F, y_F)$  is a true equilibrium of system (3.6.1) for  $\alpha_F$ , it follows from section 3.2 that  $(x_F, w_F)$  is an equilibrium of system (3.6.14) for  $\alpha_F$ . Furthermore, Proposition 1 guarantees that the critical manifold of system (3.6.14) is locally folded at  $(x_F, w_F)$  for the parameter value  $\alpha_F$ .

In general, equilibria of system (3.6.14) do not inherit their stability from their counterparts in system (3.6.1). Thus, it is not immediately apparent that  $(x_F, w_F)$  is a folded saddle-node type II singularity of the desingularized reduced system (3.6.15). Here we show that  $(x_F, w_F)$  is indeed of folded saddle-node type in system (3.6.15) at  $\alpha_F$ .

The desingularized reduced system of system (3.6.1) is (3.6.11), which can be expressed

using  $u$  and  $w$  coordinates as

$$\frac{dx}{dT} = (-\det(D_y g) \cdot f)(x, u, w, \alpha, 0), \quad (3.6.30)$$

$$\frac{d}{dT} \begin{pmatrix} u \\ w \end{pmatrix} = \left( \text{adj} \begin{pmatrix} D_u h & D_w h \\ D_u k & D_w k \end{pmatrix} \begin{pmatrix} D_x h \\ D_x k \end{pmatrix} \cdot f \right) (x, u, w, \alpha, 0). \quad (3.6.31)$$

Equations (3.6.30) and (3.6.31) describe the dynamics on the  $m$ -dimensional critical manifold. Using  $D_w K = D_w k - D_u k (D_u h)^{-1} D_w h$  and Eq. (3.6.17), the first equation becomes

$$\frac{dx}{dT} = (-\det(D_u h) \cdot (D_w K) \cdot f)(x, u, w, \alpha, 0). \quad (3.6.32)$$

The next step is to evaluate the adjoint matrix, to compare Eq. (3.6.31) with the second equation of system (3.6.15). We use LDU decomposition to factorize the adjoint matrix to

$$\text{adj} \begin{pmatrix} D_u h & D_w h \\ D_u k & D_w k \end{pmatrix} = \text{adj} \left( \begin{pmatrix} \mathbb{1} & 0 \\ D_u k (D_u h)^{-1} & \mathbb{1} \end{pmatrix} \begin{pmatrix} D_u h & 0 \\ 0 & D_w K \end{pmatrix} \begin{pmatrix} \mathbb{1} & (D_u h)^{-1} D_w h \\ 0 & \mathbb{1} \end{pmatrix} \right), \quad (3.6.33)$$

where  $\mathbb{1}$  is the identity matrix of appropriate dimension. This is equal to the product of adjoint matrices in reverse order

$$\text{adj} \begin{pmatrix} D_u h & D_w h \\ D_u k & D_w k \end{pmatrix} = \begin{pmatrix} \mathbb{1} & -(D_u h)^{-1} D_w h \\ 0 & \mathbb{1} \end{pmatrix} \begin{pmatrix} D_w K & \det(D_u h) (D_u h)^{-1} & 0 \\ 0 & \det(D_u h) \end{pmatrix} \begin{pmatrix} \mathbb{1} & 0 \\ -D_u k (D_u h)^{-1} & \mathbb{1} \end{pmatrix}. \quad (3.6.34)$$

The equation for  $w$  is then given by

$$\frac{dw}{dT} = (\det(D_u h) \cdot (D_x k - D_u k (D_u h)^{-1} D_x h) \cdot f)(x, u, w, \alpha, 0). \quad (3.6.35)$$

The desingularized reduced system after QSSR is given by Eq. (3.6.15) and using the definition of  $F(x, w, \alpha, 0) = f(x, u, w, \alpha, 0)|_{u=\bar{u}}$  can be written as

$$\begin{aligned} \frac{dx}{d\tilde{T}} &= (- (D_w K) \cdot f)(x, u, w, \alpha, 0)|_{u=\bar{u}}, \\ \frac{dw}{d\tilde{T}} &= ((D_x k - D_u k (D_u h)^{-1} D_x h) \cdot f)(x, u, w, \alpha, 0)|_{u=\bar{u}}. \end{aligned} \quad (3.6.36)$$

Comparing equations (3.6.32) and (3.6.35), restricted to  $u = \bar{u}(x, w, \alpha, 0)$ , with system (3.6.36) and noting that  $dT = \det(D_u h) \cdot d\tilde{T}$ , we see that they describe identical dynamics

on the respective critical manifolds. This means that, when each is projected to the appropriate critical manifold, the flow of system (3.6.11) is identical to the flow of system (3.6.15). Since folded singularities are characterised according to their linearisation on the critical manifold, it follows that the folded saddle-node equilibrium of system (3.6.11) corresponds to a folded saddle-node equilibrium of system (3.6.15). This completes the proof of Proposition 2.

The existence of a folded saddle-node type II singularity is generically associated with the existence of a singular Hopf bifurcation [25, 42]. Thus we have a corollary to Proposition 2:

**Corollary** *If Assumptions 1, 2 and 3 are satisfied for system (3.6.11) then (3.6.15) has a singular Hopf bifurcation within  $O(\epsilon)$  of  $\alpha_F$ .*

One subtlety worth mentioning is that the singular Hopf bifurcation in system (3.6.14) does not necessarily occur at the same parameter value as in system (3.6.1). Proposition 2 guarantees that the desingularized reduced system (3.6.15), has a folded-saddle node type II bifurcation at the same parameter value as system (3.6.11), but the singular Hopf bifurcation is only within  $O(\epsilon)$  of the folded-saddle node type II bifurcation and can occur at different parameter values in system (3.6.14) compared to system (3.6.1).

The persistence of a singular Hopf bifurcation in system (3.6.14) does not mean that the onset of oscillations is unchanged by QSSR. It is evident from the examples discussed in 2.2 that even when Hopf bifurcations persist under QSSR, the amplitude and frequency of the oscillations near the bifurcation can change significantly. Less evident is that the criticality of the Hopf bifurcation, and hence the stability of the branch of oscillations at the onset, can also change under QSSR.

### 3.6.2 Criticality of singular Hopf bifurcations

The criticality of a Hopf bifurcation is determined by the sign of the first Lyapunov coefficient [57]. In the following, we show the general derivation of the criticality of a Hopf bifurcation and then make an argument of how the criticality of a singular Hopf bifurcation may be affected by QSSR. The argument for the change in criticality of QSSR is inspired by the argument given in [97]. The authors of [97] show that the criticality

of a Hopf bifurcation that exists in the full model and persists in the layer problem can be different in the full model compared to the layer problem. We focus on changes in criticality of singular Hopf bifurcations in slow-fast systems of the form Eq. (3.6.13) as fast variables are removed.

Consider the system

$$\dot{z} = G(z, \mu), \quad (3.6.37)$$

where  $z \in \mathbb{R}^N$  and  $\mu \in \mathbb{R}^K$ . Under the assumption that Eq. (3.6.37) has a Hopf bifurcation at  $z = 0$  and  $\mu = \mu_H$ , the Taylor expansion around  $(0, \mu_H)$  is

$$G(z, \mu_H) = Az + \frac{1}{2}B(z, z) + \frac{1}{6}C(z, z, z) + O(\|z^4\|), \quad (3.6.38)$$

where  $A$  is the Jacobian matrix evaluated at  $(0, \mu_H)$ , and  $B(x, y)$  and  $C(x, y, z)$  are the following multilinear forms:

$$B_j(x, y) = \sum_{k,l=1}^N \frac{\partial^2 G_j(\xi, \mu_H)}{\partial \xi_k \partial \xi_l} \Big|_{\xi=0} x_k y_l, \quad (3.6.39)$$

$$C_j(x, y, z) = \sum_{k,l,r=1}^N \frac{\partial^3 G_j(\xi, \mu_H)}{\partial \xi_k \partial \xi_l \partial \xi_r} \Big|_{\xi=0} x_k y_l z_r, \quad (3.6.40)$$

for  $j = 1, 2, \dots, N$ . At  $(0, \mu_H)$ ,  $A$  has two complex conjugate eigenvalues  $\pm i\omega$ . We denote the eigenvector corresponding to  $i\omega$  by  $q$ , and the adjoint eigenvector by  $p$ , so that

$$Aq = i\omega q, \quad (3.6.41)$$

$$A^T p = -i\omega p. \quad (3.6.42)$$

The first Lyapunov coefficient is

$$l_1 = \frac{1}{2\omega} \operatorname{Re} [\langle p, C(q, q, \bar{q}) \rangle - 2\langle p, B(q, A^{-1}B(q, \bar{q})) \rangle + \langle p, B(\bar{q}, (2i\omega \mathbb{1} - A)^{-1}B(q, q)) \rangle]. \quad (3.6.43)$$

where  $\langle \cdot, \cdot \rangle$  denotes the usual inner product. The sign of  $l_1$  determines the criticality of the Hopf bifurcation and, hence, the stability of the resulting periodic orbit at the onset of the oscillations.

Without loss of generality we assume that system (3.6.13) has a singular Hopf bifurcation at  $(x, u, w) = (0, 0, 0)$  for  $\alpha = \alpha_H$ , and that Assumptions 1, 2 and 3 from the previous subsection are satisfied so that the Hopf bifurcation persists in the reduced system (3.6.14).

In order to get comparable expressions for the eigenvectors  $q$  and  $p$ , we revert to system (3.1.6). For  $\delta = 1$  system (3.1.6) is the same as system (3.6.13); in the limit  $\delta \rightarrow 0$  it represents Eq. (3.6.14) embedded in the  $(m+n)$ -dimensional phase space of Eq. (3.6.13). That means it follows the dynamics of the system (3.6.14), restricted to the quasi-steady-state manifold (as defined in Eq. (3.2.2)), in the phase space of the full system.

As mentioned in the last subsection, the singular Hopf bifurcation in Eq. (3.6.14) does not necessarily occur at the origin nor at the same value of the parameter,  $\alpha$ , as in Eq. (3.6.13). We assume that the singular Hopf bifurcation in Eq. (3.1.6) for  $\delta \leq 1$  occurs at a position in phase space given by  $\tilde{o}(\delta)$  for the parameter value  $\tilde{\alpha}_H(\delta)$ .

In the last subsection we have seen that the folded saddle-node singularity of type II occurs in system (3.6.14) at the same parameter value  $\alpha_F$  and at the same location in phase space as in system (3.6.13). It follows from the corollary in the previous subsection that

$$\|\tilde{o}(\delta)\| = O(\epsilon), \quad (3.6.44)$$

$$\tilde{\alpha}_H(\delta) = \alpha_H + O(\epsilon). \quad (3.6.45)$$

This means that  $\tilde{o}(\delta)$  is within  $O(\epsilon)$  of the origin, and the parameter value  $\tilde{\alpha}_H(\delta)$  is within  $O(\epsilon)$  of  $\alpha_H$ .

Zhang et al. [97] present an argument that the criticality of a Hopf bifurcation in a slow-fast system can be different in the layer problem compared to the full slow-fast problem. The argument is based on evaluating Eq. (3.6.43) for the layer problem and the full slow-fast problem and comparing the individual summands. If the summands differ by  $O(1)$ , the resulting first Lyapunov coefficient may also differ by  $O(1)$ . We follow this procedure and compare the three summands for  $\delta = 1$  and  $\delta \rightarrow 0$ . From this, we deduce that the criticality of a singular Hopf bifurcation may change under QSSR. We give two examples where a change of criticality occurs at the end of the subsection.

The eigenvector  $q$  satisfies

$$\begin{pmatrix} \epsilon D_x f - i\tilde{\omega}\mathbb{1} & \epsilon D_u f & \epsilon D_w f \\ \frac{1}{\delta} D_x h & \frac{1}{\delta} D_u h - i\tilde{\omega}\mathbb{1} & \frac{1}{\delta} D_w h \\ D_x k & D_u k & D_w k - i\tilde{\omega} \end{pmatrix} \begin{pmatrix} q_1 \\ q_2 \\ q_3 \end{pmatrix} (\tilde{o}, \tilde{\alpha}_H, \epsilon) = 0 \quad (3.6.46)$$

with  $q_1 \in \mathbb{C}^m$ ,  $q_2 \in \mathbb{C}^{n-1}$ ,  $q_3 \in \mathbb{C}$  and where  $\mathbb{1}$  is the identity matrix of appropriate dimension.

Note that the value of  $\tilde{\omega}$  may also change as  $\delta$  changes. The change in  $\tilde{\omega}$  is of  $O(\epsilon)$  since  $\tilde{\omega}$  is the magnitude of the complex conjugate eigenvalues at a singular Hopf bifurcation (see section (3.5)).

Eq. (3.6.46) is equal to

$$\begin{pmatrix} \mathbb{1} & 0 & 0 \\ 0 & \frac{1}{\delta} \cdot \mathbb{1} & 0 \\ 0 & 0 & 1 \end{pmatrix} \begin{pmatrix} \epsilon D_x f - i\tilde{\omega} \mathbb{1} & \epsilon D_u f & \epsilon D_w f \\ D_x h & D_u h - i\delta \tilde{\omega} \mathbb{1} & D_w h \\ D_x k & D_u k & D_w k - i\tilde{\omega} \end{pmatrix} \begin{pmatrix} q_1 \\ q_2 \\ q_3 \end{pmatrix} (\tilde{\omega}, \tilde{\alpha}_H, \epsilon) = 0. \quad (3.6.47)$$

For  $\delta > 0$  the matrix in front is regular and, hence, invertible. For  $\delta > 0$  Eq. (3.6.46) is equivalent to

$$\begin{pmatrix} \epsilon D_x f - i\tilde{\omega} \mathbb{1} & \epsilon D_u f & \epsilon D_w f \\ D_x h & D_u h - i\delta \tilde{\omega} \mathbb{1} & D_w h \\ D_x k & D_u k & D_w k - i\tilde{\omega} \end{pmatrix} \begin{pmatrix} q_1 \\ q_2 \\ q_3 \end{pmatrix} (\tilde{\omega}, \tilde{\alpha}_H, \epsilon) = 0. \quad (3.6.48)$$

The matrix in Eq. (3.6.48) is not invertible, and has determinant zero. A consequence is that small changes in coefficients do not necessarily lead to small changes in the solution. Hence, the eigenvector  $q$  for  $\delta < 1$  is not necessarily a small perturbation of the eigenvector  $q$  at  $\delta = 1$ . A similiar argument can be made for the right eigenvector  $p$ .

In order to compare terms in Eq. (3.6.43) for the singular Hopf bifurcation of system (3.6.14) with the singular Hopf bifurcation in (3.6.13), it is useful to obtain an expression for the eigenvector  $p$ :

$$\begin{pmatrix} \epsilon D_x f + i\tilde{\omega} \mathbb{1} & \frac{1}{\delta} D_x h & D_x k \\ \epsilon D_u f & \frac{1}{\delta} D_u h + i\tilde{\omega} \mathbb{1} & D_u k \\ \epsilon D_w f & \frac{1}{\delta} D_w h & D_w k + i\tilde{\omega} \end{pmatrix} \begin{pmatrix} p_1 \\ p_2 \\ p_3 \end{pmatrix} (\tilde{\omega}, \tilde{\alpha}_H, \epsilon) = 0. \quad (3.6.49)$$

The second row yields

$$\left( \epsilon D_u f \cdot p_1 + \left( \frac{1}{\delta} D_u h + i\omega_\delta \mathbb{1} \right) \cdot p_2 + D_u k \cdot p_3 \right) (\tilde{\omega}, \tilde{\alpha}_H, \epsilon) = 0. \quad (3.6.50)$$

For  $\delta > 0$ , the matrix  $\left( \frac{1}{\delta} D_u h + i\omega_\delta \mathbb{1} \right)$  is invertible. It follows that

$$p_2 = -\delta (D_u h + i\delta \tilde{\omega} \mathbb{1})^{-1} (\epsilon D_u f \cdot p_1 + D_u k \cdot p_3). \quad (3.6.51)$$



The multilinear forms defined above become:

$$\begin{aligned}
B_1(x, y) &= \sum_{k,l=1}^{m+n} \epsilon \frac{\partial^2 f(\xi, \tilde{\alpha}_H, \epsilon)}{\partial \xi_k \partial \xi_l} \Big|_{\xi=\tilde{\omega}} x_k y_l, \\
B_2(x, y) &= \sum_{k,l=1}^{m+n} \frac{1}{\delta} \frac{\partial^2 h(\xi, \tilde{\alpha}_H, \epsilon)}{\partial \xi_k \partial \xi_l} \Big|_{\xi=\tilde{\omega}} x_k y_l, \\
B_3(x, y) &= \sum_{k,l=1}^{m+n} \frac{\partial^2 k(\xi, \tilde{\alpha}_H, \epsilon)}{\partial \xi_k \partial \xi_l} \Big|_{\xi=\tilde{\omega}} x_k y_l, \\
C_1(x, y, z) &= \sum_{k,l,r=1}^{m+n} \epsilon \frac{\partial^3 f(\xi, \tilde{\alpha}_H, \epsilon)}{\partial \xi_k \partial \xi_l \partial \xi_r} \Big|_{\xi=\tilde{\omega}} x_k y_l z_r, \\
C_2(x, y, z) &= \sum_{k,l,r=1}^{m+n} \frac{1}{\delta} \frac{\partial^3 h(\xi, \tilde{\alpha}_H, \epsilon)}{\partial \xi_k \partial \xi_l \partial \xi_r} \Big|_{\xi=\tilde{\omega}} x_k y_l z_r, \\
C_3(x, y, z) &= \sum_{k,l,r=1}^{m+n} \frac{\partial^3 k(\xi, \tilde{\alpha}_H, \epsilon)}{\partial \xi_k \partial \xi_l \partial \xi_r} \Big|_{\xi=\tilde{\omega}} x_k y_l z_r.
\end{aligned} \tag{3.6.52}$$

The first Lyapunov coefficient  $l_1$  is a function of  $\delta$ , and we are interested in the difference:

$$|l_1(1) - l_1(\delta)|. \tag{3.6.53}$$

Evaluating the scalar products in the expressions  $\langle p, C(q, q, \bar{q}) \rangle$ ,  $\langle p, B(q, A^{-1}B(q, \bar{q})) \rangle$  and  $\langle p, B(\bar{q}, (2i\omega\mathbb{1} - A)^{-1}B(q, q)) \rangle$  one notes that  $\delta$  only appears as factor in front of  $\tilde{\omega}$ . The  $\delta$  in the denominator of  $B_2$  and  $C_2$  is cancelled by  $\delta$  in the numerator of Eq. (3.6.51). The  $\delta$  appears in front of a small value ( $\tilde{\omega}$ ) and in combination with a non-zero term ( $D_u h$ ). Hence the explicit  $\delta$  in each of these summands does not lead to large changes. On the other hand, the eigenvectors  $p$  and  $q$  may change significantly as  $\delta$  is varied. Hence  $l_1(\delta)$  is in general not a small perturbation of  $l_1(1)$ .

In summary, the first Lyapunov coefficient corresponding to a singular Hopf bifurcation may change by an order one amount under QSSR. This can, in principle, result in a sign change in  $l_1$  and, hence, in a change of criticality of the Hopf bifurcation.

In fact, in two of the motivating examples considered in section 2.2, singular Hopf bifurcations persist but change criticality under QSSR. In particular, we observe a change from subcritical to supercritical of  $HB_1$  in the Hindmarsh-Rose model (Fig. 3.1) and in the Chay-Keizer model (Fig. 3.2).

We note that a change in the criticality of a Hopf bifurcation does not necessarily correspond to observable changes on the scale of interest. For instance, the branches of periodic

orbits arising from  $HB_1$  in Fig. 2.2 and in Fig. 2.3 are essentially vertical on the scale of those figures, and one needs to look very close to each bifurcation to see the change of criticality. For instance, the branch of periodic orbits produced in the Hopf bifurcation labelled  $HB_1$  in the full Hindmarsh-Rose model is initially unstable (Fig. 3.1, left panel) while the corresponding branch in the model reduced by QSSR is initially stable (Fig. 3.1, right panel). However, both branches increase in amplitude very rapidly over a very small interval of the bifurcation parameter and emerge as stable branches lying to the right of  $HB_1$ . As a consequence, the change in criticality of the Hopf bifurcation is not important from a modelling point of view. Similar comments apply to the Hopf bifurcation labelled  $HB_1$  in the Chay-Keizer model (see Fig. 3.2).

## 3.7 Other effects of QSSR

Various other changes to the dynamics can be introduced by the application of QSSR; we describe two possibilities in this section. The statements in this section are based on numerical observations and have not been proved rigorously.

### 3.7.1 Homoclinic bifurcations

Homoclinic bifurcations may be destroyed by QSSR. We have observed this in the HR model (see Fig. 2.2). The periodic orbits emanating from  $HB_1$  and  $HB_2$  terminate in homoclinic bifurcations in the full model but in the simplified model, a family of periodic orbits connects the two Hopf bifurcations (red dashed curve).

In the CK model we also observed the creation of homoclinic bifurcations in response to the removal of  $v$  by QSSR. In the full model the families of periodic orbits connect two Hopf bifurcations (see Fig. 2.3, blue curve), but when  $v$  is removed, the emanating branches of periodic orbits terminate in homoclinic bifurcations (see Fig. 2.5). However, as already noted, the periodic orbits in the full system have very small frequencies near the parameter values for the homoclinic bifurcations of the system with  $v$  reduced (see Fig. 2.5). This is because the orbits of the simplified system come very close to the equilibrium solutions at these parameter values. It is likely that a slight modification of other parameters would lead to a homoclinic bifurcation in the full system.

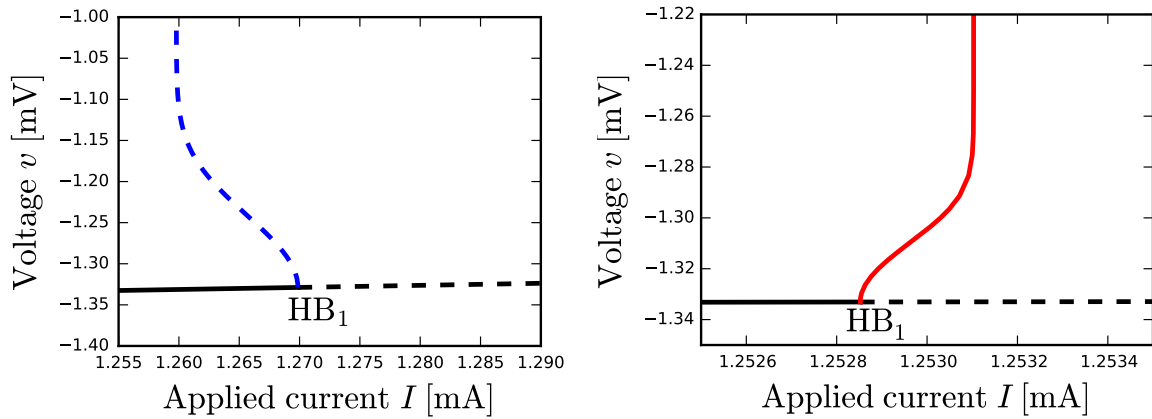


Figure 3.1: The panel on the left is a partial bifurcation diagram for the Hindmarsh-Rose model near the singular Hopf bifurcation  $HB_1$  (Eq. (2.2.11)-Eq. (2.2.13), c.f. Fig. 2.2). The bifurcation is subcritical and the resulting periodic orbits are unstable. The panel on the right shows the singular Hopf bifurcation  $HB_1$  after removing  $m$  by QSSR (Eq. (2.2.14)-Eq. (2.2.15)). The criticality has changed and the resulting periodic orbits are stable. Stable equilibria and periodic orbits are indicated by solid lines and unstable equilibria and periodic orbits are shown by dashed lines.

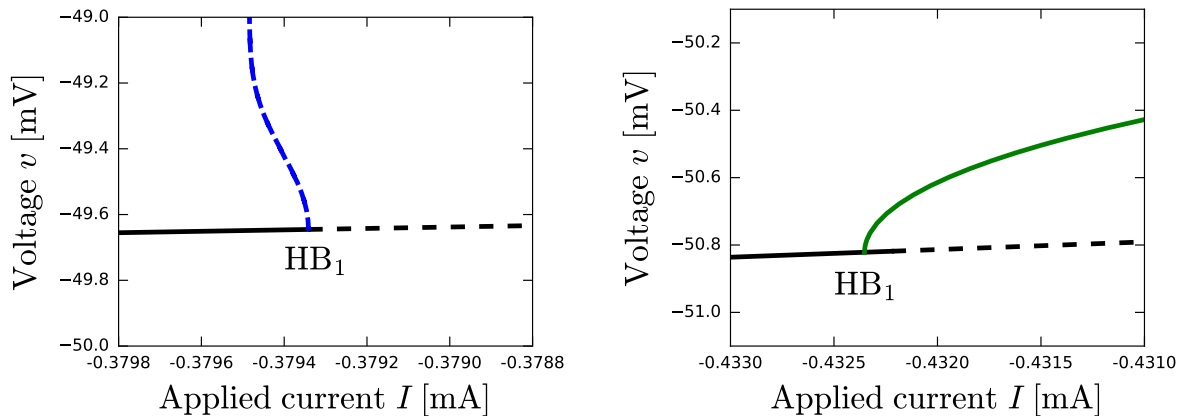


Figure 3.2: The panel on the left shows a subcritical singular Hopf bifurcation in the Chay-Keizer model Eq. (2.2.16)-Eq. (2.2.20) (c.f. Fig. 2.3). The panel on the right shows the CK model with  $v$  removed by QSSR. This leads to a supercritical singular Hopf bifurcation. Stable equilibria and periodic orbits are indicated by solid lines and unstable equilibria and periodic orbits are shown by dashed lines.

### 3.7.2 Saddle-node bifurcations of periodic orbits

QSSR may change the number of saddle-node bifurcations of periodic orbits, thereby potentially significantly changing the range of parameter values in which there is an attracting periodic solution. An example of this is seen when QSSR is applied to a model of the Gonadotropin Releasing Hormone (GnRH) neuron.

The GnRH neuron sits in the pituitary gland and is involved in the control of fertility of all mammals. Lee et al. proposed a mathematical model of this neuron formulated as a system of eight ordinary differential equations [59]. The model was revised in [67] and it was concluded that a six-dimensional version captures the main features of the dynamics of the full model.

The six-dimensional model is given by

$$\begin{aligned}
 C_m \frac{dV}{dt} &= I_{\text{app}} - I_{\text{km}} - I_{\text{cal}} - I_{\text{naf}} - sI_{\text{AHP-SK}} - sI_{\text{AHP-UCL}} + I_{\text{leak}}, \\
 \frac{dN_{\text{km}}}{dt} &= \frac{1}{\tau_{N_{\text{km}}}} (N_{\text{km}\infty} - N_{\text{km}}), \\
 \frac{dH_{\text{naf}}}{dt} &= \frac{1}{\tau_{H_{\text{naf}}}} (H_{\text{naf}\infty} - H_{\text{naf}}), \\
 \frac{dO_{\text{ucl}}^*}{dt} &= k_{\text{new}} \cdot (1 - O_{\text{ucl}}^*) - k_{33} O_{\text{ucl}}^*, \\
 \frac{dc}{dt} &= J_{\text{release}} - J_{\text{serca}} + \rho (J_{\text{in}} - J_{\text{pm}}), \\
 \frac{dc_t}{dt} &= \rho (J_{\text{in}} - J_{\text{pm}}),
 \end{aligned} \tag{3.7.1}$$

where  $V$  is the voltage across the neuron's membrane,  $N_{\text{km}}$ ,  $H_{\text{naf}}$  and  $O_{\text{ucl}}^*$  are gating variables,  $c$  is the calcium concentration in the cytosol and  $c_t$  is the total calcium concentration in the cell. The functions and parameter values can be found in Appendix A. On variation of  $I_{\text{app}}$  it is seen that the full model has a Hopf bifurcation which produces the branch of periodic orbits shown in blue in Fig. 3.3. Note that the branch of periodic orbits has a single fold (saddle-node bifurcation of periodic orbits).

By comparing time scales and magnitudes of the variables, Nan [67] concluded that  $V$ ,  $N_{\text{km}}$  and  $H_{\text{naf}}$  evolve at a rate at least an order of magnitude faster than the remaining variables, suggesting that one or more of these variable might plausibly be removed by QSSR. A simplified version of the model obtained by setting  $N_{\text{km}} = N_{\text{km}\infty}$  produces a bifurcation diagram that is also shown in Fig. 3.3. By comparing the two versions of the bifurcation diagram, it can be seen that QSSR causes the Hopf bifurcation to move to the

left, and similarly moves the rightmost fold. The curve of periodic orbits also gains two additional folds ( $SP_1$  and  $SP_2$ ), with each fold being associated with a change in stability of the branch of periodic orbits. The combined effect of movement of the rightmost fold and the introduction of two new folds is to drastically reduce the interval of parameter values for which the branch of periodic solutions is stable. Significantly, part of the stable branch of periodic solutions lost under QSSR corresponded to bursting solutions [67]. Thus, the simplified model would not normally be regarded as an acceptable approximation to the full model, at least over the range of values of applied current shown in Fig. 3.3.

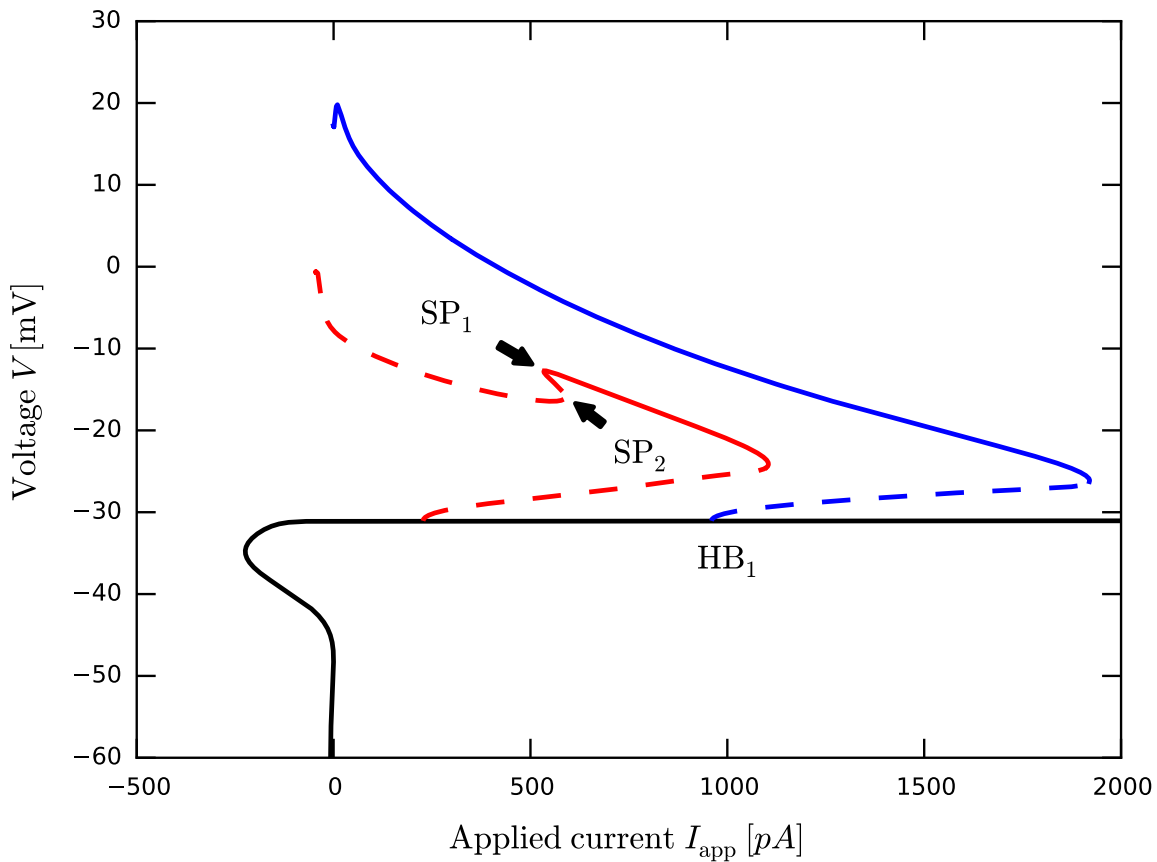


Figure 3.3: Partial bifurcation diagram for the GnRH neuron model, equations Eq. (3.7.1) with parameters as in Appendix A.3. Equilibrium solutions are indicated by the black curve. The blue curve shows the maximum voltage of the periodic orbits emanating from the Hopf bifurcation  $HB_1$  in the six-dimensional version of the model (solid for stable, dashed for unstable). For small applied currents (near  $I_{app} = 0$ ) the periodic orbits are bursting oscillations. The red curve shows the corresponding family of periodic orbits in the five-dimensional system obtained by setting  $N_{km} = N_{km\infty}$  (again, solid for stable, dashed for unstable). None of the periodic solutions corresponding to this branch are bursting solutions. Both curves (red and blue) terminate in homoclinic bifurcations when the applied current is near zero.

# 4

## Applying quasi-steady-state reduction

### 4.1 Appropriate application of quasi-steady-state reduction

We have shown that when a model has oscillatory solutions, the application of QSSR can significantly change the qualitative behaviour of solutions by, for example, moving or removing Hopf bifurcations or folds of periodic orbits. Thus, when confronted with a model in which oscillatory solutions are thought to be important, it would be safest to avoid using QSSR in an attempt to simplify the model. On the other hand, QSSR is a widely used reduction method that is simple to apply, and can in some cases vastly simplify a model without appearing to adversely affect model predictions; it is very tempting, therefore, for modellers and others to use QSSR. In this section we present some guidelines for how and when to apply QSSR if one wishes to minimise the risk of inadvertently destroying essential features of the original model.

It is worth noting that, with the current wide availability of fast computers and software packages such as XPPAUT [30], AUTO [27] and MatCont [26] that enable easy numerical integration of ordinary differential equations and the accurate detection and continua-

tion of bifurcations, the historical imperative for model reduction is somewhat diluted; adequate information about model dynamics might well be obtained by numerical computations using the full model. However, model reduction can make numerical computations faster (particularly for stiff systems, where removing fast variables can reduce or eliminate the stiffness). This may be important if the “full” model is just one component of a larger model. Furthermore, reducing the dimension of a model frequently simplifies explanations about underlying mathematical causes for complicated dynamics, since visualisation of geometric features, and hence understanding of dynamical properties, is only feasible for low-dimensional systems. We proceed on the assumption that working with the full model is undesirable for some reason.

The first step in our recommended approach to using QSSR is to perform numerical computations on the full model, with the aim of determining typical behaviour for the full model; either look at time series by integrating the system for typical initial conditions and parameter values, or compute a bifurcation diagram using continuation software like XPPAUT or AUTO. If the system has oscillations, it is reasonable to look at typical time series of oscillating solutions to get an idea about the time scales involved. Of course, this step can only be carried out if the modeller has access to the full model.

The next step is to decide which variables might be considered fast and which ones slow. This can be a difficult and subjective decision, and identifying clear, globally valid time scale separation between variables may not always be possible. A common way to start is to look for a nondimensionalized formulation of the model by

- (i) algebraically manipulating the model equations to aggregate parameters, and
- (ii) multiplying variables by characteristic scales, which take the units of a physical quantity and rescale the corresponding variables so that the maximum magnitude of each is about 1.

An example illustrating the construction of a nondimensionalized model in this way can be found in [83].

High dimensional systems or systems with many parameters might be very hard to manipulate into meaningful nondimensionalized systems, and time scales often can only be identified roughly based on the modeller’s intuition. Most commonly, a two time scale splitting of variables is assumed. In many models there are actually more than two time scales involved and it is not clear how to divide variables into fast and slow groups. For example, both the Hodgkin-Huxley model and the Chay-Keizer model from section 2.2 can

plausibly be considered to be three time scale problems. Recent work of Vo et al. [92] suggests that if more than two timescales are involved, or there is ambiguity about whether a variable should be grouped with the fast or slow variables, insight might be gained by comparing different assignments of variables to fast or slow groups. Furthermore, for conductance-based models where the equations of the gating variables depend only on voltage and the respective gating variable, a systematic approach to identifying timescales has been proposed by [53]. Nevertheless, for the purposes of QSSR, a reasonable aim is to identify the fastest group of variables, regardless of whether the slower variables form one or more subgroups; the fastest variables are the ones that might justifiably be removed using QSSR.

Another problem that arises is that some variables might be fast in some regions of the phase space but slower in other regions of the phase space, making it difficult to define a globally valid splitting. In such cases, some division of time scales is assumed, with the justification for that particular splitting being made after the fact (if at all) based on whether the resulting model has the desired properties. More work on a mathematically rigorous way to proceed in cases where there is no globally valid splitting of time scales is needed. A systematic approach to identifying an explicit splitting of slow and fast variables in the context of globally attracting critical manifolds is presented in [41].

Once a decision has been made about which variables form the fast subsystem, the next step is to analyse the fast subsystem alone. In analysis of the fast subsystem (also known as the *layer problem*), the slow variables are treated as parameters. It is in this step that an informed decision can be made about the validity of using QSSR. In particular, one should use a numerical package such as XPPAUT or AUTO, and look for bifurcations producing oscillations by varying one or more slow variables and the main bifurcation parameter. If it is found that the layer problem has a globally, exponentially attracting manifold of equilibria (and provided that the identification of the fast variables is correct), the modeller may remove all fast variables by QSSR and expect that the simplified system captures the dynamics of the full system apart from the initial transient period.

On the other hand, if oscillations are found in the layer problem, the modeller has to be careful when applying QSSR. It cannot, without further investigation, be decided which variables have to be kept to preserve the oscillations in a simplified model, although it is certain that at least two fast variables are needed in the simplified model to preserve this type of oscillation.

If oscillations are seen in the full problem but are not found in the layer problem then slow variables are needed for the oscillation, and QSSR might well preserve important features



of the oscillations. In particular, if the manifold of equilibria of the layer problem is folded relative to a fast variable, then there is a chance that oscillations in the full model are induced by a singular Hopf bifurcation. In this case at least one fast variable must be kept when applying QSSR, but QSSR will preserve the Hopf bifurcation; the resulting oscillations will have segments on which the evolution is fast and segments on which it is slow.

Alternatively, the full system oscillations may involve only slow variables. One can check if this is the case by examining the *reduced problem*, which is the system obtained by assuming that all fast variables have equilibrated. More formally, one obtains the reduced problem for a system in the form of (3.1.1) by setting  $f = 0$  and rescaling time by  $t = \tau/\epsilon$  to get the differential-algebraic system

$$\begin{aligned} 0 &= f(x, y, \alpha), \\ y' &= g(x, y, \alpha), \end{aligned} \tag{4.1.1}$$

where the prime denotes differentiation with respect to the new time  $\tau$ . Oscillations in this system can be searched for using XPPAUT or AUTO. Oscillations of this type will be preserved under QSSR.

At the end of this process, there will be better information about whether QSSR is advisable. In short:

- if there are oscillations in the layer problem, QSSR should not be attempted without further investigation into which fast variables are involved. If QSSR is used at least two fast variables must be retained;
- if oscillations arise through a singular Hopf bifurcation or relaxation oscillations are observed, at least one fast variable must be retained under QSSR;
- in all other cases, one would expect QSSR to preserve any Hopf bifurcations even if all fast variables are removed.

Note that our rigorous results tell us about the persistence of Hopf bifurcations only; as discussed in chapter 3, QSSR may substantially alter the dynamics of a system by introducing or removing other bifurcations (e.g., by the introduction of folds of periodic solutions, as discussed in section 3.7). Furthermore, even if Hopf bifurcations persist, QSSR may significantly change the amplitude or frequency of oscillation, change the range of parameters for which oscillations exist, or change the stability of the periodic orbits emanating from the Hopf bifurcation (see 3.6). For this reason, the last step in

a careful application of QSSR is to compute the bifurcation diagram for the simplified system and compare this with the full system bifurcation diagram.

We now illustrate the process outlined above for the HR model, equations (2.2.11)-(2.2.13). The time scale separation for the HR model is explicit in the equations: the right hand sides of the  $\dot{v}$  and  $\dot{m}$  equations are already appropriately nondimensionalized, so for small  $\epsilon$ ,  $v$  and  $m$  are fast and  $n$  is slow. The layer problem is obtained by taking the limit  $\epsilon \rightarrow 0$  in equations (2.2.11)-(2.2.13), yielding

$$\begin{aligned}\dot{v} &= I - v^3 + 3v^2 + m - n_0, \\ \dot{m} &= 1 - 5v^2 - m.\end{aligned}$$

The slow variable  $n$  is here replaced by the parameter  $n_0$ . Since the parameters  $I$  and  $n_0$  enter the equations only in the combination  $I - n_0$ , the two parameters can be replaced by one parameter,  $\bar{I} = I - n_0$ . The layer problem then becomes

$$\begin{aligned}\dot{v} &= \bar{I} - v^3 + 3v^2 + m, \\ \dot{m} &= 1 - 5v^2 - m.\end{aligned}\tag{4.1.2}$$

A partial bifurcation diagram for the layer problem is shown in Fig. 4.1, from which it is clear that the layer problem has two Hopf bifurcations which are connected by a family of periodic orbits. According to the guidelines outlined above, the HR system is therefore a poor candidate for QSSR; one knows *a priori* that full system oscillations that are preserved in the layer problem might be removed by QSSR. In fact, for the HR system, a stronger statement can be made: since a Hopf bifurcation can only occur in systems with two or more dimensions, removing one of the fast variables by QSSR must destroy the ‘fast’ Hopf bifurcation. This is precisely what was seen in Fig. 2.2. We note that only two of the four Hopf bifurcations observed in the full HR model (Fig. 2.2) persist in the layer problem (with their positions moved somewhat). The other two Hopf bifurcations must involve at least one slow variable, and are therefore expected to be preserved by QSSR. This expectation is confirmed by Fig. 2.2.

In this example, analysis of the layer problem in the HR model was particularly easy, because the HR model has only one slow variable and the slow variable can be aggregated with the applied current  $I$  to give a single parameter  $\bar{I}$ . In other models analysing the layer problem may not be so easy. To illustrate this, we look at the GnRH model, Eq. (3.7.1). Nondimensionalization of the model suggests that the model possesses three fast variables

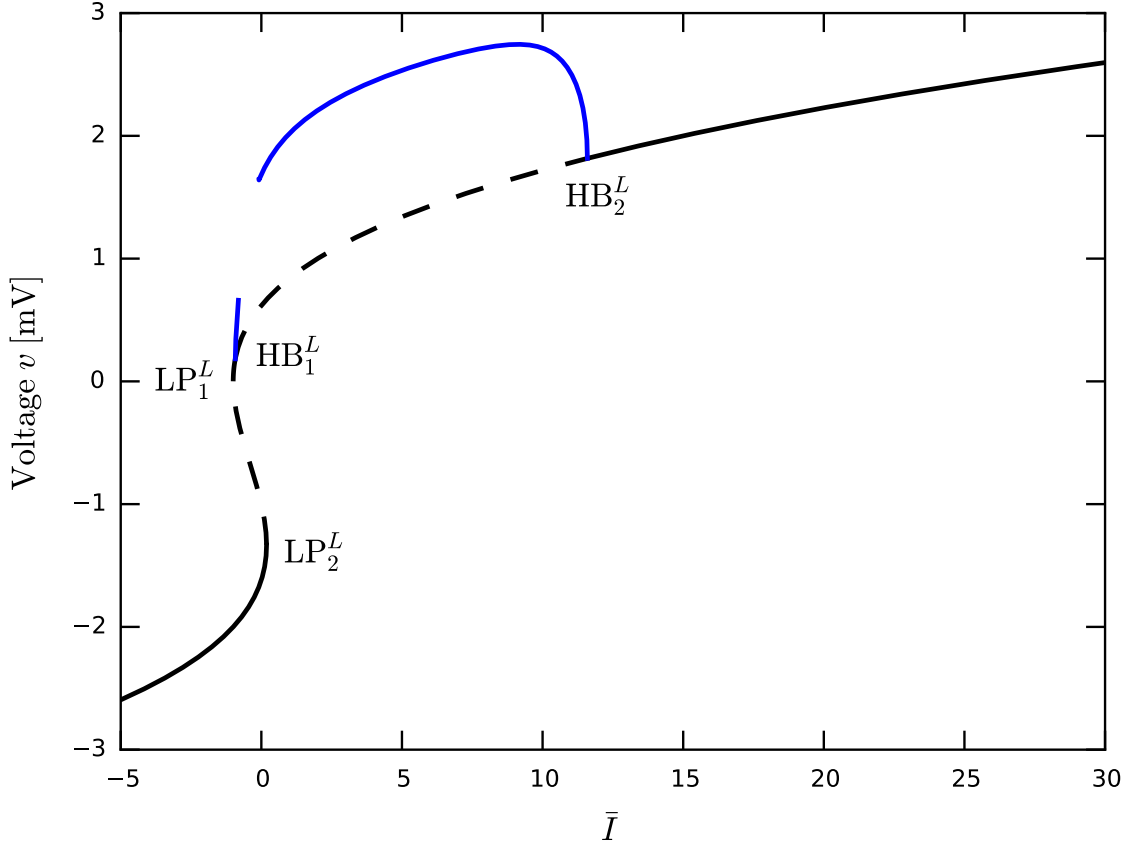


Figure 4.1: Partial bifurcation diagram for the fast subsystem of the HR model given by Eq. (4.1.2). Equilibria are indicated by the black curve (solid for stable, dashed for unstable). This subsystem has two Hopf bifurcations, at  $HB_1^L$  and  $HB_2^L$ . The blue curves show the maximum value of  $V$  for each periodic orbit on the branches emanating from the Hopf bifurcations; stability of the periodic orbits is not indicated. The labels  $LP_1^L$  and  $LP_2^L$  mark saddle-node bifurcations of equilibria.

and three slow variables [67]. This leads to the following layer problem:

$$\begin{aligned}
 C_m \frac{dV}{dt} &= I_{\text{app}} - I_{\text{km}} - I_{\text{cal}} - I_{\text{naf}} - sI_{\text{AHP-SK}} - sI_{\text{AHP-UCL}} + I_{\text{leak}}, \\
 \frac{dN_{\text{km}}}{dt} &= \frac{1}{\tau_{N_{\text{km}}}} (N_{\text{km}\infty} - N_{\text{km}}), \\
 \frac{dH_{\text{naf}}}{dt} &= \frac{1}{\tau_{H_{\text{naf}}}} (H_{\text{naf}\infty} - H_{\text{naf}}).
 \end{aligned} \tag{4.1.3}$$

The main parameter is the applied current  $I_{\text{app}}$ , but the slow variables of Eq. (3.7.1) are now treated as three additional parameters  $O_{\text{ucl},0}^*$ ,  $c_0$  and  $c_{t,0}$ . In principle, one would have to explore the four-dimensional parameter space to check for bifurcations in the layer problem. In this case it is sufficient for our purposes to take representative combinations of  $O_{\text{ucl},0}^*$ ,  $c_0$  and  $c_{t,0}$  while varying the parameter  $I_{\text{app}}$ . Partial bifurcation diagrams for

two choices of parameter values are shown in Fig. 4.2 and Fig. 4.3. For the parameter values used for the bifurcation diagram shown in Fig. 4.2, the layer problem has no Hopf bifurcations and the manifold of equilibria is exponentially attracting, suggesting that there would be no problem with using QSSR. However, for the parameter values used for the bifurcation diagram shown in Fig. 4.3, the layer problem shows two Hopf bifurcations ( $HB_1^L$  and  $HB_2^L$ ) and a family of periodic orbits (blue curve); in this case the critical manifold is not globally attracting, meaning that the dynamics of a simplified model may be qualitatively different from that of the full model, and, hence, that it is not advisable to attempt the removal of one or more fast variables by QSSR.

This example illustrates the point that it may not be straightforward to determine whether the layer problem has a globally exponentially attracting manifold of equilibria based on numerical integration of the layer problem; specifically, in cases where there is more than one parameter of the layer problem (remembering to include slow variables of the full problem as parameters of the layer problem) an exhaustive search of the parameter space looking for parameter values where the layer problem loses asymptotic stability may be difficult, and crucial regions of parameter space may easily be missed, possibly leading to erroneous conclusions about the validity of using QSSR.

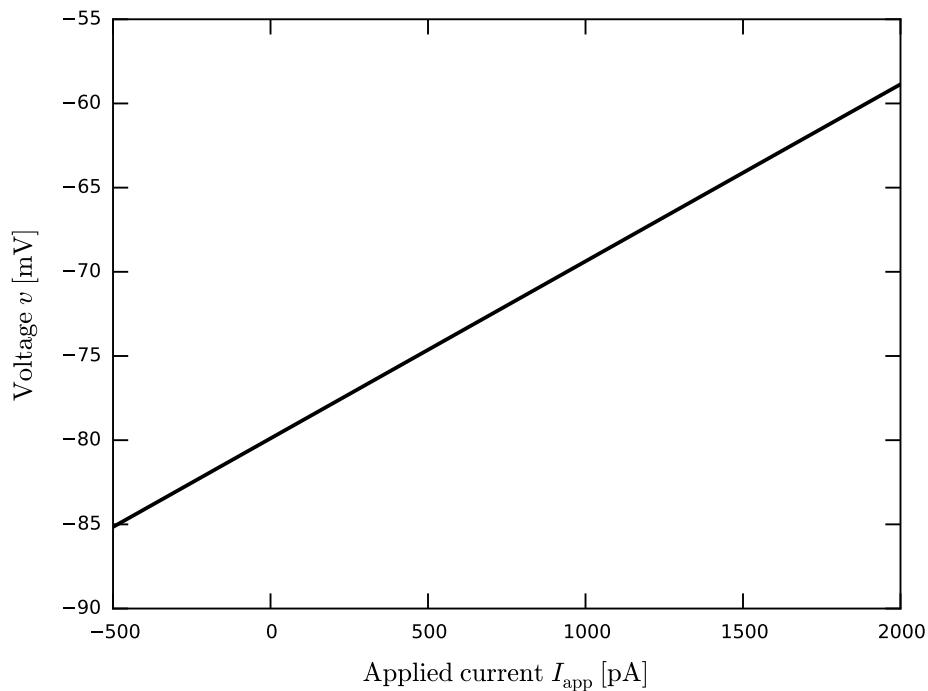


Figure 4.2: Partial bifurcation diagram for the fast subsystem of the GnRH model given by Eq. (4.1.3) with  $O_{uc1,0}^* = 0.1$ ,  $c_0 = 0.5$  and  $c_{t,0} = 80$ . The black curve represents stable equilibria.

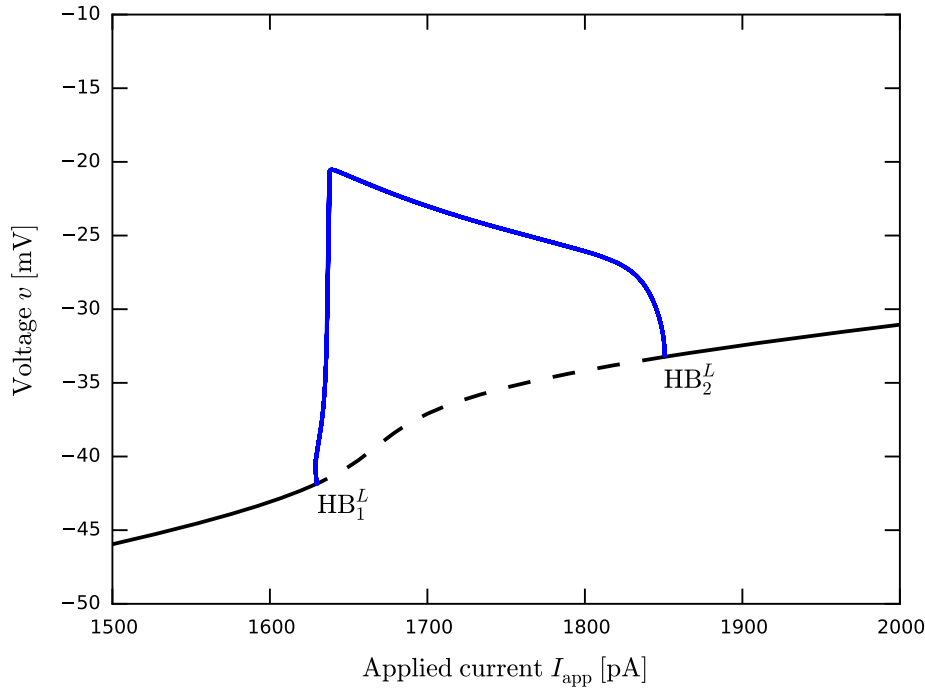


Figure 4.3: Partial bifurcation diagram for the fast subsystem of the GnRH model given by Eq. (4.1.3) with  $O_{ucl,0}^* = 0.0454$ ,  $c_0 = 50.3688$  and  $c_{t,0} = 52.9475$ . Equilibria are indicated by the black curve (solid for stable, dashed for unstable). This subsystem has two Hopf bifurcations, at  $HB_1^L$  and  $HB_2^L$ . The blue curve shows the maximum value of  $V$  for each periodic orbit on the branch connecting the Hopf bifurcations; stability of the periodic orbits is not indicated.

## 4.2 Conclusions

QSSR is a technique that is widely used to simplify mathematical models with multiple time scales, particularly models of chemical kinetics or biophysical phenomena. This is the case despite it being known for some time that QSSR may introduce qualitative changes to the dynamics by removing oscillations [37], [32]. The method is popular because it is intuitive and easy to apply, and can lead to significantly simpler models. Our aim in this part of the thesis has been to increase understanding of the circumstances under which QSSR leads to qualitatively correct predictions about model dynamics, especially when the original model shows oscillations, and hence to provide guidance on when it is appropriate to use QSSR for model simplification.

We have shown examples where application of QSSR significantly changes the oscillatory behaviour in a model, either by destroying one or more Hopf bifurcations or by moving Hopf bifurcations a relatively long way in the parameter space or by introducing new bifurcations (such as folds of periodic orbits) to the dynamics. In a two time scale setting, we proved that singular Hopf bifurcations, which involve both fast and slow variables, are

robust in the sense that they are preserved under QSSR when at least one fast variable is kept and the matrix defined in Eq. (3.1.4) is invertible. The persistence of a singular Hopf bifurcation does not imply that all features of the oscillations near the Hopf bifurcation are unchanged, and changes in stability of the emanating periodic orbits as well as changes in their amplitude and frequency near onset can occur.

We have argued that Hopf bifurcations involving only slow variables are also robust under QSSR, but that Hopf bifurcations involving only fast variables can be destroyed by QSSR. Our results were formulated in the context of models that are expressed globally in standard slow-fast form, as in Eq. (3.1.1). We conjecture that similar results about persistence of Hopf bifurcations would hold in systems which only allow a local decomposition into standard slow-fast form near the Hopf bifurcation.

The dynamics associated with Hopf bifurcations is not the only concern when applying QSSR. We saw in the examples that QSSR can also remove or introduce homoclinic bifurcations and folds of periodic orbits, thereby altering the oscillatory behaviour of the model in a major way.

With these results in mind, we have proposed a way to determine whether the dynamics of a particular system is likely to be adversely affected by QSSR; this method relies on being able to identify which system variables are fast and which are slow, and then analysing the fast subsystem (layer problem). We acknowledge that finding an explicit time scale separation and analysing the fast subsystem can be tedious and is sometimes not feasible, but doing so does provide information about one of the likely problems of the application of QSSR, i.e., the removal of oscillations involving only fast variables.

Despite all words of warning, we believe that QSSR will continue to be widely used for simplification of biophysical models with multiple time scales. Hence, more work is necessary to understand as well as possible the conditions under which QSSR leads to qualitatively accurate models.



# 5

## Excitation-contraction coupling in airway smooth muscle cells

### 5.1 Introduction

During asthma attacks or airway hyperresponsiveness the airway diameter can reduce dramatically in size. The reduction of the airway diameter is induced by a contraction of airway smooth muscle cells (ASMC) [24, 77]. ASMC, like skeletal and cardiac muscle cells, are regulated by transient changes of the cytosolic  $\text{Ca}^{2+}$  concentration ( $[\text{Ca}^{2+}]_i$ ). The contractile mechanisms are different for different muscle types; an overview including mathematical models of contraction mechanisms can be found in [52].

In this thesis, we focus on the  $\text{Ca}^{2+}$  signalling that drives the contraction. Intracellular  $\text{Ca}^{2+}$  acts as a messenger which activates the contractile apparatus following an extracellular stimulus. Typically,  $[\text{Ca}^{2+}]_i$  oscillates and the frequency directly influences the strength of contraction [6, 24, 64, 74].

There are two different types of stimuli that can lead to oscillations of the cytosolic  $\text{Ca}^{2+}$



concentration. One pathway is via depolarization, e.g., by changing the ion concentrations in the extracellular space. Depolarization leads to opening of voltage-gated  $\text{Ca}^{2+}$  channels (VGCC) which are located in the plasma membrane [47]. The  $\text{Ca}^{2+}$  concentration in the extracellular space is higher than in the cytosol [51], and the opening of VGCC increases  $[\text{Ca}^{2+}]_i$ . An initial increase of  $[\text{Ca}^{2+}]_i$  can result in overfilling of the SR. As a consequence, ryanodine receptors (RyR) can open and release  $\text{Ca}^{2+}$  from the SR into the cytosol. This mechanism is called calcium-induced calcium release (CICR). When the SR has lost the excess  $\text{Ca}^{2+}$ , the RyR close and the pumps transport  $\text{Ca}^{2+}$  back into the SR and out of the cell [88]. This process can repeat periodically and cause oscillations in  $[\text{Ca}^{2+}]_i$ . The period of depolarization-induced  $[\text{Ca}^{2+}]_i$  oscillations, set by the time it takes to refill the SR, is 20 s - 60 s [5, 74].

In other muscle cells (striated muscle [38], vascular smooth muscle [48], gastrointestinal smooth muscle [14] and heart muscle [10]) depolarization followed by increased  $[\text{Ca}^{2+}]_i$  and contraction provides the main pathway for muscle contraction.

A second pathway is that an agonist (e.g., 5-hydroxytryptamine (5-HT), acetylcholine (ACh), histamine or methacholine (MCh)) binds to G-protein coupled receptors in the plasma membrane [24]. This leads to the production of inositol (1,4,5)-trisphosphate ( $\text{IP}_3$ ), which diffuses into the cytosol and binds to  $\text{IP}_3$ -receptors (IPR) in the membrane of the SR. IPR have an increased open probability in the presence of  $\text{IP}_3$  and release  $\text{Ca}^{2+}$  from the SR into the cytosol. Periodic release from the IPR and reuptake by the SR via pumps lead to  $[\text{Ca}^{2+}]_i$  oscillations with periods of 1 s - 15 s [74].

Both pathways rely on  $\text{Ca}^{2+}$  release and reuptake from the SR. A schematic overview of the  $\text{Ca}^{2+}$  fluxes is shown in Fig. 5.1. The pathways involve different release mechanisms from the SR. In general, both release mechanisms can interact, and  $[\text{Ca}^{2+}]_i$  oscillations are controlled by the interaction of IPR and RyR [88].

During  $[\text{Ca}^{2+}]_i$  oscillations the cell loses  $\text{Ca}^{2+}$  through the plasma membrane pump (PM) and sustained oscillations require  $\text{Ca}^{2+}$  influx through plasma membrane channels (see Fig. 5.1). In ASMC store-operated  $\text{Ca}^{2+}$  channels (SOCC), receptor-operated  $\text{Ca}^{2+}$  channels (ROCC) and VGCC have been identified [64].

All  $\text{Ca}^{2+}$  influxes depend on the voltage across the plasma membrane. Some channels (VGCC) are actively-gated by changes in voltage, and for other channels the difference in voltage provides an electrical forcing which aids or hinders the transport of  $\text{Ca}^{2+}$  ions into the cell. ZhuGe et al. [98] present experimental evidence that local  $\text{Ca}^{2+}$  releases lead to biphasic responses in the voltage across the membrane. In order to study the

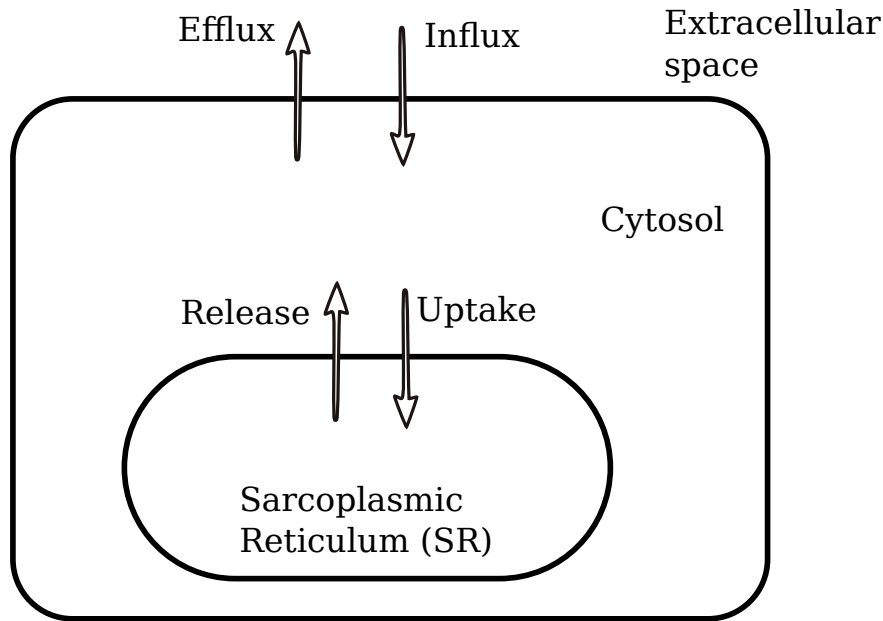


Figure 5.1: Schematic diagram of  $\text{Ca}^{2+}$  fluxes. During  $[\text{Ca}^{2+}]_i$  oscillations most of the  $\text{Ca}^{2+}$  transport is between the SR and the cytosol (release and uptake). When  $[\text{Ca}^{2+}]_i$  is elevated, the cell also loses  $\text{Ca}^{2+}$  to the extracellular space (efflux). Oscillations can be triggered by the presence of  $\text{IP}_3$  or by an increased influx due to depolarization.

contributions of  $\text{Ca}^{2+}$  fluxes for the two different stimuli, the effect of changes in voltage on the influxes need to be included.

The importance of SOCC in ASMC has been reported by various studies [3, 4, 11, 23, 70, 72, 75]. SOCC are activated by interaction of stromal interaction molecules (STIM) and Orai proteins. The STIM molecules, located in the SR membrane, function as sensors for the SR  $\text{Ca}^{2+}$  concentration. When the  $\text{Ca}^{2+}$  concentration in the SR is low, STIM oligomerize and collocate near Orai proteins in the plasma membrane. The Orai proteins provide the gating mechanism and open in response to STIM binding [11, 63, 69, 72, 73].

The contributions to the overall influx of the different types of  $\text{Ca}^{2+}$  channels are unknown. The main aim of the work in the second half of this thesis was to determine relative contributions of SOCC and VGCC. The balance between the fluxes through SOCC and VGCC is important to understand the effect of depolarization in controlling the  $\text{Ca}^{2+}$  dynamics.

The voltage across the membrane is affected by other ion fluxes across the membrane. Following the work of [82], we have included  $\text{Na}^+$ ,  $\text{K}^+$  and  $\text{Cl}^-$  channels. An overview of all channels can be found in Fig. 5.2.

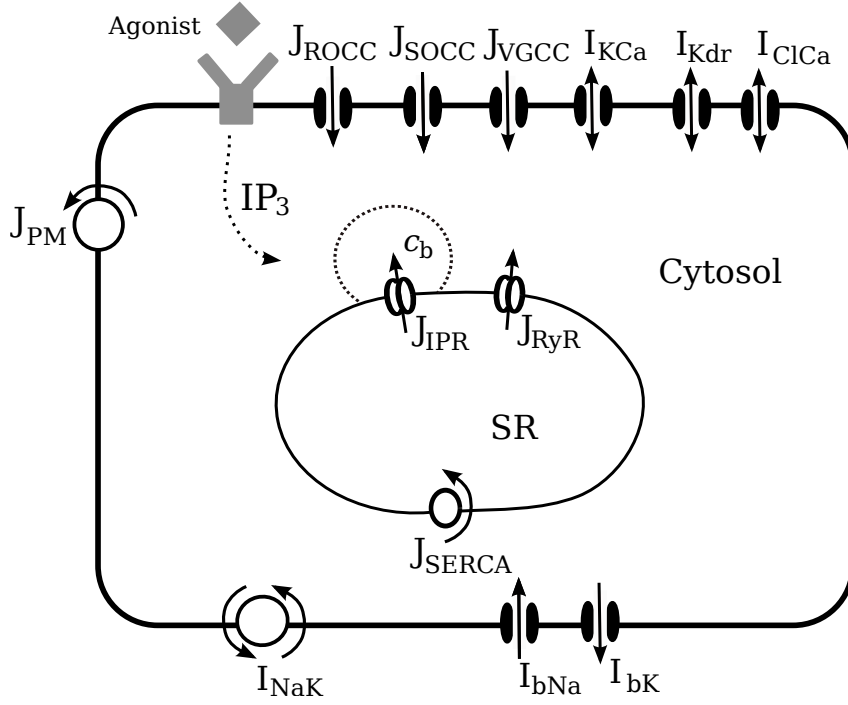


Figure 5.2: Schematic diagram of the model. Agonist binding to G-coupled receptors stimulates the production and diffusion of  $\text{IP}_3$  into the cytosol. Calcium is released from the sarcoplasmic reticulum (SR) through IPR and RyR. The  $\text{Ca}^{2+}$  release from the IPR is released into the microdomain with concentration  $c_b$ , and diffuses into the cytosol. Reuptake is via the pumps (SERCA). Calcium efflux is via the plasma membrane pump (PM) and influx is through receptor-operated (ROCC), store-operated (SOCC) and L-type voltage-gated (VGCC)  $\text{Ca}^{2+}$  channels. The model includes  $\text{Ca}^{2+}$ -activated  $\text{K}^+$  and  $\text{Cl}^-$  channels (KCa) and (ClCa), the delayed rectifier  $\text{K}^+$  currents (Kdr), basal  $\text{Na}^+$  (bNa) and  $\text{K}^+$  currents (bK) and the  $\text{Na}^+$ - $\text{K}^+$  exchanger (NaK).

## 5.2 Model construction

The differential equations of the full model are:

$$\dot{c} = J_{\text{Release}} - J_{\text{SERCA}} - \delta (J_{\text{VGCC}} + J_{\text{ROCC}} + J_{\text{SOCC}} + J_{\text{PM}}), \quad (5.2.1)$$

$$\dot{c}_b = \gamma_1 (J_{\text{IPR}} - J_{\text{diff}}), \quad (5.2.2)$$

$$\dot{c}_t = -\delta (J_{\text{VGCC}} + J_{\text{ROCC}} + J_{\text{SOCC}} + J_{\text{PM}}), \quad (5.2.3)$$

$$\dot{h}_{42} = \lambda_{h42} \left( \frac{k_{-42}^3}{c_b^3 + k_{-42}^3} - h_{42} \right), \quad (5.2.4)$$

$$\dot{P}_{\text{so}} = \frac{1}{T_{\text{Socc}}} (P_{\text{so}}^\infty - P_{\text{so}}), \quad (5.2.5)$$

$$\begin{aligned} \dot{V} = & -\frac{1}{C_m} (J_{\text{PM}} + J_{\text{ROCC}} + J_{\text{SOCC}} + J_{\text{VGCC}} + I_{\text{Kdr}} + I_{\text{ClCa}} \\ & + I_{\text{bK}} + I_{\text{bNa}} + I_{\text{NaK}} + I_{\text{KCa}}). \end{aligned} \quad (5.2.6)$$

The variable  $c$  is the  $\text{Ca}^{2+}$  concentration in the cytosol ( $[\text{Ca}^{2+}]_i$ ), while  $c_b$  is the  $\text{Ca}^{2+}$  concentration in a microdomain around the cytosolic side of the IPR to account for high  $\text{Ca}^{2+}$  after release (see Fig. 5.2); details can be found in [19]. The variable  $c_t$  is the total  $\text{Ca}^{2+}$  concentration in the cell and  $h_{42}$  is a gating variable of the IPR; low values of  $h_{42}$  inhibit the IPR.  $P_{\text{so}}$  is a gating variable for the store-operated  $\text{Ca}^{2+}$  channel as introduced in [94] and  $V$  is the voltage across the plasma membrane.

The constant  $\gamma_1$  is the volume ratio between the volume of the cytoplasm and the volume of the microdomain. The function  $\lambda_{h_{42}}$  (Eq. (5.2.19)) is responsible for the timescale of opening and closing of the IPR. Likewise, the constant  $T_{\text{SOCC}}$  sets the timescale over which the SOCC adapt. The  $[\text{IP}_3]$ -dependent function  $k_{-42}$  determines the strength of the  $c_b$ -dependent inhibition of the IPR and  $P_{\text{so}}^\infty$  (Eq. (5.2.26)) is the deterministic equivalent of the steady-state open probability of SOCC. The factor  $C_m$  is the capacitance of the plasma membrane. Calcium fluxes are denoted by  $J$ , and  $\text{K}^+$ ,  $\text{Na}^+$  and  $\text{Cl}^-$  fluxes are represented by the letter  $I$ .

The fluxes across the plasma membrane are measured in nA, where the fluxes that contribute to the  $\text{Ca}^{2+}$  concentrations are effective fluxes measured in  $\frac{\mu\text{M}}{\text{s}}$ . Effective fluxes contribute to the free  $\text{Ca}^{2+}$  concentration and are not buffered [51].

The factor  $\delta$  takes the different units into account and we have estimated it to be

$$\delta = \frac{1}{2F \cdot \text{Vol}} \cdot 10^{-3} \approx 1.449 \frac{\text{mol}}{\text{C} \cdot l}, \quad (5.2.7)$$

where  $F$  is the Faraday constant and  $\text{Vol}$  is the volume of the cell in mol. We approximate the volume to be  $\text{Vol} = 3.58 \cdot 10^{-12} l$  based on the data in [49]. Since most of the  $\text{Ca}^{2+}$  influx is directly taken up by buffers and only the free cytosolic  $\text{Ca}^{2+}$  is taken into account in Eq. (5.2.1) and Eq. (5.2.3), it is estimated that the effective flux is 1000 times smaller than the flux across the cell membrane.

The ionic currents across the plasma membrane depend on the voltage difference between the Nernst potential of the ion and the voltage across the plasma membrane [51]. The Nernst potentials of the ions  $\text{Ca}^{2+}$ ,  $\text{Na}^+$ ,  $\text{K}^+$  and  $\text{Cl}^-$  are

$$E_{\text{Ion}} = \frac{RT}{nF} \log \left( \frac{[\text{Ion}]_{\text{ext}}}{[\text{Ion}]_{\text{int}}} \right), \quad (5.2.8)$$

where  $R$  is the gas constant,  $F$  is the Faraday constant and  $T$  is the temperature. The constant  $n$  takes the charge of the ion into account and is two for  $\text{Ca}^{2+}$ , one for  $\text{Na}^+$  and  $\text{K}^+$  and minus one for  $\text{Cl}^-$ .

### 5.2.1 Calcium transport between the cytosol and the SR

The  $\text{Ca}^{2+}$  concentration in the SR is determined by the conservation relationship  $c_t = c + c_b/\gamma_1 + c_s/\gamma_2$ , where  $\gamma_2$  is the volume ratio between cytoplasm and SR, and  $\gamma_1$  is as before. The  $\text{Ca}^{2+}$  concentration in the SR is:

$$c_s = \gamma_2 \left( c_t - c - \frac{c_b}{\gamma_1} \right). \quad (5.2.9)$$

The release of  $\text{Ca}^{2+}$  from internal stores into the cytosol is given by

$$\begin{aligned} J_{\text{Release}} &= J_{\text{diff}} + J_{\text{leak}} + J_{\text{RyR}}, \\ J_{\text{diff}} &= k_{\text{diff}}(c_b - c), \\ J_{\text{leak}} &= k_{\text{leak}}(c_s - c), \\ J_{\text{RyR}} &= k_{\text{RyR}} P_{\text{RyR}}(c_s - c), \end{aligned} \quad (5.2.10)$$

where  $J_{\text{diff}}$  is the  $\text{Ca}^{2+}$  current from the microdomain at the cytosolic site of the IPR,  $J_{\text{leak}}$  is a generic leak from the SR to the cytosol and  $J_{\text{RyR}}$  is the current through the RyR. The constants  $k_{\text{diff}}$  and  $k_{\text{leak}}$  are proportionality constants and  $k_{\text{RyR}}$  represents the density of RyR. The function  $P_{\text{RyR}}$  determines the fraction of open RyR and is a deterministic equivalent of the open probability.

We include RyR by a model proposed for bullfrog sympathetic neurons [39], extended by a store-dependent term by [86, 94]. The open state of the RyR is determined by:

$$P_{\text{RyR}} = \left( k_{\text{ryr0}} + \frac{k_{\text{ryr1}} c^3}{k_{\text{ryr2}} + c^3} \right) \frac{c_s^4}{k_{\text{ryr3}} + c_s^4}, \quad (5.2.11)$$

where  $k_{\text{ryr0}}$  represents the  $c$ -independent fraction of open RyR,  $k_{\text{ryr1}}$  represents the  $c$ -dependent fraction of open RyR and  $k_{\text{ryr2}}$  determines the  $\text{Ca}^{2+}$  concentration where the second term is half-maximally activated.

For ASMC, it has been shown that  $[\text{Ca}^{2+}]_i$  oscillations can be elicited with constant  $\text{IP}_3$  concentration [19, 94], demonstrating that the system has a class I feedback mechanism. A class I feedback mechanism means that oscillations are the result of the IPR kinetics, and oscillations of the  $\text{IP}_3$  concentration are not necessary. A class II feedback mechanism requires oscillations of the  $\text{IP}_3$  concentration to produce agonist-induced  $[\text{Ca}^{2+}]_i$  oscillations [89]. Hence, the concentration of  $\text{IP}_3$  appears as parameter  $p$  in our model.

The model for the IPR has been proposed by [19], and is a deterministic version of

the stochastic model of [87]. While  $\text{Ca}^{2+}$  puffs originating from IPR cluster activity are inherently stochastic, it has been shown that periodic  $[\text{Ca}^{2+}]_i$  oscillations can be described accurately by a deterministic model [19].

The current through the IPR is modelled by:

$$J_{\text{IPR}} = k_{\text{IPR}} P_{\text{IPR}} (c_s - c_b), \quad (5.2.12)$$

where the constant  $k_{\text{IPR}}$  represents the density of IPR, and  $P_{\text{IPR}}$  is the open probability.

The authors show that the receptors have two modes, the drive and park mode (see Fig. 5.3). The drive mode has three closed states and one open state. In order to simplify the six state model, the states  $C_1$ ,  $C_3$  and  $O_5$  are neglected, since the probability that IPR are in any of those states is less than 0.03 [19].

The transition rates between park and drive mode are

$$\begin{aligned} q_{24} &= a_{24} + V_{24}(1 - m_{24}h_{24}), \\ q_{42} &= a_{42} + V_{42}m_{42}h_{42}, \end{aligned} \quad (5.2.13)$$

which involve the functions

$$\begin{aligned} a_{42} &= 1.8 \frac{p^2}{p^2 + 0.34}, \\ a_{24} &= 1 + \frac{5}{p^2 + 0.25}, \\ V_{24} &= 62 + \frac{880}{p^2 + 4}, \\ V_{42} &= \frac{110p^2}{p^2 + 0.01}. \end{aligned}$$

When the IPR are in the drive mode, the transition between the states are independent of ligands. The open probability within the drive mode is roughly 0.7. Hence, Cao et al. introduced a new, partially open state  $D$  [19].

The fraction of IPR in the partially open state  $D$  are:

$$\frac{dD}{dt} = q_{42}(1 - D) - \frac{q_{24}q_{62}}{q_{62} + q_{26}}D, \quad (5.2.14)$$

where the transition rate  $q_{24}$  has been rescaled to account for the fact that a transition into the park mode is only allowed from state  $C_2$ .

The open probability of the IPR becomes

$$P_{\text{IPR}} = D \frac{q_{26}}{q_{62} + q_{26}}. \quad (5.2.15)$$

The authors [19] eliminated three gating variables and  $D$  by QSSR

$$\begin{aligned} D &= \frac{q_{42}(q_{62} + q_{26})}{q_{42}q_{62} + q_{42}q_{26} + q_{24}q_{62}}, \\ m_{24} &= m_{24,\infty}, \\ h_{24} &= h_{24,\infty}, \\ m_{42} &= m_{42,\infty}. \end{aligned}$$

The justification of using QSSR to eliminate the gating variables  $m_{24}$ ,  $h_{24}$ ,  $m_{42}$  and  $D$  is entirely based upon comparing the simplified model with experimental data [19]. The authors conclude that the agreement between experimental data and model simulations of the simplified model is sufficiently good that using QSSR is reasonable. We do not investigate the effects of QSSR on this particular model any further.

The steady-state functions are:

$$\begin{aligned} h_{24,\infty} &= \frac{k_{-24}^2}{c_p^2 + k_{-24}^2}, \\ m_{42,\infty} &= \frac{c_b^3}{c_b^3 + k_{42}^3}, \\ m_{24,\infty} &= \frac{c_p^3}{c_p^3 + k_{24}^3}. \end{aligned}$$

The functions  $h_{24,\infty}$  and  $m_{24,\infty}$  depend on the  $\text{Ca}^{2+}$  concentration at the channel pore located inside the SR ( $c_p$ ), which is approximated by a linear function of  $c_s$

$$c_p = c_{p0}c_s/100. \quad (5.2.16)$$

The following functions have been chosen by [19] to generate accurate  $[\text{IP}]_3$ -dependent open probabilities:

$$k_{-42} = 0.41 + 25 \frac{p^3}{p^3 + 274.6}, \quad (5.2.17)$$

$$k_{42} = 0.49 + \frac{0.543p^3}{p^3 + 64}. \quad (5.2.18)$$

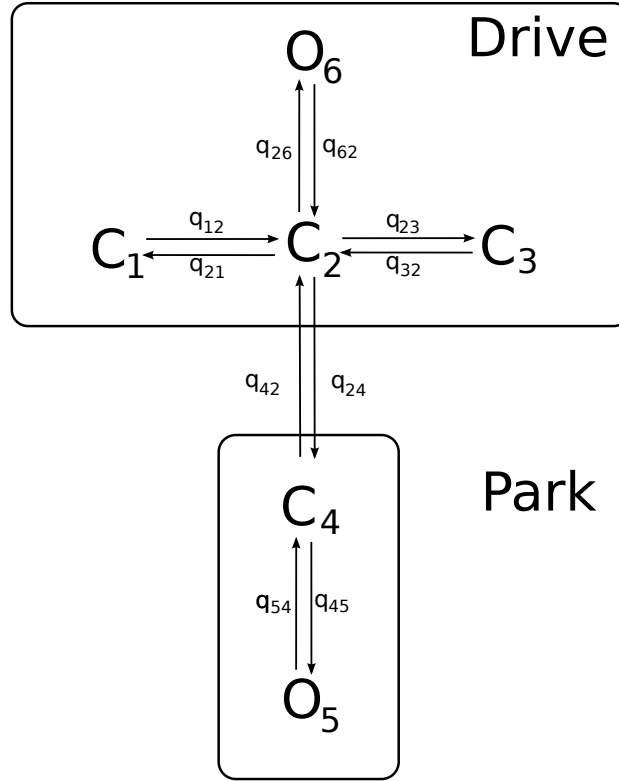


Figure 5.3: Overview of the six-state IPR model, reproduced from [19]. The model has two modes, park and drive. In the park mode the receptor is mostly closed and in the drive mode the receptor is open about 70% of the time. The transitions within a mode are independent of  $\text{Ca}^{2+}$ . The mode transitions  $q_{42}$  and  $q_{24}$  are  $\text{Ca}^{2+}$ -dependent.

The IPR are quickly inhibited by large concentrations of  $c_b$  and recover slowly. Hence, the timescale of the inhibition of the IPR depends on the state of the IPR.

Cao et al. modelled the timescale on which the gating variable  $h_{42}$  evolves by

$$\lambda_{h_{42}} = (1 - D)L + DH, \quad (5.2.19)$$

where  $H$  is significantly larger than  $L$  (see table 5.3).

The flux through the SERCA pump is modelled by

$$J_{\text{SERCA}} = \frac{V_s c^{\text{ns}}}{K_s^{\text{ns}} + c^{\text{ns}}}, \quad (5.2.20)$$

which is a Hill function with Hill coefficient  $\text{ns}$  and maximal pump strength  $V_s$ . This form of the model is taken from [20]. The constant  $K_s$  sets the concentration  $c$  for which the pump is operating at half of its full strength.



### 5.2.2 Calcium transport across the plasma membrane

Elevated  $[IP_3]$  causes an increased  $Ca^{2+}$  influx that is neither voltage-gated nor dependent on the  $Ca^{2+}$  concentration in the SR. These channels are called receptor-operated channels (ROCC), and are modelled by a linear function of  $IP_3$ , as has been done previously [90, 94].

We modify the model of ROCC by a voltage-dependent forcing term, which leads to:

$$J_{ROCC} = V_{rocc}p(V - E_{Ca}), \quad (5.2.21)$$

where the constant  $V_{rocc}$  represents the density of ROCC.

Voltage-gated  $Ca^{2+}$  entry by VGCC is modelled by an activation-gating variable and a Goldman-Hodgkin-Katz driving force:

$$J_{VGCC} = g_{Ca}m_{Vocc}^2V_{Ca}, \quad (5.2.22)$$

as has been previously suggested [58, 94]. The constant  $g_{Ca}$  represents the conductivity,  $m_{Vocc}$  is the activation-gating function, and the function  $V_{Ca}$  represents a driving force which originates from a Goldman-Hodgkin-Katz equation [61]. The activation-gating function for the VGCC is [94]:

$$m_{Vocc} = \frac{1}{1 + \exp(-(V - V_m)/k_m)}, \quad (5.2.23)$$

where  $V_m$  represents the voltage where VGCC are half-maximally activated and  $k_m$  determines the steepness of the activation. The driving force is given by the Goldman-Hodgkin-Katz equation:

$$V_{Ca} = V \frac{c - [Ca]_{ext} \exp(-2VF/(RT))}{1 - \exp(-2VF/(RT))}. \quad (5.2.24)$$

The SOCC model consists of a steady-state open probability (Eq. (5.2.26)) and a dynamic variable, which takes into account that SOCC do not adjust instantaneously to changes in the SR  $Ca^{2+}$  concentration. The equation is:

$$J_{SOCC} = V_{socc}P_{so}(V - E_{Ca}), \quad (5.2.25)$$

which has been adapted from [23];  $V_{socc}$  represents the density of SOCC, and  $P_{so}$  determines the fraction of open receptors (Eq. (5.2.5)) and is the deterministic equivalent to the open probability. Furthermore, we added the voltage-dependent forcing term.

The steady-state open probability of the store-operated  $\text{Ca}^{2+}$  channel is

$$P_{\text{so}}^{\infty} = \frac{K_{\text{SOCC}}^4}{K_{\text{SOCC}}^4 + c_s^4}, \quad (5.2.26)$$

which is modelled as a Hill function with Hill coefficient 4 [23]. The constant  $K_{\text{SOCC}}$  determines where SOCC are half-maximally activated.

The plasma membrane pump for the extrusion of  $\text{Ca}^{2+}$  is modelled by

$$J_{\text{PM}} = \frac{V_p c^{\text{np}} - \omega[\text{Ca}]_{\text{ext}}}{K_p^{\text{np}} + c^{\text{np}}}. \quad (5.2.27)$$

The pump is derived from a Hill function with maximal pumping strength  $V_p$  with Hill coefficient np and half activation constant  $K_p$  [94]. We have added an additional term  $-\omega[\text{Ca}]_{\text{ext}}$  that depends on the external  $\text{Ca}^{2+}$  concentration, which can cause the pump to run in reverse mode [51]. The additional term leads to lower, more realistic fluxes at rest.

### 5.3 Sodium, potassium and chloride transport across the plasma membrane

The big-conductance  $\text{Ca}^{2+}$ -activated  $\text{K}^+$  channels ( $I_{\text{KCa}}$ ) are an important contributor to membrane hyperpolarization [56, 62, 96, 98]. The model for  $I_{\text{KCa}}$  is taken from [82].

The  $\text{Ca}^{2+}$ -activated  $\text{K}^+$  current is

$$I_{\text{KCa}} = g_{\text{KCa}} x_{\text{Ca1},\infty} B(V - E_{\text{K}}), \quad (5.3.1)$$

where  $g_{\text{KCa}}$  is the conductivity,  $x_{\text{Ca1},\infty}$  and  $B$  are gating functions. The gating functions for the  $\text{Ca}^{2+}$ -activated  $\text{K}^+$  current are [82]:

$$\begin{aligned} x_{\text{Ca1},\infty} &= \frac{c^2 + K_4 c}{c^2 + K_4 c(1 + (\alpha/\beta)) + K_4 K_2 (\alpha/\beta)}, \\ B &= \frac{K_1 c x_{\text{Ca1},\infty}}{K_{-1}}, \end{aligned} \quad (5.3.2)$$

which depend on the voltage-dependent transition rates:

$$\begin{aligned}
 K_1 &= 0.85 \exp(0.04V), \\
 K_{-1} &= 0.24 \exp(-0.012V), \\
 K_2 &= 0.000275 \exp\left(\frac{-1.51VF}{RT}\right), \\
 K_4 &= 0.0000125 \exp\left(\frac{-1.99VF}{RT}\right).
 \end{aligned} \tag{5.3.3}$$

The delayed-rectifier  $K^+$  channel ( $I_{Kdr}$ ) further hyperpolarizes the cell. The model is taken from [82] based on work in porcine and canine airway smooth muscle cells [16, 54].

The delayed-rectifier  $K^+$  current is

$$I_{Kdr} = g_{Kdr}(\gamma_{KSS} + (x_{i1,\infty} + x_{i2,\infty})(1 - \gamma_{KSS}))x_{a,\infty}^2(V - E_K), \tag{5.3.4}$$

where  $g_{Kdr}$  is the conductivity. The  $\gamma_{KSS}$  is the ratio of activity at rest [82],  $x_a$  is the voltage-dependent activation-gating function and  $x_{i1,\infty}$ ,  $x_{i2,\infty}$  are voltage-dependent inactivation-gating functions. The activation-gating function  $x_{a,\infty}$  and the inactivation-gating functions  $x_{i1,\infty}$ ,  $x_{i2,\infty}$  of the delayed rectifier  $K^+$  current are [82]:

$$\begin{aligned}
 x_{i1,\infty} &= \frac{1}{1 + \exp((V + 4.3)/7.5)}, \\
 x_{i2,\infty} &= \frac{1}{1 + \exp((V + 4.3)/7.5)}, \\
 x_{a,\infty} &= \frac{1}{1 + \exp((5.5 - V)/6)}.
 \end{aligned} \tag{5.3.5}$$

The  $Ca^{2+}$ -activated  $Cl^-$  channel ( $I_{ClCa}$ ) depolarizes the cell [40]. The model has been constructed by [82] using experimental data of rat tracheal myocytes [81].

The  $Ca^{2+}$ -activated  $Cl^-$  current is modelled by

$$I_{ClCa} = g_{Cl} \frac{V - E_{Cl}}{1 + (Ca_{CT}/c)^3}, \tag{5.3.6}$$

where  $g_{Cl}$  is the conductivity,  $E_{Cl}$  is the Nernst potential of  $Cl^-$  and  $Ca_{CT}$  represents the  $Ca^{2+}$  concentration for which the  $Ca^{2+}$ -activated  $Cl^-$  channel is half-maximally activated.

Furthermore, contributions of  $Na^+$ - $K^+$  ATPases ( $I_{NaK}$ ), background  $Na^+$  ( $I_{bNa}$ ) and  $K^+$  ( $I_{bK}$ ) channels are included.

The  $\text{Na}^+$ - $\text{K}^+$  exchanger current is

$$I_{\text{NaK}} = I_{\text{NaK,max}} \frac{[K]_{\text{ext}}}{K_{\text{mK}} + [K]_{\text{ext}}} \frac{[\text{Na}]_{\text{int}}}{K_{\text{mNa}} + [\text{Na}]_{\text{int}}}, \quad (5.3.7)$$

where  $I_{\text{NaK,max}}$  is the maximum current,  $[K]_{\text{ext}}$  is the extracellular  $\text{K}^+$  concentration,  $K_{\text{mK}}$  is the  $\text{K}^+$  concentration for which the first term is half of its maximum,  $[\text{Na}]_{\text{int}}$  is the intracellular  $\text{Na}^+$  concentration and  $K_{\text{mNa}}$  is the  $\text{K}^+$  for which the second term is half of its maximum.

The background currents for  $\text{K}^+$  and  $\text{Na}^+$  are

$$I_{\text{bK}} = g_{\text{bK}}(V - E_{\text{K}}), \quad (5.3.8)$$

$$I_{\text{bNa}} = g_{\text{bNa}}(V - E_{\text{Na}}), \quad (5.3.9)$$

where  $g_{\text{bK}}$  and  $g_{\text{bNa}}$  are the conductivities of the background  $\text{K}^+$  and  $\text{Na}^+$  currents and  $E_{\text{K}}$  and  $E_{\text{Na}}$  (Eq. (5.2.8)) are the respective Nernst potentials of  $\text{K}^+$  and  $\text{Na}^+$ .

In their model, Roux et al. [82] take non-specific  $\text{Ca}^{2+}$ ,  $\text{K}^+$  and  $\text{Na}^+$  channels into account but mention that their contributions are very small, hence, we omit them from the model.

Parameter values can be found in the table below:

Parameter	Value	Parameter	Value
$c_{p0}$	120 $\mu\text{M}$	$\gamma_1$	100
$q_{26}$	10500 $s^{-1}$	$q_{62}$	4010 $s^{-1}$
$\gamma_2$	10	$H$	40 $s^{-1}$
$L$	1.0 $s^{-1}$	$k_{\text{diff}}$	10 $s^{-1}$
$k_{\text{leak}}$	0.0032 $s^{-1}$	$K_s$	0.26 $\mu\text{M}$
$V_s$	13.25 $\mu\text{M}s^{-1}$	$n_s$	1.75
$K_{\text{socc}}$	450 $\mu\text{M}$	$V_{\text{rocc}}$	0.0005 $\mu\text{S } \mu\text{mol}^{-1}$
$V_{\text{socc}}$	0.0015 $\mu\text{S } s^{-1}$	$K_p$	0.5 $\mu\text{M}$
$V_p$	0.614 nA	$n_p$	2
$k_{\text{IPR}}$	0.07 $s^{-1}$	$k_{24}$	0.35 $\mu\text{M}$
$k_{-24}$	80 $\mu\text{M}$	$k_{\text{ryr}0}$	0.0072 $s^{-1}$
$T_{\text{socc}}$	30 s	$k_{\text{RyR}}$	0.1 $s^{-1}$
$k_{\text{ryr}1}$	0.12 $s^{-1}$	$k_{\text{ryr}2}$	0.33 $\mu\text{M}$
$k_{\text{ryr}3}$	700 $\mu\text{M}$	$T$	310 K
$C_m$	0.00002 $\mu\text{F}$	$R$	8314.4621 mJ (mol K) $^{-1}$
$F$	96485.3415 C mol $^{-1}$	$[K]_{\text{ext}}$	8 mM
$[K]_{\text{int}}$	120 mM	$[Na]_{\text{ext}}$	130 mM
$[Na]_{\text{int}}$	12 mM	$[Cl]_{\text{int}}$	55 mM
$[Cl]_{\text{ext}}$	140 mM	$[Ca]_{\text{ext}}$	2 mM
$g_{\text{Kdr}}$	0.035 $\mu\text{S}$	$\gamma_{\text{Kss}}$	0.15
$g_{\text{Ca}}$	0.009 $\mu\text{S } \mu\text{M}^{-1}$	$V_m$	-18 mV
$\delta$	1.449 mol (C l) $^{-1}$	$k_m$	17.5 mV
$g_{\text{KCa}}$	2.45 $\mu\text{S}$	$\alpha$	280 $s^{-1}$
$\beta$	480 $s^{-1}$	$g_{\text{Cl}}$	0.01 $\mu\text{S}$
$Ca_{\text{CT}}$	0.5 $\mu\text{M}$	$K_{\text{mnsCa}}$	1.2 mM
$g_{\text{bK}}$	0.008729 $\mu\text{S}$	$I_{\text{NaKMax}}$	0.7 nA
$K_{\text{mK}}$	1 mM	$K_{\text{mNa}}$	40 mM
$g_{\text{bNa}}$	0.003263 $\mu\text{S}$	$\omega$	$2.8 \cdot 10^{-6} (\mu\text{M})^{-1}$

Table 5.1: Parameter values for model as presented in 5.2.

# 6

## Contributions of plasma membrane calcium channels

### 6.1 Importance of voltage-gated $\text{Ca}^{2+}$ entry

In this section we look at the contributions of VGCC during agonist-induced and depolarization-induced  $[\text{Ca}^{2+}]_i$  oscillations in mouse airway smooth muscle cells. We use experimental data on blocking VGCC to parametrize our mathematical model. The experimental data presented in the first two panels in Fig. 6.1 and the first two rows in Fig. 6.2 in chapter 6 were obtained by Jun Chen and Michael J. Sanderson at the University of Massachusetts Medical School. The experimental measurements show changes in fluorescence intensity, corresponding to changes in cytosolic  $\text{Ca}^{2+}$  concentration, in airway smooth muscle cells in mice lung slices. A detailed description of the experimental procedure can be found in [12].

This data was used to adjust the parameters of the voltage-gated  $\text{Ca}^{2+}$  channels ( $g_{\text{Ca}}$ ,  $k_{\text{m}}$  and  $V_{\text{m}}$ ), such that the mathematical model reproduced the qualitative behaviour. By observing the effect of blocking VGCC on  $[\text{Ca}^{2+}]_i$  oscillations, we get an indirect measure

of the relative contribution of VGCC to total influx for the two different stimuli.

First, the cells are stimulated by 50 mM KCl, which causes depolarization and increased voltage-gated  $\text{Ca}^{2+}$  entry. Internal stores overflow and CICR follows, as can be seen in the top panel of Fig. 6.1. Subsequently inhibiting the VGCC by 10  $\mu\text{M}$  nifedipine abolishes the slow  $[\text{Ca}^{2+}]_i$  oscillations quickly (see middle panel of Fig. 6.1). Model simulations for depolarization-induced  $[\text{Ca}^{2+}]_i$  oscillations by 50 mM KCl and subsequent blocking of VGCC by nifedipine are shown in the bottom panel of Fig. 6.1.

In the top row of Fig. 6.2 the cells were treated with 400 nM MCh, which causes fast  $[\text{Ca}^{2+}]_i$  oscillations (periods of about 1.3 s). The second row shows oscillations triggered by 400 nM MCh (left panel), followed by blocking VGCC by 100  $\mu\text{M}$  nifedipine (right panel). The oscillations gradually slow down to a period of approximately 2.3 s. Hence, the frequency has reduced by roughly a half after blocking VGCC. The corresponding model simulations are shown in the bottom panel of Fig. 6.2.

Both experiments are reproduced in the mathematical model. During depolarization-induced  $[\text{Ca}^{2+}]_i$  oscillations the flux through the VGCC is the largest  $\text{Ca}^{2+}$  influx (see Fig. 6.3, top panel). The depolarization leads to substantial opening VGCC and the current through VGCC increases nearly threefold. During agonist-induced  $[\text{Ca}^{2+}]_i$  oscillations, the contributions due to VGCC and SOCC are of similar magnitude (see Fig. 6.3, bottom panel). We will make predictions about blocking SOCC in section 6.2.

Agonist-induced  $[\text{Ca}^{2+}]_i$  oscillations are accompanied by oscillations in the membrane voltage (see Fig. 6.4). During  $\text{Ca}^{2+}$  release from the SR, the cell hyperpolarizes to nearly -54 mV and during the reuptake of  $\text{Ca}^{2+}$  the cell depolarizes to about -44 mV. The range about which the voltage oscillates is consistent with experimental recordings by [98].

In the bottom panels of Fig. 6.4 we compare a model with oscillating membrane voltage (blue curves) to a model with voltage fixed at the resting value of  $V_{\text{rest}} = -46.7$  mV (red curves). Oscillations in the membrane voltage do not have a significant effect on  $[\text{Ca}^{2+}]_i$  oscillations. Transient changes in the membrane voltage do not affect intracellular  $\text{Ca}^{2+}$  handling significantly.

For a measurable reduction in frequency, hyperpolarization has to be sustained over many  $\text{Ca}^{2+}$  oscillation periods, and consequently VGCC have to be inhibited for a long period of time. During agonist-induced  $[\text{Ca}^{2+}]_i$  oscillations, the timescale of the  $[\text{Ca}^{2+}]_i$  oscillations is set by IPR kinetics. While a reduced total  $\text{Ca}^{2+}$  concentration, i.e., the available  $\text{Ca}^{2+}$  in the cytosol and SR, manifests in slower oscillations,  $\text{Ca}^{2+}$  is extruded

slowly compared to the timescale of individual spikes in  $[\text{Ca}^{2+}]_i$ .

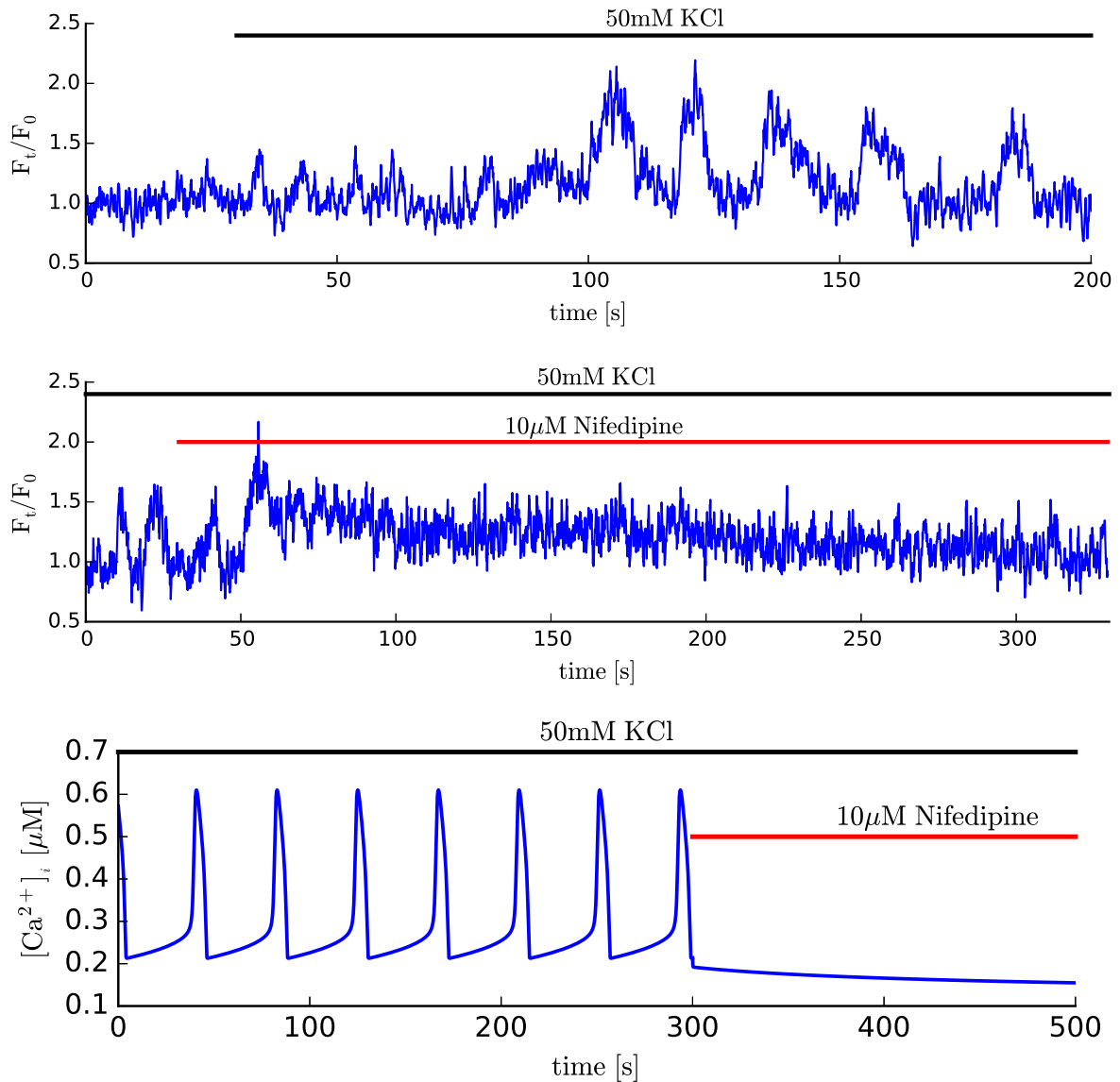


Figure 6.1: Intracellular  $[\text{Ca}^{2+}]_i$  oscillations in mouse airway smooth muscle cells induced by depolarization by 50 mM KCl. Depolarization causes elevated  $\text{Ca}^{2+}$  entry through VGCC and leads to overfilling of internal stores. The result is periodic CICR with periods about 30 s (top panel). Subsequently blocking VGCC by 10  $\mu\text{M}$  nifedipine causes the oscillations to stop abruptly (middle panel). The elevated cytosolic  $\text{Ca}^{2+}$  is extruded and the  $\text{Ca}^{2+}$  concentration slowly returns to values close to the resting state before depolarization. Measurements are shown as relative fluorescence values  $F_t/F_0$ . Simulations of oscillations in the  $\text{Ca}^{2+}$  concentration by depolarization by 50 mM KCl (bottom panel). Blocking VGCC, in the model, leads to an abrupt stop of  $[\text{Ca}^{2+}]_i$  oscillations and the plateau of  $\text{Ca}^{2+}$  concentration decreases back to baseline. The model results are shown in  $\mu\text{M}$ .



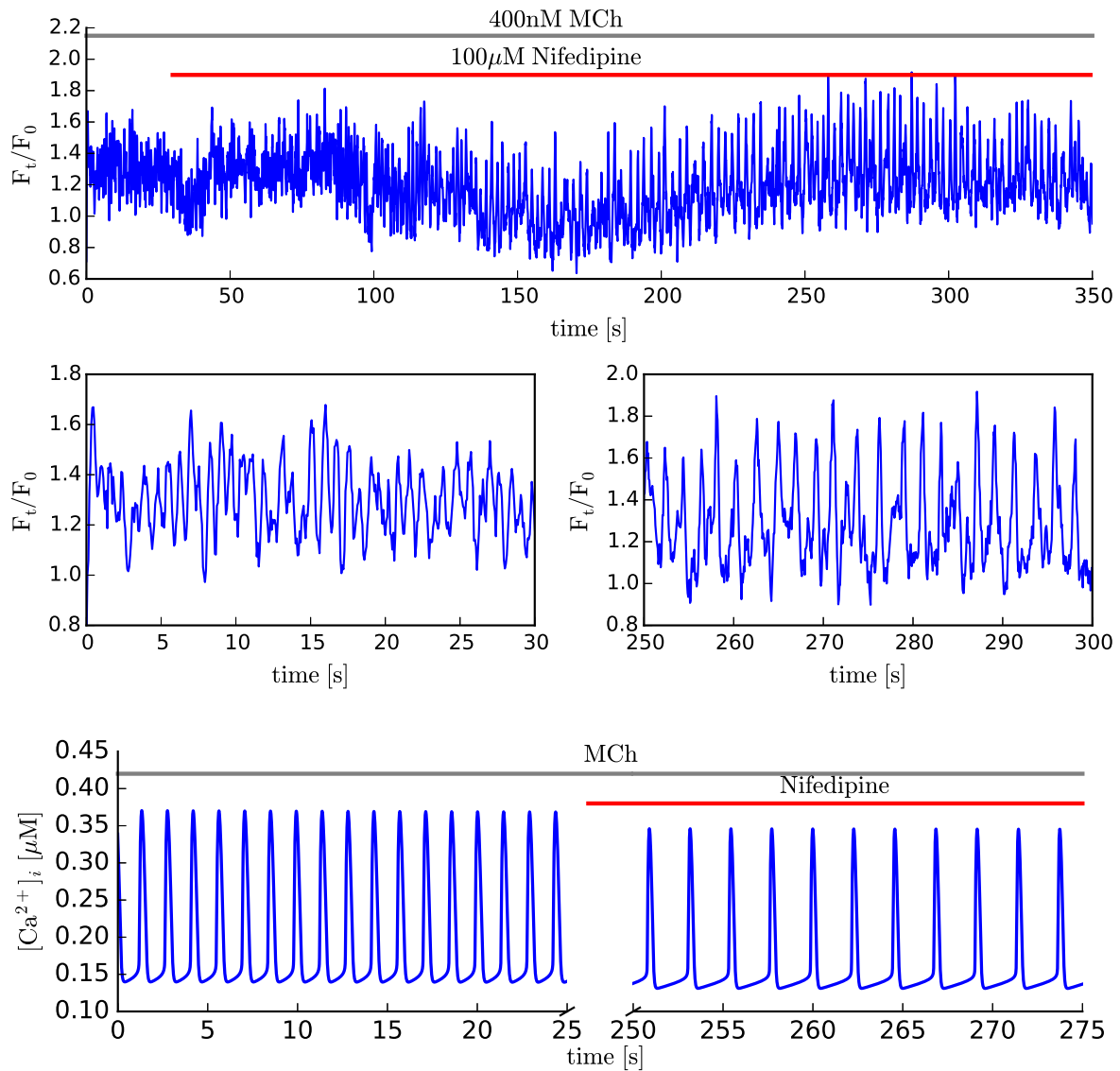


Figure 6.2: The top panel shows oscillations triggered by 400 nM MCh followed by consecutively blocking voltage-gated  $Ca^{2+}$  entry by 100  $\mu$ M nifedipine. The first 30 s (middle left) show fast oscillations with periods of about 1 s. Nifedipine slows down the oscillations to a period of about 2 s (middle right). The third row shows model simulations. An agonist binding to the G-coupled receptor leads to the production of  $IP_3$ . For the simulations of the left panel  $[IP_3] = 0.05 \mu$ M. The period is in good agreement with the results of Fig. 6.2 (about 1.3 s). Blocking VGCC by nifedipine leads to slower oscillations with period about 2.3 s (Note the different scale on the x-axis).

## 6.2 Importance of store-operated $Ca^{2+}$ entry

It has been observed by various groups that SOCC are upregulated under conditions where the SR  $Ca^{2+}$  concentration is low in ASMC [11, 72, 75]. Furthermore, some groups argue that the  $Ca^{2+}$  influx during agonist-induced oscillations is largely due to SOCC [11, 91]. This hypothesis is consistent with all aforementioned findings. We simulate the

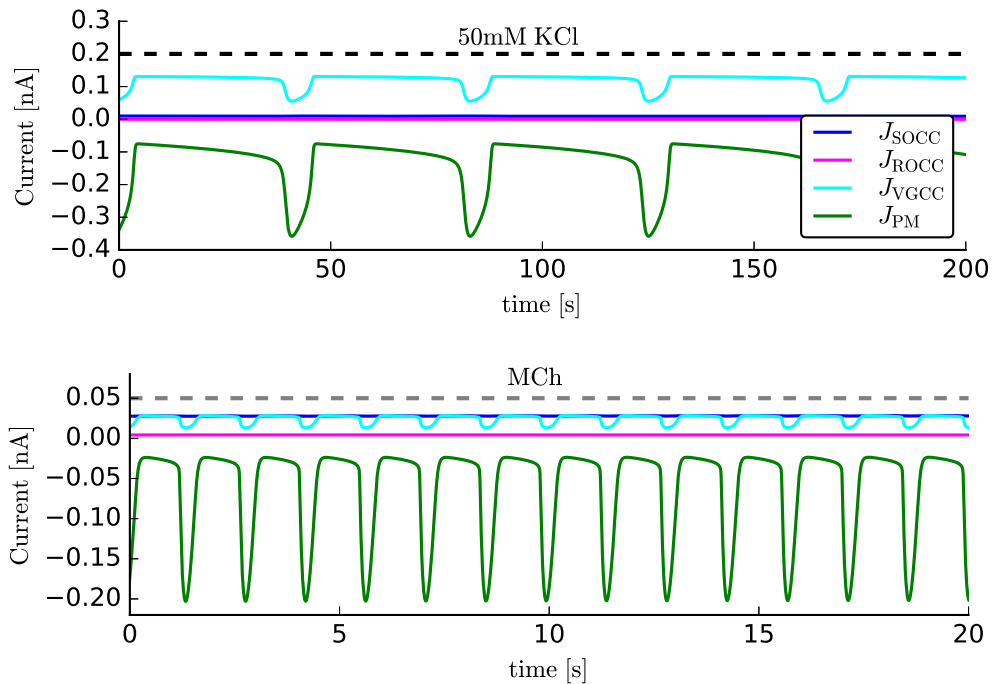


Figure 6.3: Simulations of the currents through plasma membrane  $\text{Ca}^{2+}$  channels for different stimuli. The top panel shows the currents of SOCC, ROCC, VGCC and PM for depolarization-induced  $[\text{Ca}^{2+}]_i$  oscillations (50 mM KCl). The bottom panel shows the same currents for agonist-induced  $[\text{Ca}^{2+}]_i$  oscillations ( $[\text{IP}_3] = 0.05 \mu\text{M}$ ).

effect of partially blocking SOCC on  $[\text{Ca}^{2+}]_i$  oscillations. The  $[\text{Ca}^{2+}]_i$  oscillations slow down with reduced  $\text{Ca}^{2+}$  influx through SOCC as can be seen in the top panel of Fig. 6.5. We show two time series with the contributions of SOCC reduced to 50% (middle panel of Fig. 6.5) and to 20% (bottom panel in Fig. 6.5).

If the influx through SOCC is reduced to less than roughly 10%, the  $[\text{Ca}^{2+}]_i$  oscillations cease entirely. We simulate blocking SOCC completely and compare this to agonist-induced  $[\text{Ca}^{2+}]_i$  oscillations in a  $\text{Ca}^{2+}$ -free medium (Fig. 6.6). As predicted in Fig. 6.5, the  $[\text{Ca}^{2+}]_i$  oscillations cease completely. Furthermore, it takes about three times as long as in the absence of extracellular  $\text{Ca}^{2+}$ . The difference of blocking SOCC to simulations in a  $\text{Ca}^{2+}$ -free medium is that ROCC and VGCC are still transporting  $\text{Ca}^{2+}$  into the cell.

Based on our simulations we make the following predictions:

- During agonist-induced  $[\text{Ca}^{2+}]_i$  oscillations the influx through SOCC is larger than the influx through VGCC. This balance changes to a much stronger contribution of VGCC in depolarized cells (see Fig. 6.3).
- Fully blocking VGCC has the same effect on the frequency of  $[\text{Ca}^{2+}]_i$  oscillations as

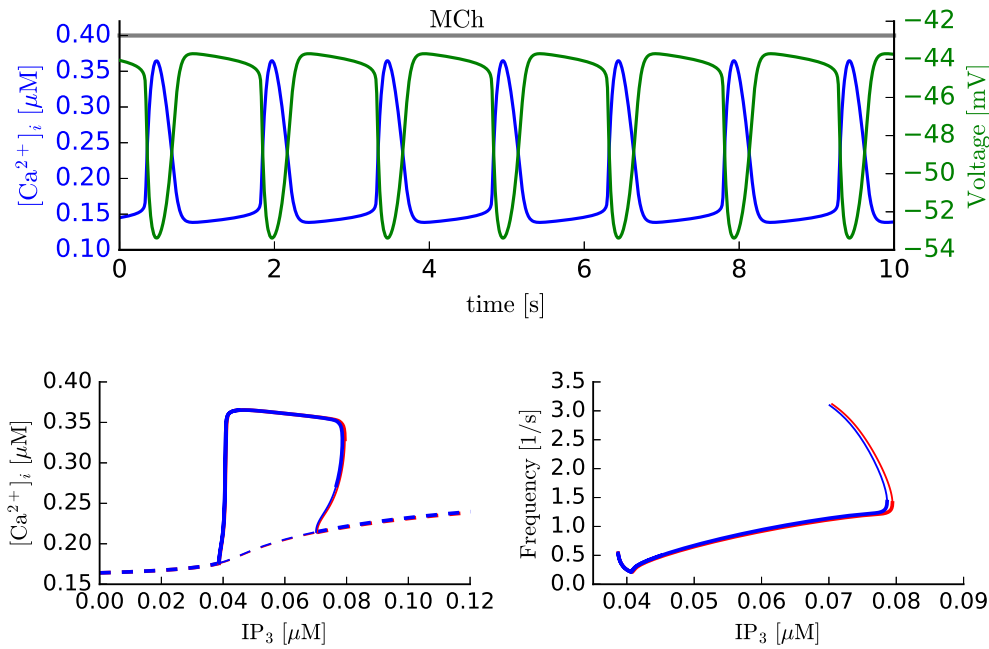


Figure 6.4: Top panel: Simulations of  $[Ca^{2+}]_i$  oscillations triggered by  $[IP_3] = 0.05 \mu M$  and corresponding changes in Voltage across the plasma membrane. Calcium release from the SR is accompanied by hyperpolarization of the cell, followed by a depolarization during the reuptake of  $Ca^{2+}$  by the SR. Bottom panel: Comparison of models with oscillating voltage (blue curves) versus fixed voltage at  $V_{rest} = -46.7$  mV (red curves). The left panel shows the resting state (dashed lines) and the maximum of the  $Ca^{2+}$  concentration during oscillations (solid lines) for different values of  $IP_3$ -concentration. Thick lines indicate stable solutions and thin lines indicate unstable solutions. The frequency as a function of  $IP_3$  is shown in the right panel. A higher  $IP_3$ -concentration is associated with a higher oscillation frequency.

blocking SOCC partially to about 25% of its full strength (see Fig. 6.5). Blocking SOCC partially slows down oscillations of  $[Ca^{2+}]_i$ .

- If the influx through SOCC is completely blocked,  $[Ca^{2+}]_i$  oscillations disappear. Our model predicts that it takes about three times longer until the  $[Ca^{2+}]_i$  oscillations cease when SOCC are fully blocked compared to agonist-induced  $[Ca^{2+}]_i$  oscillations in a  $Ca^{2+}$ -free medium (see Fig. 6.6).

These predictions remain to be tested experimentally by our collaborators.

### 6.3 Dynamics of store-operated $Ca^{2+}$ channels

Given the prediction that SOCC is the most significant  $Ca^{2+}$ -entry pathway during agonist-induced  $[Ca^{2+}]_i$  oscillations, a natural question to investigate is how the SOCC

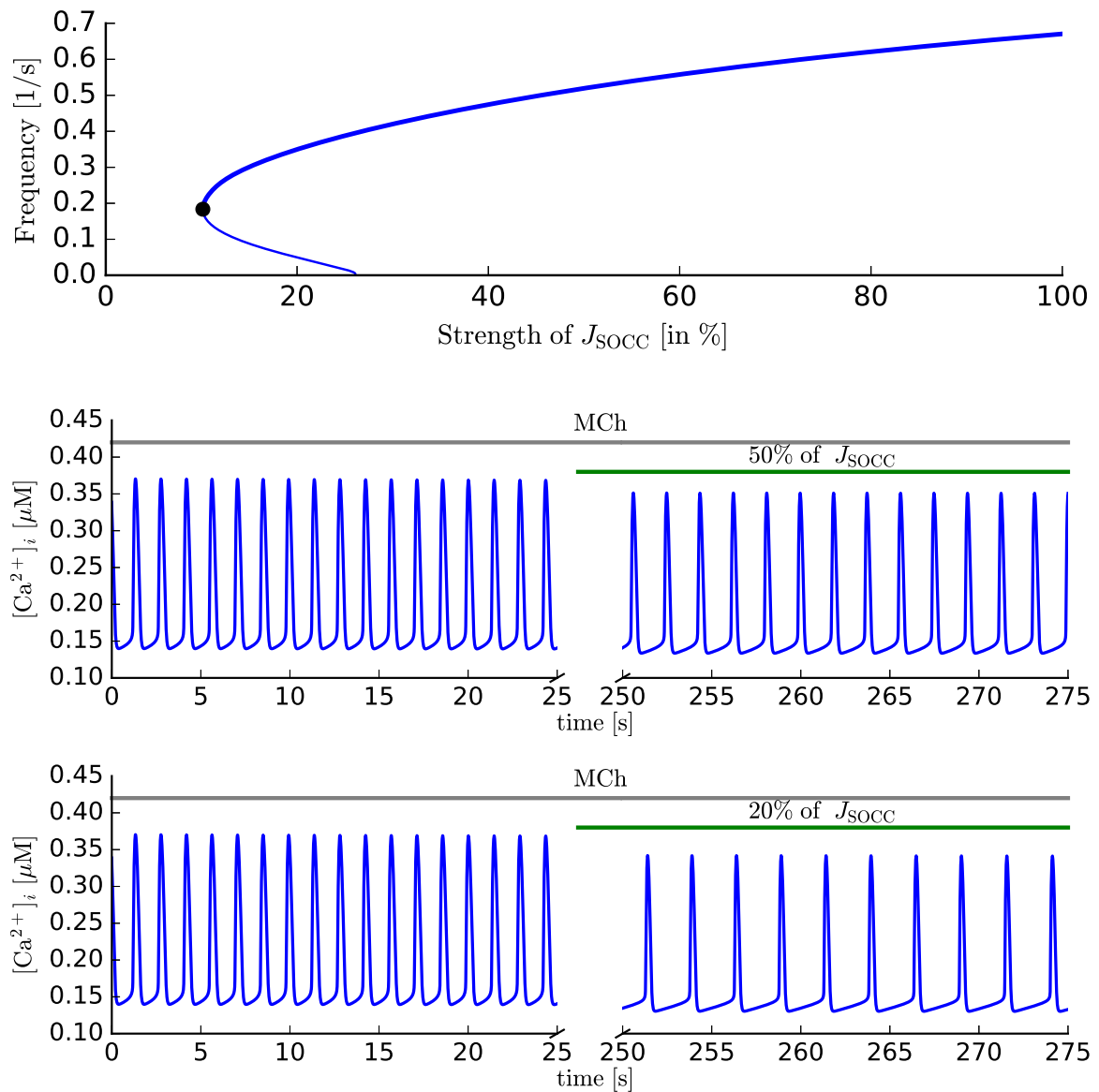


Figure 6.5: The top panel shows simulations of partially blocking  $J_{\text{SOCC}}$  for fixed concentration of  $[\text{IP}_3] = 0.05 \mu\text{M}$ . The x-axis shows the strength of  $J_{\text{SOCC}}$  relative to the full strength. Thick lines indicate stable solutions and thin lines indicate unstable solutions. The black dot indicates where unstable and stable solutions meet and disappear. To the left of the black dot, no stable oscillations are found. The middle and bottom panel show stable oscillations of  $[\text{Ca}^{2+}]_i$  at  $[\text{IP}_3] = 0.05 \mu\text{M}$ , followed by partially blocking  $J_{\text{SOCC}}$  (50% and 20% of the full strength respectively).

gating kinetics affects oscillations of  $[\text{Ca}^{2+}]_i$ . Store-operated  $\text{Ca}^{2+}$  channels are controlled by a complex set of reactions. Stromal interaction molecules (STIM1 and STIM2) are located in the SR membrane. STIM are mobile and able to oligomerize, yet it is not clear how many molecules form oligomers [46]. STIM molecules function as  $\text{Ca}^{2+}$  sensors to the  $\text{Ca}^{2+}$  concentration in the SR. STIM2 tend to form oligomers for higher  $\text{Ca}^{2+}$  concentration in the SR compared to STIM1 [1, 46]. STIM1 oligomers form at lower

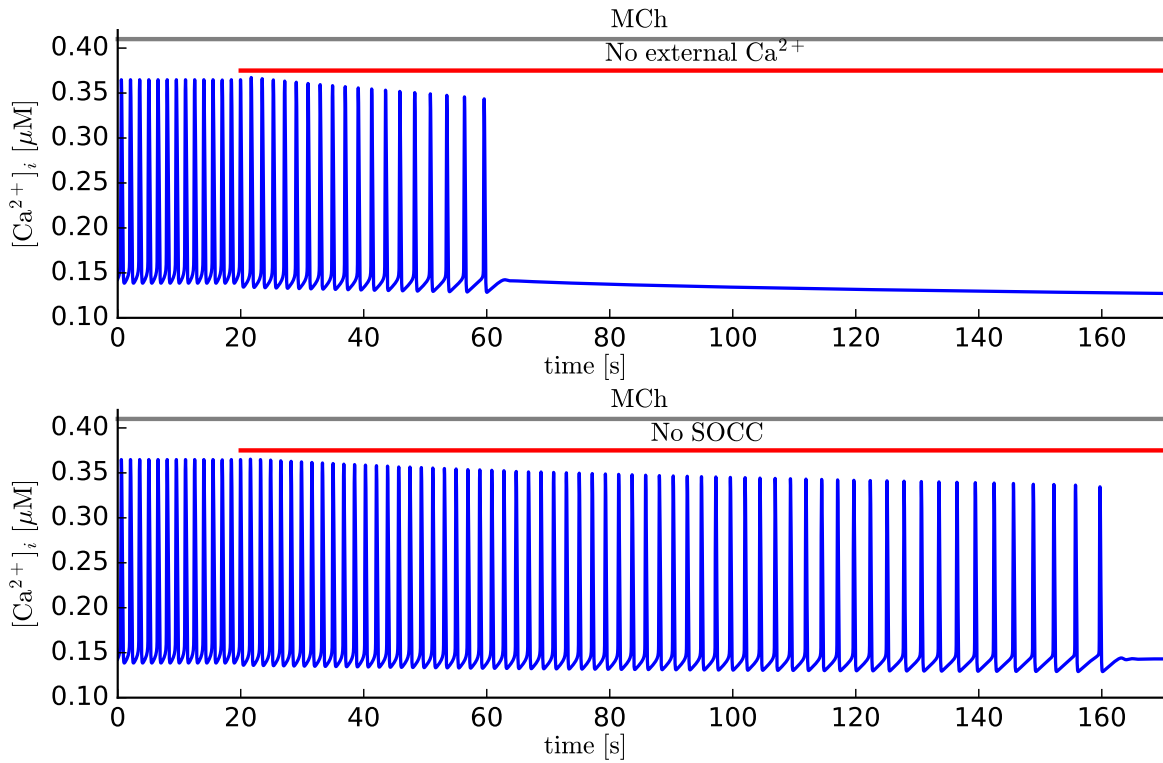


Figure 6.6: The top panel shows  $[Ca^{2+}]_i$  oscillations stimulated by  $[IP_3] = 0.05 \mu M$  in the absence of extracellular  $Ca^{2+}$ . During the oscillations the cell loses  $Ca^{2+}$  and the oscillations cease after 40 s. In the bottom panel the cell is subjected to the same stimulus and then the SOCC are blocked. Blocking SOCC stops the oscillations after about 140 s.

$Ca^{2+}$  concentration in the SR, but lead to a stronger  $Ca^{2+}$  influx through Orai proteins. The STIM colocalize near Orai proteins located in the plasma membrane. There are three Orai homologs (Orai1, Orai2 and Orai3). STIM bind to N- and C-terminals of the Orai proteins and induce conformational changes in the Orai proteins [1, 46, 69, 76]. Ong et al. suggest that STIM2 activity promotes mobility of STIM1 and supports puncta formation with Orai under conditions of low agonist concentration and minimal  $Ca^{2+}$  store depletion. This increases the agonist sensitivity of SOCC [69].

A model with a single gating variable for the open probability ( $P_{so}$ ) and adaptation time ( $T_{socc}$ ), taking the delay between  $Ca^{2+}$  depletion of the SR and channel opening into account, certainly does not do justice to the complex channel kinetics. Yet, simple models are a first step to study the effect of different gating kinetics on the  $[Ca^{2+}]_i$  oscillations. The adaptation time determines how rapidly SOCC react to changes in  $[Ca^{2+}]_{SR}$  (Eq. (5.2.5)). For small values of  $T_{socc}$  the SOCC reach their steady-state open probability ( $P_{so}^\infty$ ) rapidly and large values of  $T_{socc}$  cause a longer delay between the open probability and  $P_{so}^\infty$ .

A comparison of SR  $\text{Ca}^{2+}$  concentrations during agonist-induced  $[\text{Ca}^{2+}]_i$  oscillations for different values of  $T_{\text{socc}}$  can be seen in Fig. 6.7. The counter-intuitive result is that the SR  $\text{Ca}^{2+}$  concentration is not significantly affected by the SOCC gating kinetics (Fig. 6.7, top panel).

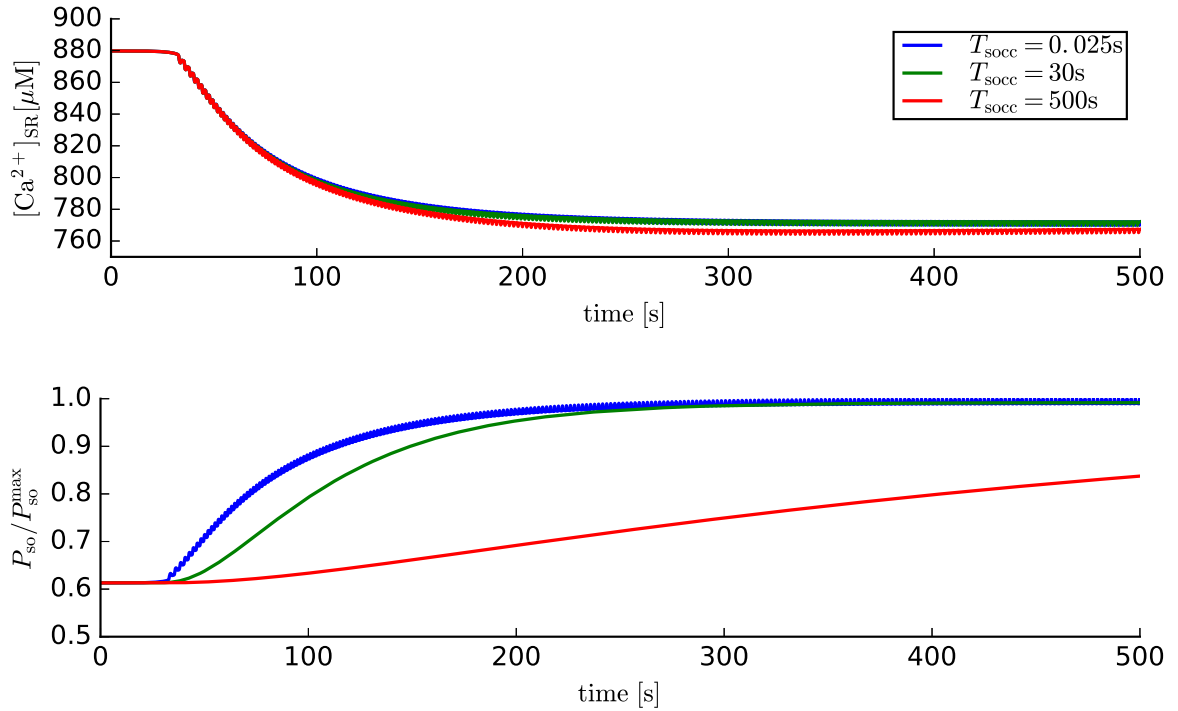


Figure 6.7: Comparison of  $[\text{Ca}^{2+}]_i$  oscillations with different SOCC gating kinetics. Oscillations have been triggered by  $[\text{IP}_3] = 0.045 \mu\text{M}$ . The constant  $T_{\text{socc}}$  represents the adaptation time with which SOCC adapts to changes in the SR  $\text{Ca}^{2+}$  concentration. The top panel shows the  $\text{Ca}^{2+}$  concentration in the SR, which decreases slowly over many oscillation periods and plateaus near 80% of the resting value for different  $T_{\text{socc}}$ . The bottom panel shows the relative open probability of SOCC for different adaptation times. The SOCC adaptation time has little influence on the SR  $\text{Ca}^{2+}$  concentration. Note that for  $T_{\text{socc}} = 0.0025 \text{ s}$  the SOCC open probability oscillates and for  $T_{\text{socc}} = 500 \text{ s}$  the SOCC open probability increases slowly in a non-oscillating manner.

During each  $\text{Ca}^{2+}$  oscillation the SR only gets minimally depleted and the  $\text{Ca}^{2+}$  loss of the SR becomes significant only after many oscillation cycles. Furthermore, agonist-induced  $[\text{Ca}^{2+}]_i$  oscillations do not fully deplete the SR; the  $\text{Ca}^{2+}$  concentration in the SR plateaus around 80% of the resting value. Hence, while SOCC are crucial in sustaining  $[\text{Ca}^{2+}]_i$  oscillations, their gating kinetics do not affect the cytosolic  $\text{Ca}^{2+}$  signal significantly.

Note, that the SOCC open probability oscillates for fast adapting channels (bottom panel, blue curve) whereas slower kinetics leads to gradual opening of SOCC (bottom panel, green and red curve). These findings suggest that modellers who are interested only in whole-cell  $[\text{Ca}^{2+}]_i$  oscillations may not need a detailed model of SOCC gating kinetics.



# 7

## Discussion of model predictions

In the second part of the thesis we focus on the role of VGCC, SOCC and voltage dynamics in airway smooth muscle cells. Our work is based on the work on plasma membrane ion channels by [82]. We have adapted their models for  $K^+$ ,  $Na^+$  and  $Cl^-$  channels, and use models for VGCC and ROCC from [94]. The model for SOCC is from [23].

Roux et al. used forced equations to mimic the release of  $Ca^{2+}$  from internal stores and studied the voltage dynamics of ASMC. We, on the other hand, use a model for  $Ca^{2+}$  handling that allows  $[Ca^{2+}]_i$  oscillations based on  $Ca^{2+}$  release through  $IP_3$ -receptors [19] and ryanodine receptors [94] and reuptake by the SR through pumps.

Roux et al. find that cholinergic stimulation (e.g., stimulation by an agonist) does not lead to substantial  $Ca^{2+}$  influx through VGCC. We confirm this indirectly by demonstrating the reduction of the agonist-induced  $[Ca^{2+}]_i$  oscillation frequency in response to blocking voltage-gated  $Ca^{2+}$  entry.

When ASMC are depolarized (by 50 mM KCl) increased  $Ca^{2+}$  influx results in overfilling of the SR and CICR. Blocking VGCC stops depolarization-induced  $[Ca^{2+}]_i$  oscillations abruptly. This shows that voltage-gated  $Ca^{2+}$  entry is the main  $Ca^{2+}$  entry pathway in depolarized conditions.



In summary, our modelling shows that voltage-gated  $\text{Ca}^{2+}$  entry is the main driving force behind CICR when ASMC are in conditions of sustained depolarization, e.g., when the extracellular ion concentrations change. Agonists that trigger  $[\text{Ca}^{2+}]_i$  oscillations do not result in sustained depolarizations or hyperpolarizations. Only sustained and significant changes in membrane voltage affect the  $\text{Ca}^{2+}$  handling significantly. The main  $\text{Ca}^{2+}$  influx during agonist-induced  $[\text{Ca}^{2+}]_i$  oscillations is via SOCC.

Spatial inhomogeneities may affect the depolarization and hyperpolarization during  $[\text{Ca}^{2+}]_i$  oscillations. The hyperpolarization is mainly established by the big-conductance  $\text{K}^+$  and the delayed-rectifier  $\text{K}^+$  channels. Depolarization is mainly induced by the activity of the  $\text{Ca}^{2+}$ -activated  $\text{Cl}^-$  channels. In our case these channels “see” the cytosolic  $\text{Ca}^{2+}$  concentration whereas in reality the  $\text{Ca}^{2+}$  at their respective channel mouth may be very different. Yet, the time course of the membrane potential in our model is consistent with recordings by [98].

Our results are in contrast with a conclusion drawn by [96]. The authors measure the effect of L-Type VGCC blockers in isolated mouse ASMC. They find that specific VGCC blockers are a potent drug to reverse the MCh-induced contraction of ASMC. From this finding they deduce that the VGCC are the major contributor to  $\text{Ca}^{2+}$  influx during agonist-induced contraction. They employ a protocol of depolarization (by 20 mM KCl) combined with MCh. Such a depolarization upregulates VGCC and shifts the balance to a stronger contribution of VGCC compared to SOCC.

We predict that changes in voltage during agonist-induced  $[\text{Ca}^{2+}]_i$  oscillations do not have a significant effect on  $\text{Ca}^{2+}$  oscillation frequency. The  $\text{Ca}^{2+}$  signaling components that set the timescale of agonist-induced  $[\text{Ca}^{2+}]_i$  oscillations are the IPR and the refilling of internal stores. Changes in voltage only manifest by changes in total  $\text{Ca}^{2+}$  available inside the cell. Significant changes in the total available  $\text{Ca}^{2+}$  occur much slower than individual oscillations in  $[\text{Ca}^{2+}]_i$ .

In ASMC there is evidence that SOCC are upregulated when SR  $\text{Ca}^{2+}$  concentration is sufficiently depleted [3, 4, 70, 75]. We predict that partially blocking SOCC leads to a reduced frequency of  $[\text{Ca}^{2+}]_i$  oscillations. Furthermore, blocking SOCC entirely leads to a complete stop of  $[\text{Ca}^{2+}]_i$  oscillations. Our model shows that fully blocking SOCC stops  $[\text{Ca}^{2+}]_i$  oscillations, but it takes about three times longer compared to oscillations with all influxes blocked (such as in  $\text{Ca}^{2+}$ -free medium).

There are two remaining questions concerning the role of SOCC during  $[\text{Ca}^{2+}]_i$  oscillations in ASMC.

1. To what extent is the SR depleted during sustained  $[Ca^{2+}]_i$  oscillations?

Our mathematical model shows that sustained  $[Ca^{2+}]_i$  oscillations do not fully deplete the SR but rather that SR  $Ca^{2+}$  concentration plateaus around 80% of the resting  $Ca^{2+}$  concentration. The depletion of the SR  $Ca^{2+}$  depends on the amplitude of the  $[Ca^{2+}]_i$  oscillations, as well as on the size of the SR, which is different for different species. Hence, the exact value of the plateau found in our simulations might not be universally valid. However, the existence of a plateau demonstrates that stable  $[Ca^{2+}]_i$  oscillations are possible without dramatically depleting the SR. We discuss the general caveats of the mathematical model at the end of this chapter.

2. Given that agonist-induced  $[Ca^{2+}]_i$  oscillations do not lead to dramatic depletion of the SR, what are the contributions of SOCC to  $Ca^{2+}$  influx during submaximal depletion of the SR  $Ca^{2+}$  concentration?

Sweeney et al. [91] show that the SOCC contributes significantly to agonist-induced contraction in rat and human ASMC. They argue that the maintenance of strong contraction is due to significant  $Ca^{2+}$  influx through SOCC when cells are stimulated by ACh. We confirm this by blocking SOCC in our mathematical model and find that  $[Ca^{2+}]_i$  oscillations stop after over 2 minutes. While the quantitative prediction of the time it takes until the oscillations cease should be treated with caution, we believe that the qualitative prediction that the oscillations cease is robust.

The type of model (ordinary differential equations) is appropriate when  $Ca^{2+}$  and  $IP_3$  are in sufficient supply and homogeneously distributed. For low cellular  $Ca^{2+}$  concentrations the stochastic nature of  $IP_3$ -receptor kinetics becomes more important, leading to longer interspike intervals when  $[Ca^{2+}]_i$  is low during stimulation in a  $Ca^{2+}$ -free medium or when SOCC are blocked (Fig. 6.6). Likewise spatial inhomogeneity in the distribution of IPR and RyR may affect the time it takes until oscillations cease.

Stromal interaction molecules (STIM1 and STIM2) are located in the SR membrane and have a  $Ca^{2+}$  binding side exposed to  $Ca^{2+}$  in the SR. Upon depletion of the SR, STIM1 undergo a conformational change that increases their mobility and they oligomerize and collocate near Orai proteins in the plasma membrane pump. The binding of STIM1 to C- and N-terminals of Orai proteins provide the gating mechanism of SOCC [1, 46, 76].

STIM2 are mobilized by minimal depletion of the SR. The activity of STIM2 may explain the strong contribution of SOCC to  $Ca^{2+}$  influx during agonist-induced  $[Ca^{2+}]_i$  oscillations while the SR is not substantially depleted [69]. The time course of this SOCC

gating mechanism is far from clear. The mobility of STIM2 in the SR membrane and the time constants of STIM2-STIM1 interaction and puncta formation with Orai proteins are unknown. Thus, we have investigated the effect of different gating kinetics on agonist-induced  $[Ca^{2+}]_i$  oscillations. We demonstrate that SR and cytosolic  $Ca^{2+}$  concentrations are not significantly affected by the precise gating kinetics of SOCC. This suggests that a detailed model of SOCC may not be necessary for  $[Ca^{2+}]_i$  oscillations in ASMC.

The following word of caution by Roux et al. applies to our study as well [82]. The mathematical model is constructed based on data for different species. The models for the ion channels are constructed and parametrized for canine, porcine, rat and mice. Likewise the model for RyR is based on bullfrog sympathetic neurons and the model for IPR is parametrized by IPR data obtained in DT40 cells [93]. There is no dataset available characterizing the main ion channels and  $Ca^{2+}$  handling pathways for a single species.

Despite all words of caution, the qualitative predictions of the mathematical model agree with all available experimental data of  $Ca^{2+}$  measurements during agonist-induced and depolarization-induced  $[Ca^{2+}]_i$  oscillations and yield testable predictions about the importance of voltage dynamics on the intracellular  $Ca^{2+}$  handling, the effect of (partially) blocking SOCC and the time it takes until oscillations stop in the absence of influx through SOCC. The qualitative predictions are not sensitive to parameter fine tuning, which gives us confidence in the model's predictive power and the predicted behaviour.

# 8

## Concluding remarks and future directions

### 8.1 Quasi-steady-state reduction

Quasi-steady-state reduction is a commonly used technique for the simplification of mathematical models with multiple timescales. It has been known for some time that the application of QSSR to a model can result in significant qualitative differences in the dynamics of a model [32, 37]. In particular, qualitative changes can be introduced by QSSR in mathematical models that show oscillations.

This prompts the question why QSSR is often used even in models that have oscillatory solutions, given that computational power and efficient algorithms for solving ordinary differential equations is often widely available. The appeal of QSSR is that it is based on an intuitively satisfying approach and often easy to utilize. QSSR may reduce stiffness of a given model and may allow for easier geometrical understanding of underlying mathematical structures.

Despite the fact that quasi-steady-state reduction (QSSR) can lead to erroneous predictions about the behaviour of a given model, we believe that QSSR will remain widely used in the modelling community. Hence, it is an important task to understand the conditions under which dynamical properties of a given model are preserved by QSSR.

A common mechanism for the onset of oscillations is a Hopf bifurcation, in which an equilibrium changes stability as a system parameter is varied. We have shown examples where oscillations are removed by QSSR through removing Hopf bifurcations. We have made progress on establishing conditions under which Hopf bifurcations are robust. In particular, we showed rigorously that singular Hopf bifurcations, involving fast and slow variables, are generically preserved under QSSR. Furthermore, we have demonstrated with examples that Hopf bifurcations involving only fast variables may be removed by QSSR, and have argued that Hopf bifurcations only involving slow variables are preserved by QSSR.

Persistence of a Hopf bifurcation does not mean that the resulting periodic orbits are unchanged. We have shown that the criticality of a singular Hopf bifurcation may be changed by QSSR, which implies that the resulting periodic orbits are of different stability in the vicinity of the singular Hopf bifurcation. This result is similar to the result of Zhang et al. [97].

Furthermore, we have shown that the frequency and amplitude of the branches of the periodic orbits resulting from persistence of Hopf bifurcations may be changed by QSSR. Bifurcations of periodic orbits other than Hopf bifurcations may also be affected by QSSR. We have also seen numerically that homoclinic bifurcations may be removed or introduced by QSSR. In one example, QSSR introduced a saddle-node bifurcation of periodic orbits, changing the stability of the corresponding branch of periodic orbits for a wide range of parameters.

We have suggested a way to mitigate the risks of using QSSR. Specifically, we recommend that the fast subsystem of a model (with slow variables treated as parameters) be explored. If the fast subsystem possesses a manifold of equilibria that is not globally attracting, adverse effects of QSSR can be expected.

There are many open questions about the consequences of using QSSR in mathematical models with oscillations. For example, bursting oscillations frequently arise through other mechanisms than Hopf bifurcations. We have not studied the effect of QSSR on bursting solutions that don't arise through Hopf bifurcations. Furthermore, we have only studied systems with explicit timescale splitting. Much less is known about the effect of QSSR in

systems without an explicit timescale splitting.

A natural extension of this work would be to explore the changes of stability of the critical manifold induced by QSSR. In this work, we have used the Leibniz formula for determinants (Eq. (3.6.17)) to show that a zero eigenvalue of the *layer problem* is preserved by QSSR. In fact, this approach can also be used to see the changes in stability of normally hyperbolic sheets of the critical manifold. This allows a connection between eigenvalues of the critical manifold of the full system, treated as equilibria of the fast subsystem, and eigenvalues of the critical manifold of the system after QSSR. Normally hyperbolic sheets of the critical manifold perturb to sheets in the full system, along which the evolution of a trajectory is “slow”. These sheets inherit their stability properties from the critical manifold. Such an extension would be a first step towards obtaining results valid away from the neighbourhood of equilibria.

Many important properties of periodic solutions can be affected by changes away from the critical manifold. It is not clear how to study the effect of QSSR on dynamic structures away from the critical manifold if one does not restrict the investigations to concrete examples.

## 8.2 Airway smooth muscle cells

We have constructed a model for the excitation-contraction coupling based on previously published models for the voltage dynamics [23, 82, 94] and  $\text{Ca}^{2+}$  handling [19, 23, 94] in airway smooth muscle cells. The model is parametrized to reproduce available experimental data on blocking voltage-gated  $\text{Ca}^{2+}$  channels, which was obtained by our collaborators at the University of Massachusetts Medical School.

The modelling effort is an attempt to understand the influence of voltage dynamics during agonist-induced  $\text{Ca}^{2+}$  oscillations in ASMC. Like all muscle cells, ASMC contract as a result of action potentials opening voltage-gated  $\text{Ca}^{2+}$  channels increasing  $[\text{Ca}^{2+}]_i$ . When  $[\text{Ca}^{2+}]_i$  exceeds a (local) threshold, ryanodine receptors open and yield  $\text{Ca}^{2+}$ -induced  $\text{Ca}^{2+}$  release from internal stores, initiating muscle contraction.

On the other hand, ASMC show stronger contraction in response to agonists binding to G-coupled receptor proteins in the plasma membrane [74]. This pathway relies on production of  $\text{IP}_3$ , which binds to IPR and results in  $\text{IP}_3$ -mediated  $\text{Ca}^{2+}$  release from internal stores.

Both types of  $\text{Ca}^{2+}$  release mechanisms can support periodic changes of  $[\text{Ca}^{2+}]_i$  when combined with the activity of pumps, which transport most of the  $\text{Ca}^{2+}$  back into internal stores, and some  $\text{Ca}^{2+}$  ions out of the cell. The voltage across the plasma membrane changes with each  $\text{Ca}^{2+}$  release from internal stores, based on the feedback that  $[\text{Ca}^{2+}]_i$  exerts on the plasma membrane channels [98].

We have shown in the mathematical model, in the work described in chapter 6, that variations in voltage have little influence on frequency and amplitude of oscillations in  $[\text{Ca}^{2+}]_i$ . Voltage modulates the transport of  $\text{Ca}^{2+}$  across the plasma membrane. Overall, the  $\text{Ca}^{2+}$  transport across the plasma membrane is smaller than the  $\text{Ca}^{2+}$  transport within internal compartments. Hence, only prolonged elevated or reduced influxes change total  $\text{Ca}^{2+}$  concentration significantly and affect the dynamics of  $[\text{Ca}^{2+}]_i$ .

Based on our simulations we make the following predictions:

- During agonist-induced  $\text{Ca}^{2+}$  oscillations store-operated  $\text{Ca}^{2+}$  channels are the most significant  $\text{Ca}^{2+}$  entry pathways. Our model predicts that after fully blocking SOCC the  $\text{Ca}^{2+}$  oscillations cease. Furthermore, the model shows that the exact kinetics of SOCC do not affect the  $\text{Ca}^{2+}$  oscillations significantly. This is consistent with the idea that only sustained changes in influx or efflux has a significant effect on the intracellular  $\text{Ca}^{2+}$  handling.
- Our model also shows that variations in voltage due to agonist-induced  $\text{Ca}^{2+}$  oscillations do not lead to prolonged elevation or reduction of  $\text{Ca}^{2+}$  influx from the extracellular space. Furthermore, fixing the voltage does not change agonist-induced  $\text{Ca}^{2+}$  oscillations significantly.
- During  $\text{Ca}^{2+}$  oscillations the SR does not fully deplete. Our simulations show that agonist-induced oscillations only deplete the SR to about 80% of its resting value. While the exact value of the predicted depletion may not be quantitatively accurate (see chapter 7), the model robustly shows that stable oscillations are possible without full SR depletion.

These predictions remain to be tested experimentally. Our model is based on data obtained in mouse lung slices. Hence, the second and third prediction may be challenging to validate experimentally, since it is very hard to measure the  $\text{Ca}^{2+}$  concentration in the SR as well as to measure or clamp the voltage for cells inside lung slices. The first prediction will be tested in the future by our collaborators.

A potentially very useful model modification would be to take calmodulin and other  $\text{Ca}^{2+}$

buffers explicitly into account. The model presented is a model for effective fluxes, based on the assumptions that buffers are fast and do not saturate. Saturating buffers or buffers with different kinetic properties may well have a large impact on the observed behaviour. Only a small fraction of  $\text{Ca}^{2+}$  (less than 1%) are available as free  $\text{Ca}^{2+}$ . Even small changes in buffer kinetics or (local) concentrations may have large consequences on the  $\text{Ca}^{2+}$  dynamics. A problem with including buffer kinetics is that experimental results are coarse and only allow for fluorescence measurements indicative of the whole-cell free  $[\text{Ca}^{2+}]_i$ , and it would not be clear which buffer concentrations and binding kinetics are realistic. It would be helpful to study the effect of the buffer kinetics systematically with saturating and non-saturating buffers.





# A

## Model functions and parameters

### A.1 Hodgkin-Huxley model

The discussion of the Hodgkin-Huxley model in section 2.2 uses the model in the form found in [83], i.e.,

$$\begin{aligned}C_m \frac{dv}{dt} &= I - g_{\text{Na}} m^3 h (v - E_{\text{Na}}) - g_{\text{K}} n^4 (v - E_{\text{K}}) - g_{\text{L}} (v - E_{\text{L}}), \\ \frac{dm}{dt} &= \frac{1}{\tau_m t_m(v)} (m_{\infty}(v) - m), \\ \frac{dh}{dt} &= \frac{1}{\tau_h t_h(v)} (h_{\infty}(v) - h), \\ \frac{dn}{dt} &= \frac{1}{\tau_n t_n(v)} (n_{\infty}(v) - n),\end{aligned}$$

with the definitions

$$\begin{aligned}x_{\infty}(v) &= \frac{a_x(v)}{a_x(v) + b_x(v)}, \\ t_x(v) &= \frac{1}{a_x(v) + b_x(v)},\end{aligned}\tag{A.1.1}$$

for  $x = m, h, n$ . The functions are:

$$a_m(v) = 0.1 \frac{v + 40}{1 - \exp\left[-\frac{v+40}{10}\right]}, \quad (\text{A.1.2})$$

$$b_m(v) = 4 \exp\left[-\frac{v + 65}{18}\right], \quad (\text{A.1.3})$$

$$a_h(v) = 0.07 \exp\left[-\frac{v + 65}{20}\right], \quad (\text{A.1.4})$$

$$b_h(v) = \frac{1}{1 + \exp\left[-\frac{v+35}{10}\right]}, \quad (\text{A.1.5})$$

$$a_n(v) = 0.01 \frac{v + 55}{1 - \exp\left[-\frac{v+55}{10}\right]}, \quad (\text{A.1.6})$$

$$b_n(v) = 0.125 \exp\left[-\frac{v + 65}{80}\right]. \quad (\text{A.1.7})$$

$$(\text{A.1.8})$$

The parameters are given in the following table:

$g_{\text{Na}}$	120 mS/cm <sup>2</sup>	$E_{\text{Na}}$	50 mV
$g_{\text{K}}$	36 mS/cm <sup>2</sup>	$E_{\text{K}}$	-77 mV
$g_{\text{L}}$	0.3 mS/cm <sup>2</sup>	$E_{\text{L}}$	-54.4 mV
$C_{\text{m}}$	1 $\mu\text{F}/\text{cm}^2$	$\tau_m$	1
$\tau_h$	1	$\tau_n$	1

Table A.1: Functions and parameters for the Hodgkin-Huxley model as used in section 2.2.

## A.2 Chay-Keizer model

The Chay-Keizer model for the pancreatic  $\beta$ -cell was first proposed in [21]. In the discussion in section 2.2 we use the model in the form presented in [51]:

$$\begin{aligned}
 C_m \frac{dv}{dt} &= I - \left( g_{K,Ca} \frac{c}{K_d + c} + g_K n^4 \right) (v - E_K) \\
 &\quad - 2g_{Ca} m^3 h (v - E_{Ca}) - g_L (v - E_L), \\
 \frac{dm}{dt} &= \frac{1}{\tau_m t_m(v)} (m_\infty(v) - m), \\
 \frac{dh}{dt} &= \frac{1}{\tau_h t_h(v)} (h_\infty(v) - h), \\
 \frac{dn}{dt} &= \frac{1}{\tau_n t_n(v)} (n_\infty(v) - n), \\
 \frac{dc}{dt} &= f(-k_1 g_{Ca} m^3 h (v - E_{Ca}) - k_c c).
 \end{aligned}$$

In the equations for the gating variables  $m$ ,  $h$  and  $n$  we use the definitions

$$\begin{aligned}
 x_\infty(v) &= \frac{a_x(v)}{a_x(v) + b_x(v)}, \\
 t_x(v) &= \frac{1}{a_x(v) + b_x(v)},
 \end{aligned} \tag{A.2.1}$$

for  $x = m, h, n$ . The functions are:

$$\begin{aligned}
 a_m(v) &= 0.1 \frac{25 - (v + v')}{\exp\left[\frac{25 - (v + v')}{10}\right] - 1}, \\
 b_m(v) &= 4 \exp\left[-\frac{v + v'}{18}\right], \\
 a_h(v) &= 0.07 \exp\left[-\frac{v + v'}{20}\right], \\
 b_h(v) &= \frac{1}{\exp\left[\frac{30 - (v + v')}{10}\right] + 1}, \\
 a_n(v) &= 0.01 \frac{10 - (v + v^*)}{\exp\left[\frac{10 - (v + v^*)}{10}\right] - 1}, \\
 b_n(v) &= 0.125 \exp\left[-\frac{v + v^*}{80}\right].
 \end{aligned}$$

The parameters are given in the following table:

$g_{K,Ca}$	0.09 mS/cm <sup>2</sup>	$g_K$	12 mS/cm <sup>2</sup>
$g_{Ca}$	6.5 mS/cm <sup>2</sup>	$g_L$	0.04 mS/cm <sup>2</sup>
$\tau_m$	0.3	$k_1$	0.035 $\mu\text{Mcm}^2/\text{nC}$
$k_c$	0.04 ms <sup>-1</sup>	$v^*$	30 mV
$v'$	50 mV	$K_d$	1 $\mu\text{M}$
$E_K$	-75 mV	$E_{Ca}$	100 mV
$E_L$	-40 mV	$\tau_n$	0.3
$\tau_h$	0.3	$C_m$	1 $\mu\text{F}/\text{cm}^2$
$f$	0.002		

Table A.2: Parameter values for the Chay-Keizer model as used in section 2.2.

### A.3 GnRH neuron model

A model for the GnRH neuron was proposed by Lee et. al in [59]. We use a simplified version from [67], in which some of the ionic currents are averaged:

$$\begin{aligned}
 C_m \frac{dV}{dt} &= I_{\text{app}} - I_{\text{km}} - I_{\text{cal}} - I_{\text{naf}} - sI_{\text{AHP-SK}} - sI_{\text{AHP-UCL}} + I_{\text{leak}}, \\
 \frac{dN_{\text{km}}}{dt} &= \frac{1}{\tau_{N_{\text{km}}}} (N_{\text{km}\infty} - N_{\text{km}}), \\
 \frac{dH_{\text{naf}}}{dt} &= \frac{1}{\tau_{H_{\text{naf}}}} (H_{\text{naf}\infty} - H_{\text{naf}}), \\
 \frac{dO_{\text{ucl}}^*}{dt} &= k_{\text{new}} \cdot (1 - O_{\text{ucl}}^*) - k_{33} O_{\text{ucl}}^*, \\
 \frac{dc}{dt} &= J_{\text{release}} - J_{\text{serca}} + \rho (J_{\text{in}} - J_{\text{pm}}), \\
 \frac{dc_t}{dt} &= \rho (J_{\text{in}} - J_{\text{pm}}),
 \end{aligned}$$

with the currents being

$$\begin{aligned}
I_{\text{km}} &= g_{\text{km}} N_{\text{km}} (V - V_{\text{K}}), \\
I_{\text{cal}} &= g_{\text{cal}} M_{\text{cal}\infty}^2 (V - V_{\text{Ca}}), \\
I_{\text{naf}} &= g_{\text{naf}} M_{\text{naf},\infty}^3 H_{\text{naf}} (V - V_{\text{Naf}}), \\
sI_{\text{AHP-SK}} &= g_{\text{sk}} \left( \frac{c^{n_{\text{sk}}}}{c^{n_{\text{sk}}} + K_{\text{sk}}^{n_{\text{sk}}}} \right) (V - V_{\text{K}}), \\
sI_{\text{AHP-UCL}} &= g_{\text{ucl}} (O_{\text{ucl}} + O_{\text{ucl}}^*) (V - V_{\text{K}}), \\
I_{\text{leak}} &= g_{\text{leak}} (V - V_{\text{leak}}), \\
J_{\text{release}} &= (k_{\text{f}} O_4 + J_{\text{er}}) \cdot (c_{\text{e}} - c), \\
J_{\text{serca}} &= P_{\text{rate}} \frac{c - a_1 c_{\text{e}}}{a_2 + a_3 c + a_4 c_{\text{e}} + a_5 c c_{\text{e}}}, \\
J_{\text{in}} &= -\alpha I_{\text{cal}} + \beta \cdot \text{IP}_3, \\
J_{\text{pm}} &= V_{\text{p}} \frac{c^2}{K_{\text{p}}^2 + c^2} + V_{\text{naca}} \frac{c^4}{K_{\text{naca}}^4 + c^4}.
\end{aligned}$$

The functions are:

$$\begin{aligned}
M_{\text{naf}\infty} &= \frac{1}{1 + \exp[-(V + 40)/4.3]}, \\
H_{\text{naf}\infty} &= \frac{1}{1 + \exp[(V + 66.1)/10.8]}, \\
N_{\text{km}\infty} &= \frac{1}{1 + \exp[-(V + 37)/4]}, \\
M_{\text{cal}\infty} &= \frac{1}{1 + \exp[-(V + 30)/2]}, \\
\tau_{h_{\text{naf}}} &= \frac{75}{\exp[(V + 80)/19] + 2 \exp[-2 \cdot (V + 80)/19]}, \\
\tau_{n_{\text{km}}} &= \frac{11.5}{\exp[(V + 30)/15] + \exp[-(V + 30)/15]}, \\
O_4 &= \frac{q_{12} q_{32} q_{24}}{q_{12} q_{32} q_{24} + q_{23} q_{12} + q_{42} q_{32} q_{12} + q_{42} q_{32} q_{21}}, \\
q_{23} &= a_{23} - \left( \frac{V_{23}}{k_{23}^2 + c^2} + b_{23} \right) \left( \frac{V_{-23} c^5}{k_{-23}^5 + c^5} + b_{-23} \right), \\
q_{32} &= \left( \frac{V_{32}}{k_{32}^3 + c^3 + b_{32}} \right) \left( \frac{V_{-32} c^7}{k_{-32}^7 + c^7} + b_{-32} \right), \\
c_{\text{e}} &= 27 \cdot (c_{\text{t}} - c).
\end{aligned}$$

The parameters are given in the following table.

$C_m$	16 pF	$V_{\text{Naf}}$	60 mV
$V_K$	-80 mV	$V_{\text{Ca}}$	100 mV
$V_{\text{leak}}$	100 mV	$g_{\text{naf}}$	200 nS
$g_{\text{km}}$	8.14 nS	$g_{\text{cal}}$	0.05 nS
$g_{\text{sk}}$	0.1 nS	$g_{\text{ucl}}$	950 nS
$g_{\text{leak}}$	0.04 nS	$K_{\text{sk}}$	1 $\mu\text{M}$
$O_{\text{ucl}}$	0	$n_{\text{sk}}$	2
$k_f$	$1.92 \cdot 10^{-4} \text{ ms}^{-1}$	$k_{33}$	$3 \cdot 10^{-5} \text{ ms}^{-1}$
$\rho$	0.5	$J_{\text{er}}$	$4 \cdot 10^{-7} \text{ ms}^{-1}$
$a_1$	$10^{-4}$	$q_{12}$	$0.74 \text{ ms}^{-1}$
$q_{21}$	$0.11 \text{ ms}^{-1}$	$q_{24}$	$7.84 \text{ ms}^{-1}$
$q_{42}$	$3.6 \text{ ms}^{-1}$	$\alpha$	$4.8 \cdot 10^{-3} \mu\text{M pA}^{-1}$
$\beta$	$2 \cdot 10^{-5} \text{ ms}^{-1}$	$\text{IP}_3$	0.3 $\mu\text{M}$
$V_{-32}$	1.06	$V_p$	$4.2 \cdot 10^{-3} \mu\text{M ms}^{-1}$
$a_4$	7 $\mu\text{M ms}^{-1}$	$b_{-32}$	0.03
$K_p$	0.425 $\mu\text{M}$	$K_{\text{naca}}$	0.05 $\mu\text{M}$
$P_{\text{rate}}$	1	$a_{23}$	$1/1.023 \text{ ms}^{-1}$
$a_2$	35 ms	$a_3$	300 $\mu\text{M}^{-1} \text{ ms}$
$V_{\text{naca}}$	$3.5 \cdot 10^{-4} \mu\text{M ms}^{-1}$	$a_5$	35 $\mu\text{M}^{-2} \text{ ms}^{-1}$
$V_{23}$	$1.08 \mu\text{M}^2 \text{ ms}^{-1}$	$k_{23}$	2 $\mu\text{M}$
$b_{23}$	$2.2 \text{ ms}^{-1}$	$V_{-23}$	0.3545
$k_{-23}$	0.072 $\mu\text{M}$	$b_{-23}$	0.042
$V_{32}$	$0.007 \mu\text{M}^3 \text{ ms}^{-1}$	$k_{32}$	0.52 $\mu\text{M}$
$b_{32}$	$0.005 \text{ ms}^{-1}$	$k_{\text{new}}$	$2.9 \cdot 10^{-8}$
$k_{-32}$	0.15 $\mu\text{M}$		

Table A.3: Parameter values for the Gonadotropin Releasing Hormone neuron model as used in section 4.1.

# Bibliography

- [1] A. AMCHESLAVSKY, M. L. WOOD, A. V. YEROMIN, I. PARKER, J. A. FREITES, D. J. TOBIAS, AND M. D. CAHALAN, *Molecular Biophysics of Orai Store-Operated  $Ca^{2+}$  Channels*, *Biophysical Journal*, 108 (2015), pp. 237–246.
- [2] A. ATRI, J. AMUNDSON, D. CLAPHAM, AND J. SNEYD, *A Single-Pool Model for Intracellular Calcium Oscillations and Waves in the *Xenopus Laevis* Oocyte*, *Biophysical Journal*, 65 (1993), pp. 1727–1739.
- [3] B. AY, A. IYANOYE, G. C. SIECK, Y. S. PRAKASH, AND C. M. PABELICK, *Cyclic Nucleotide Regulation of Store-Operated  $Ca^{2+}$  Influx in Airway Smooth Muscle*, *American Journal of Physiology - Lung Cellular and Molecular Physiology*, 290 (2006), pp. L278–L283.
- [4] B. AY, Y. S. PRAKASH, C. M. PABELICK, AND G. C. SIECK, *Store-Operated  $Ca^{2+}$  Entry in Porcine Airway Smooth Muscle*, *American Journal of Physiology - Lung Cellular and Molecular Physiology*, 286 (2004), pp. L909–L917.
- [5] Y. BAI, M. EDELMANN, AND M. J. SANDERSON, *The Contribution of Inositol 1,4,5-Trisphosphate and Ryanodine Receptors to Agonist-Induced  $Ca^{2+}$  Signaling of Airway Smooth Muscle Cells*, *American Journal of Physiology - Lung Cellular and Molecular Physiology*, 297 (2009), pp. L347–L361.
- [6] Y. BAI AND M. J. SANDERSON, *Airway Smooth Muscle Relaxation Results from a Reduction in the Frequency of  $Ca^{2+}$  Oscillations Induced by a cAMP-Mediated Inhibition of the  $IP_3$  Receptor*, *Respiratory Research*, 7 (2006), pp. 1–20.
- [7] M. J. BERRIDGE, *Smooth Muscle Cell Calcium Activation Mechanisms*, *The Journal of Physiology*, 586 (2008), pp. 5047–5061.
- [8] M. J. BERRIDGE, M. D. BOOTMAN, AND H. L. RODERICK, *Calcium Signalling: Dynamics, Homeostasis and Remodelling*, *Nature Reviews Molecular Cell Biology*, 4 (2003), pp. 517–529.



- [9] M. J. BERRIDGE, P. LIPP, AND M. D. BOOTMAN, *The Versatility and Universality of Calcium Signalling*, *Nature Reviews Molecular Cell Biology*, 1 (2000), pp. 11–21.
- [10] D. M. BERS, *Cardiac Excitation–Contraction Coupling*, *Nature*, 415 (2002), pp. 198–205.
- [11] C. K. BILLINGTON, I. P. HALL, AND C. P. NELSON, *Mechanisms Underlying  $Ca^{2+}$  Store Refilling in Airway Smooth Muscle*, in *Calcium Signaling In Airway Smooth Muscle Cells*, Springer, 2014, pp. 177–193.
- [12] S. BOIE, J. CHEN, M. J. SANDERSON, AND J. SNEYD, *Excitation Contraction Coupling in Airway Smooth Muscle Cells and the Role of Store-Operated  $Ca^{2+}$  Channels*. In Preparation.
- [13] S. BOIE, V. KIRK, J. SNEYD, AND M. WECHSELBERGER, *Effects of Quasi-Steady-State Reduction on Biophysical Models with Oscillations*, *Journal of Theoretical Biology*, 393 (2016), pp. 16–31.
- [14] T. B. BOLTON, S. A. PRESTWICH, A. V. ZHOLOS, AND D. V. GORDIENKO, *Excitation–Contraction Coupling in Gastrointestinal and Other Smooth Muscles*, *Annual Review of Physiology*, 61 (1999), pp. 85–115.
- [15] J. A. M. BORGHANS, R. J. DE BOER, AND L. A. SEGEL, *Extending the Quasi-Steady State Approximation by Changing Variables*, *Bulletin of Mathematical Biology*, 58 (1996), pp. 43–63.
- [16] J. BOYLE, M. TOMASIC, AND M. KOTLIKOFF, *Delayed Rectifier Potassium Channels in Canine and Porcine Airway Smooth Muscle Cells*, *The Journal of Physiology*, 447 (1992), pp. 329–350.
- [17] O. BRANDMAN, J. LIU, W. S. PARK, AND T. MEYER, *STIM2 is a Feedback Regulator that Stabilizes Basal Cytosolic and Endoplasmic Reticulum  $Ca^{2+}$  Levels*, *Cell*, 131 (2007), pp. 1327–1339.
- [18] G. E. BRIGGS AND J. B. S. HALDANE, *A Note on the Kinetics of Enzyme Action*, *Biochemical Journal*, 19 (1925), pp. 338–339.
- [19] P. CAO, X. TAN, G. DONOVAN, M. J. SANDERSON, AND J. SNEYD, *A Deterministic Model Predicts the Properties of Stochastic Calcium Oscillations in Airway Smooth Muscle Cells*, *PLoS Computational Biology*, 10 (2014), p. e1003783.
- [20] P. C. CHANDRASEKERA, M. E. KARGACIN, J. P. DEANS, AND J. LYTTON, *Determination of Apparent Calcium Affinity for Endogenously Expressed Human*

- Sarco(endoplasmic Reticulum Calcium-ATPase Isoform SERCA3*, American Journal of Physiology - Cell Physiology, 296 (2009), pp. C1105–C1114.
- [21] T. R. CHAY AND J. KEIZER, *Minimal Model for Membrane Oscillations in the Pancreatic Beta-Cell*, Biophysical Journal, 42 (1983), pp. 181–190.
- [22] A. CILIBERTO, F. CAPUANI, AND J. J. TYSON, *Modeling Networks of Coupled Enzymatic Reactions Using the Total Quasi-Steady State Approximation*, PLoS Computational Biology, 3 (2007), p. e45.
- [23] H. CROISIER, X. TAN, J. F. PEREZ-ZOGHBI, M. J. SANDERSON, J. SNEYD, AND B. S. BROOK, *Activation of Store-Operated Calcium Entry in Airway Smooth Muscle Cells: Insight from a Mathematical Model*, PLoS One, 8 (2013), p. e69598.
- [24] P. DELMOTTE, A.-R. RESSMEYER, Y. BAI, AND M. J. SANDERSON, *Mechanisms of Airway Smooth Muscle Relaxation Induced by Beta2-Adrenergic Agonists*, Frontiers in Bioscience, 15 (2010), pp. 750–764.
- [25] M. DESROCHES, J. GUCKENHEIMER, B. KRAUSKOPF, C. KUEHN, H. OSINGA, AND M. WECHSELBERGER, *Mixed-Mode Oscillations with Multiple Time Scales*, SIAM Review, 54 (2012), pp. 211–288.
- [26] A. DHOOGHE, W. GOVAERTS, AND Y. A. KUZNETSOV, *MATCONT: A MATLAB Package for Numerical Bifurcation Analysis of ODEs*, ACM Transactions of Mathematical Software, (2003), pp. 141–164.
- [27] E. DOEDEL, A. CHAMPNEYS, F. DERCOLE, T. FAIRGRIEVE, Y. A. KUZNETSOV, B. OLDEMAN, R. PAFFENROTH, B. SANDSTEDTE, X. WANG, AND C. ZHANG, *AUTO-07p: Continuation and Bifurcation Software for Ordinary Differential Equations*. <http://cmvl.cs.concordia.ca/auto/>.
- [28] L. DUAN AND Q. LU, *Codimension-Two Bifurcation Analysis on Firing Activities in Chay Neuron Model*, Chaos, Solitons & Fractals, (2006), pp. 1172–1179.
- [29] G. DUPONT, L. COMBETTES, AND L. LEYBAERT, *Calcium Dynamics: Spatio-Temporal Organization from the Subcellular to the Organ Level*, International Review of Cytology, 261 (2007), pp. 193–245.
- [30] B. ERMENTROUT, *XPPAUT*, in Computational Systems Neurobiology, Springer, (2012), pp. 519–531.
- [31] B. ERMENTROUT AND D. H. TERMAN, *Mathematical Foundations of Neuroscience*, Springer, (2010).

- [32] T. ERNEUX AND A. GOLDBETER, *Rescue of the Quasi-Steady-State Approximation in a Model for Oscillations in an Enzymatic Cascade*, SIAM Journal on Applied Mathematics, 67 (2006), pp. 305–320.
- [33] M. FALCKE, *On the Role of Stochastic Channel Behavior in Intracellular  $Ca^{2+}$  Dynamics*, Biophysical Journal, 84 (2003), pp. 42 – 56.
- [34] M. FALCKE, *Reading the Patterns in Living Cells – The Physics of  $Ca^{2+}$  Signaling*, Advances in Physics, (2004), pp. 255 – 440.
- [35] Y.-S. FAN AND T. R. CHAY, *Generation of Periodic and Chaotic Bursting in an Excitable Cell Model*, Biological Cybernetics, 71 (1994), pp. 417–431.
- [36] N. FENICHEL, *Geometric Singular Perturbation Theory for Ordinary Differential Equations*, Journal of Differential Equations, (1979), pp. 53–98.
- [37] E. FLACH AND S. SCHNELL, *Use and Abuse of the Quasi-Steady-State Approximation*, IEE Proceedings - Systems Biology, 153 (2006), pp. 187–191.
- [38] B. E. FLUCHER AND C. FRANZINI-ARMSTRONG, *Formation of Junctions Involved in Excitation–Contraction Coupling in Skeletal and Cardiac Muscle*, Proceedings of the National Academy of Sciences, 93 (1996), pp. 8101–8106.
- [39] D. FRIEL,  *$[Ca^{2+}]_i$  Oscillations in Sympathetic Neurons: An Experimental Test of a Theoretical Model*, Biophysical Journal, (1995), pp. 1752–1766.
- [40] G. GALLOS AND C. W. S. EMALA, *Calcium-Activated Chloride Channels*, in Calcium Signaling In Airway Smooth Muscle Cells, Springer, 2014, pp. 85–106.
- [41] A. GOEKE AND S. WALCHER, *A Constructive Approach to Quasi-Steady State Reductions*, Journal of Mathematical Chemistry, 52 (2014), pp. 2596–2626.
- [42] J. GUCKENHEIMER, *Singular Hopf Bifurcation in Systems with Two Slow Variables*, SIAM Journal on Applied Dynamical Systems, 7 (2008), pp. 1355–1377.
- [43] J. GUCKENHEIMER AND H. OSINGA, *The Singular Limit of a Hopf Bifurcation*, Discrete and Continuous Dynamical Systems - Series A, 32 (2012), pp. 2805–2823.
- [44] J. HINDMARSH AND R. M. ROSE, *A Model of Neuronal Bursting Using Three Coupled First Order Differential Equations*, Proceedings of the Royal Society of London B: Biological Sciences, (1984), pp. 87–102.
- [45] A. HODGKIN AND A. HUXLEY, *A Quantitative Description of Membrane Current and its Application to Conduction and Excitation in Nerve*, The Journal of Physiology, 117 (1952), pp. 500–544.

- [46] P. G. HOGAN, R. S. LEWIS, AND A. RAO, *Molecular Basis of Calcium Signaling in Lymphocytes: STIM and ORAI*, Annual Review of Immunology, 28 (2010), pp. 491–533.
- [47] L. J. JANSSEN, *Airway Smooth Muscle Electrophysiology in a State of Flux?*, American Journal of Physiology – Lung Cellular and Molecular Physiology, 302 (2012), pp. L730–L732.
- [48] L. J. JANSSEN, H. LU-CHAO, AND S. NETHERTON, *Excitation–Contraction Coupling in Pulmonary Vascular Smooth Muscle Involves Tyrosine Kinase and Rho Kinase*, American Journal of Physiology – Lung Cellular and Molecular Physiology, 280 (2001), pp. L666–L674.
- [49] R. L. JONES, J. G. ELLIOT, AND A. L. JAMES, *Estimating Airway Smooth Muscle Cell Volume and Number in Airway Sections. Sources of Variability*, American Journal of Respiratory Cell and Molecular Biology, 50 (2014), pp. 246–252.
- [50] H. KARAKI, H. OZAKI, M. HORI, M. MITSUI-SAITO, K.-I. AMANO, K.-I. HARADA, S. MIYAMOTO, H. NAKAZAWA, K.-J. WON, AND K. SATO, *Calcium Movements, Distribution, and Functions in Smooth Muscle*, Pharmacological reviews, 49 (1997), pp. 157–230.
- [51] J. P. KEENER AND J. SNEYD, *Mathematical Physiology: Cellular Physiology. I*, Springer, (2009).
- [52] ———, *Mathematical Physiology: Systems Physiology. II*, Springer, 2009.
- [53] T. B. KEPLER, L. F. ABBOTT, AND E. MARDER, *Reduction of Conductance-Based Neuron Models*, Biological Cybernetics, 66 (1992), pp. 381–387.
- [54] M. I. KOTLIKOFF, *Potassium Currents in Canine Airway Smooth Muscle Cells*, American Journal of Physiology – Lung Cellular and Molecular Physiology, 259 (1990), pp. L384–L395.
- [55] C. KUEHN, *Multiple Time Scale Dynamics*, Springer, (2015).
- [56] H. KUME, *Large-Conductance Calcium-Activated Potassium Channels*, in Calcium Signaling In Airway Smooth Muscle Cells, Springer, 2014, pp. 49–83.
- [57] Y. A. KUZNETSOV, *Elements of Applied Bifurcation Theory*, Springer, (2013).
- [58] A. P. LEBEAU, A. B. ROBSON, A. E. MCKINNON, R. A. DONALD, AND J. SNEYD, *Generation of Action Potentials in a Mathematical Model of Corticotrophs*, Biophysical Journal, 73 (1997), pp. 1263–1275.

- [59] K. LEE, W. DUAN, J. SNEYD, AND A. E. HERBISON, *Two Slow Calcium-Activated Afterhyperpolarization Currents Control Burst Firing Dynamics in Gonadotropin-Releasing Hormone Neurons*, *The Journal of Neuroscience*, 30 (2010), pp. 6214–6224.
- [60] Y.-X. LI AND J. RINZEL, *Equations for  $InsP_3$  Receptor-Mediated  $[Ca^{2+}]_i$  Oscillations Derived from a Detailed Kinetic Model: A Hodgkin-Huxley Like Formalism*, *Journal of Theoretical Biology*, 166 (1994), pp. 461–473.
- [61] Y.-X. LI, J. RINZEL, L. VERGARA, AND S. STOJILKOVIĆ, *Spontaneous Electrical and Calcium Oscillations in Unstimulated Pituitary Gonadotrophs*, *Biophysical Journal*, 69 (1995), pp. 785–795.
- [62] L. M. LIFSHITZ, J. D. CARMICHAEL, F. A. LAI, V. SORRENTINO, K. BELLVE, K. E. FOGARTY, AND R. ZHUGE, *Spatial Organization of RyRs and bK Channels Underlying the Activation of STOCs by  $Ca^{2+}$  Sparks in Airway Myocytes*, *The Journal of General Physiology*, 138 (2011), pp. 195–209.
- [63] J. LIOU, M. FIVAZ, T. INOUE, AND T. MEYER, *Live-Cell Imaging Reveals Sequential Oligomerization and Local Plasma Membrane Targeting of Stromal Interaction Molecule 1 after  $Ca^{2+}$  Store Depletion*, *Proceedings of the National Academy of Sciences*, 104 (2007), pp. 9301–9306.
- [64] M. MARHL, D. NOBLE, AND E. ROUX, *Modelling of Molecular and Cellular Mechanisms Involved in  $Ca^{2+}$  Signal Encoding in Airway Myocytes*, *Cell Biochemistry and Biophysics*, 46 (2006), pp. 64–87.
- [65] L. MICHAELIS AND M. L. MENTEN, *Die Kinetik der Invertinwirkung*, *Biochemische Zeitschrift*, 49 (1913), pp. 333–369.
- [66] J. MOEHLIS, *Canards for a Reduction of the Hodgkin-Huxley Equations*, *Journal of Mathematical Biology*, 52 (2005), pp. 141–153.
- [67] P. NAN, *Dynamical Systems Analysis of Biophysical Models with Multiple Timescales*, PhD thesis, The University of Auckland, (2014).
- [68] E. NEHER AND G. J. AUGUSTINE, *Calcium Gradients and Buffers in Bovine Chromaffin Cells*, *The Journal of Physiology*, 450 (1992), pp. 273–301.
- [69] H. L. ONG, L. B. DE SOUZA, C. ZHENG, K. T. CHENG, X. LIU, C. M. GOLDSMITH, S. FESKE, AND I. S. AMBUDKAR, *STIM2 Enhances Receptor-Stimulated  $Ca^{2+}$  Signaling by Promoting Recruitment of STIM1 to the Endoplasmic Reticulum – Plasma Membrane Junctions*, *Science Signaling*, 8 (2015), pp. ra3–ra3.

- [70] C. M. PABELICK, B. AY, Y. PRAKASH, AND G. C. SIECK, *Effects of Volatile Anesthetics on Store-Operated  $\text{Ca}^{2+}$  Influx in Airway Smooth Muscle*, *Anesthesiology*, 101 (2004), pp. 373–380.
- [71] M. G. PEDERSEN, A. M. BERSANI, AND E. BERSANI, *Quasi Steady-State Approximations in Complex Intracellular Signal Transduction Networks - A Word of Caution*, *Journal of Mathematical Chemistry*, 43 (2008), pp. 1318–1344.
- [72] S. E. PEEL, B. LIU, AND I. P. HALL, *A Key Role for STIM1 in Store-Operated Calcium Channel Activation in Airway Smooth Muscle*, *Respiratory Research*, 7 (2006), pp. 119–127.
- [73] ———, *ORAI and Store-Operated Calcium Influx in Human Airway Smooth Muscle Cells*, *American Journal of Respiratory Cell and Molecular Biology*, 38 (2008), pp. 744–749.
- [74] J. F. PEREZ AND M. J. SANDERSON, *The Frequency of Calcium Oscillations Induced by 5-HT, ACH, and KCl Determine the Contraction of Smooth Muscle Cells of Intrapulmonary Bronchioles*, *The Journal of General Physiology*, 125 (2005), pp. 535–553.
- [75] Y. PRAKASH, A. IYANOYE, B. AY, G. C. SIECK, AND C. M. PABELICK, *Store-Operated  $\text{Ca}^{2+}$  Influx in Airway Smooth Muscle: Interactions between Volatile Anesthetic and Cyclic Nucleotide Effects*, *Anesthesiology*, 105 (2006), pp. 976–983.
- [76] M. PRAKRIYA AND R. S. LEWIS, *Store-Operated Calcium Channels*, *Physiological Reviews*, 95 (2015), pp. 1383–1436.
- [77] A.-R. RESSMEYER, Y. BAI, P. DELMOTTE, K. F. UY, P. THISTLETHWAITE, A. FRAIRE, O. SATO, M. IKEBE, AND M. J. SANDERSON, *Human Airway Contraction and Formoterol-Induced Relaxation Is Determined by  $\text{Ca}^{2+}$  Oscillations and  $\text{Ca}^{2+}$  Sensitivity*, *American Journal of Respiratory Cell and Molecular Biology*, 43 (2010), pp. 179–91.
- [78] J. J. RICE AND M. S. JAFRI, *Modelling Calcium Handling in Cardiac Cells*, *Philosophical Transactions of the Royal Society of London A: Mathematical, Physical and Engineering Sciences*, 359 (2001), pp. 1143–1157.
- [79] J. RINZEL, *Excitation Dynamics: Insights from Simplified Membrane Models*, *Federation Proceedings*, 44 (1985), pp. 2944–2946.
- [80] J. RINZEL AND Y. S. LEE, *On Different Mechanisms for Membrane Potential Bursting*, in *Nonlinear Oscillations in Biology and Chemistry*, Springer, (1986), pp. 19–33.

- [81] E. ROUX, P. J. NOBLE, J.-M. HYVELIN, AND D. NOBLE, *Modelling of  $Ca^{2+}$ -Activated Chloride Current in Tracheal Smooth Muscle Cells*, *Acta Biotheoretica*, 49 (2001), pp. 291–300.
- [82] E. ROUX, P. J. NOBLE, D. NOBLE, AND M. MARHL, *Modelling of Calcium Handling in Airway Myocytes*, *Progress in Biophysics and Molecular Biology*, 90 (2006), pp. 64–87.
- [83] J. RUBIN AND M. WECHSELBERGER, *Giant Squid–Hidden Canard: The 3D Geometry of the Hodgkin–Huxley Model*, *Biological Cybernetics*, 97 (2007), pp. 5–32.
- [84] S. SCHUSTER, M. MARHL, AND T. HÖFER, *Modelling of Simple and Complex Calcium Oscillations*, *European Journal of Biochemistry*, 269 (2002), pp. 1333–1355.
- [85] L. A. SEGEL AND M. SLEMROD, *The Quasi-Steady-State Assumption: A Case Study in Perturbation*, *SIAM Review*, 31 (1989), pp. 446–477.
- [86] T. R. SHANNON, F. WANG, J. PUGLISI, C. WEBER, AND D. M. BERS, *A Mathematical Treatment of Integrated  $Ca^{2+}$  Dynamics within the Ventricular Myocyte*, *Biophysical Journal*, 87 (2004), pp. 3351–3371.
- [87] I. SIEKMANN, L. E. WAGNER, D. YULE, E. J. CRAMPIN, AND J. SNEYD, *A Kinetic Model for Type I and II  $IP_3R$  Accounting for Mode Changes*, *Biophysical Journal*, 103 (2012), pp. 658–668.
- [88] J. SNEYD, P. CAO, X. TAN, AND M. J. SANDERSON, *Mathematical modeling of calcium dynamics in airway smooth muscle cells*, in *Calcium Signaling in Airway Smooth Muscle Cells*, Springer, 2014, pp. 341–357.
- [89] J. SNEYD, K. TSANEVA-ATANASOVA, V. REZNIKOV, Y. BAI, M. J. SANDERSON, AND D. I. YULE, *A method for determining the dependance of calcium oscillations on inositol triphosphate oscillations*, *PNAS*, 103 (2006), pp. 1675–1680.
- [90] J. SNEYD, K. TSANEVA-ATANASOVA, D. YULE, J. THOMPSON, AND T. SHUTTLEWORTH, *Control of Calcium Oscillations by Membrane Fluxes*, *Proceedings of the National Academy of Sciences of the United States of America*, 101 (2004), pp. 1392–1396.
- [91] M. SWEENEY, S. S. MCDANIEL, O. PLATOSHYN, S. ZHANG, Y. YU, B. R. LAPP, Y. ZHAO, P. A. THISTLETHWAITE, AND J. X.-J. YUAN, *Role of Capacitative  $Ca^{2+}$  Entry in Bronchial Contraction and Remodeling*, *Journal of Applied Physiology*, 92 (2002), pp. 1594–1602.

- [92] T. VO, R. BERTRAM, AND M. WECHSELBERGER, *Multiple Geometric Viewpoints of Mixed Mode Dynamics Associated with Pseudo-plateau Bursting*, SIAM Journal on Applied Dynamical Systems, 12 (2013), pp. 789–830.
- [93] L. E. WAGNER II AND D. I. YULE, *Differential Regulation of the InsP<sub>3</sub> Receptor Type 1 and 2 Single Channel Properties by InsP<sub>3</sub>, Ca<sup>2+</sup> and ATP*, The Journal of Physiology, 590 (2012), pp. 3245–3259.
- [94] I. Y. WANG, Y. BAI, M. J. SANDERSON, AND J. SNEYD, *A Mathematical Analysis of Agonist- and KCl-Induced Ca<sup>2+</sup> Oscillations in Mouse Airway Smooth Muscle Cells*, Biophysical Journal, 98 (2010), pp. 1170–1181.
- [95] M. WECHSELBERGER, *A Propos De Canards (Apropos Canards)*, Transactions of the American Mathematical Society, (2012), pp. 3289–3309.
- [96] C.-H. ZHANG, L. M. LIFSHITZ, K. F. UY, M. IKEBE, K. E. FOGARTY, AND R. ZHUGE, *The Cellular and Molecular Basis of Bitter Tastant-Induced Bronchodilation*, PLoS Biol, 11 (2013), p. e1001501.
- [97] W. ZHANG, V. KIRK, J. SNEYD, AND M. WECHSELBERGER, *Changes in the Criticality of Hopf Bifurcations due to Certain Model Reduction Techniques in Systems with Multiple Timescales*, Journal of Mathematical Neuroscience, 1 (2011), pp. 1–22.
- [98] R. ZHUGE, R. BAO, K. E. FOGARTY, AND L. M. LIFSHITZ, *Ca<sup>2+</sup> Sparks Act as Potent Regulators of Excitation-Contraction Coupling in Airway Smooth Muscle*, The Journal of Biological Chemistry, 285 (2010), pp. 2203–2210.